The Role of Mechanical Cues in Guiding Human Pluripotent Stem Cell Fate Decisions

By

Yefim Zaltsman

A dissertation submitted in partial fulfillment of

the requirements for the degree of

Doctor of Philosophy

(Biochemistry)

at the

UNIVERSITY OF WISCONSIN- MADISON

2018

Date of final oral examination: 1/8/2018

The dissertation is approved by the following members of the Final Oral Committee:

Laura L. Kiessling, Professor, Chemistry and Biochemistry
Deane F. Mosher, Professor, Biomolecular Chemistry and Medicine
William L. Murphy, Professor, Biomedical Engineering and Orthopedics & Rehabilitation
Sean P. Palecek, Professor, Chemical and Biological Engineering
Jill C. Wildonger, Assistant Professor, Biochemistry

Abstract

Human pluripotent stem (hPS) cells possess the capacity to self-renew indefinitely and differentiate into virtually all cell types. hPS cells thus represent an unlimited source of cells with potentially transformative applications such as cell-based regenerative medicine and drug discovery. These applications, however, require robust methods for directing the differentiation of hPS cells to desired cell types. To exert control over hPS cell fate, it is imperative to understand the signal inputs that hPS cells receive from their microenvironment. While initially the focus was on elucidating the role of soluble factors such as growth factors and small molecules, insoluble cues emanating from interactions between cells as well as between cells and the extracellular matrix are also important in contributing to hPS cell fate decisions (Chapter 1).

We found that, even in the presence of soluble factors that promote pluripotency, compliant substrates—with elasticity similar to human brain tissue—override these signals to induce efficient differentiation of hPS cells to neurons (Chapter 2). Culture on soft substrates also augments soluble-factor based differentiation of hPS cells to motor neurons. The underlying molecular mechanism relies on F-actin and the transcriptional coactivator Yes-associated protein (YAP). Inhibition of F-actin polymerization or YAP depletion in hPS cells on a stiff substrate phenocopies the neuronal differentiation on a soft substrate. Our findings indicate that by modulating YAP localization, matrix elasticity can profoundly influence hPS cell fate.

Next, I identified YAP interactors in hPS cells and characterized which interactions change during differentiation (Chapter 3). I found that during neuronal differentiation YAP localization is regulated by angiomotin (AMOT). AMOT-YAP complexes increase during differentiation and forced expression of AMOT excludes YAP from the nucleus. These results suggest an overlooked role of AMOT in neurogenesis. Finally, I identified novel YAP interactors and generated hPS cell lines that facilitate monitoring of YAP interactions and localization in live cells (Chapter 4). Cumulatively, my findings elucidate YAP's role in hPS cell mechanosensing and cell fate control.

Acknowledgments

I am incredibly grateful to all who have made it possible for me to complete my graduate work. There are many individuals to acknowledge, and I will attempt to enumerate them here.

First off, I would like to thank my graduate advisor, Professor Laura Kiessling. Upon joining the group, I was excited to work on the stem cell project and learn more about cell biology and development, as well as new molecular biology and biochemical tools. My excitement for the underlying science did not waver throughout my graduate career; in fact, it continued to grow, which helped to motivate me to persevere when I would encounter setbacks. Therefore, I am grateful to Professor Kiessling for facilitating and enabling the work that led to the development of my project. In addition, I am grateful for the freedom to craft my project and drive it into the directions I found most interesting. This freedom helped me grow immensely as a scientist. Finally, I am thankful to Professor Kiessling for fostering a collegial group environment and recruiting excellent scientists who are knowledgeable and good-natured.

With that, I would like to thank the rest of the Kiessling group, both former and present members. I'm especially grateful to Dr. Samira Musah for starting this project, thus giving me a chance to follow up on very exciting work. I am thankful to Dr. Joseph Klim and Dr. Paul Wrighton for their guidance and helpful feedback. I thank the rest of stem cell lounge (Dr. Sayaka Masuko, Qiao Li, and Deena-Al Mahbuba) as well as the talented undergraduate students whom I had the distinct pleasure in mentoring (Benjamin Weber, Joshua Bensen). I thank Dr. Danny Zwick for providing great company at late hours. Finally, I'd like to thank Heather Hodges for being my baymate for so many years and providing great conversation.

I am also very thankful to my thesis committee members, as well as the Department of Biochemistry and the rest of the scientific community at the University of Wisconsin–Madison. To my thesis committee, Professors Deane Mosher, William Murphy, Jill Wildonger, and Sean

Palecek—I am grateful for their continued support and invaluable feedback throughout my graduate career. I am also thankful to the dedicated and hard-working staff in the Department, in particular to Kris Turkow, Colleen Clary, and Brenda Renaud as well as the excellent facilities staff, in particular Dr. Elle Grevstad of the Biochemistry Optical Core. I thank Prof. Karen Downs for her enlightening mammalian embryology course, and Dr. Lynne Prost for the opportunity to teach a seminar course. I'm especially thankful to the Stem Cell and Regenerative Medicine Center (SCRMC) led by Profs. William Murphy and Timothy Kamp for fostering an outstanding stem cell community on campus and providing many valuable opportunities. I'd also like to thank them for supporting the Wisconsin Stem Cell Roundtable (WiSCR), an organization I had the distinct honor of leading as well as helping to craft new initiatives like outreach and a research fellowship for undergraduates. I would also like to thank the SCRMC and the Stefaniak Fellowship from the Department of Biochemistry for providing funding.

I am very thankful to my friends, both the ones I've known for many years and the new ones I made in Madison. They've been very supportive and have accompanied me to many concerts, restaurants, and other memorable outings. I would like to extend special gratitude to Spencer Scholz with whom I've had many unforgettable adventures and the pleasure of indulging in exceptional food and drink (in particular, the great amount that was made by him). As a corollary, I would also like to thank his cat Benjamin who is an affable companion.

Finally, my biggest gratitude goes out to my family and especially my parents, Yuriy Zaltsman and Esther Rabinovitch. I owe everything to them and the upbringing they provided me with. They're incredibly supportive and loving, and instilled in me a thirst for knowledge. I will forever be grateful to them for moving us from Russia to the United States, and for supporting my college education. As my mom would remind me growing up, you can't choose your parents—of course it's true, but I very much lucked out. I'm also very thankful to my wonderful brother Ben and sister Anya, and my late grandparents for their love and support.

Table of Contents

List of Figures

List of Tables

Abbreviations

AKAP	A-kinase anchor protein
ALK	Activin receptor-like kinase
AMOT	Angiomotin
AMOTL	Angiomotin-like
AP-MS	Affinity purification-mass spectrometry
ARID	AT-rich interaction domain
BCLAF	Bcl-2-associated transcription factor
BMP	Bone morphogenetic protein
BRET	Bioluminescence resonance energy transfer
Cas	CRISPR-associated
CRISPR	Clustered regulatory interspaced short palindromic repeats
DMEM/F12	Dulbecco's modified Eagle medium/Nutrient Mixture F-12
EC	Embryonal carcinoma
E-cadherin	Epithelial cadherin
ECM	Extracellular matrix
EpiS	Epiblast stem
ERK	Extracellular signal-regulated kinase
ES	Embryonic stem
EXT	Exostosin
F-actin	Filamentous actin
FBS	Fetal bovine serum
FGF	Fibroblast growth factor
FLAG	DYKDDDDK sequence motif
GAG	Glycosaminoglycan
GDF	Growth differentiation factor
GSK	Glycogen synthase kinase
hES	Human embryonic stem
hMS	Human mesenchymal stem
hPS	Human pluripotent stem
HS	Heparan sulfate
ICM	Inner cell mass
IP	Immunoprecipiation
iPS	Induced pluripotent stem
IVF	In vitro fertilization
kPa	Kilopascal
LAP	Lamina-associated polypeptide
LIF	Leukemia inhibitory factor
LRP	Low-density lipoprotein receptor-related protein
MAPK	Mitogen-activated protein kinase
MEF	Mouse embryonic fibroblast
NEUROG	Neurogenin
NSC	Neural stem cell
OCT4	Octamer-binding transcription factor 4
PA	Polyacrylamide
PDMS	Polydimethylsiloxane
PI3K	Phosphoinositide 3-kinase
PMEDSAH	Poly[2-(methacryloyloxy)ethyl dimethyl-(3-sulfopropyl)ammonium hydroxide]
PTM	Post-translation modification

ROCK	Rho-associated kinase
SCNT	Somatic cell nuclear transfer
SMAD	C. elegans Sma and Drosphila mothers against dpp (Mad)
SSEA	Stage specific embryonic antigen
TAZ	Transcriptional coactivator with PDZ-binding domain
TEAD	Transcriptional enhancer activator domain
TGF-β	Transforming growth factor-β
TMPO	Thymopoietin
VHBD	Vitronectin heparin-binding domain
WNT	Wingless and Int
WT	Wildtype
YAP	Yes-associated protein

Chapter 1

Human pluripotent stem cells: from discovery to cell fate control

1.1 Overview

Pluripotent stem cells are remarkable for their ability to both self-renew and differentiate into virtually any cell type in the adult organism. These properties present exciting opportunities for understanding mammalian development and disease. To exert control over these cells and fully realize their potential, it is necessary to first understand the developmental origin of pluripotent cells and the signals they receive from their microenvironment.

This review covers the in vivo origins of pluripotency as well as the pursuit to isolate pluripotent cells for in vitro propagation. The successful isolation of pluripotent cells from mouse teratomas and later mouse blastocysts paved the way for the derivation of human embryonic stem cells. Human embryonic stem cells along with other human pluripotent stem (hPS) cells are shedding light onto human development and enabling exciting advances in regenerative medicine and drug discovery. These powerful applications rely on our ability to control the cell fate decision of hPS cells. Therefore, this review also covers how soluble and insoluble signals from the microenvironment influence hPS cell fate.

1.2 Pluripotency in vivo and in vitro

1.2.1 Pluripotency during mammalian embryogenesis

Pluripotency refers to a property conferred onto cells that possess the potential to generate tissues derived from the three primary germ layers (definitive endoderm, mesoderm, and definitive ectoderm). The primary germ layers give rise to the tissues and organs that form the entire fetus during development and therefore serve as the point of origin for all the cell types of an adult individual. Pluripotent cells exist transiently during embryogenesis. Their identification by classical embryologists in the 1950s-70s paved the way for the isolation and derivation of pluripotent stem cell lines in later years.

Mammalian development initiates with the formation of the zygote, a single cell that is the product of successful fertilization of an oocyte by a sperm cell. The zygote undergoes cell cleavage resulting in 2-, 4-, and 8-cell blastomeres, followed by the morula stage. The cells during these initial stages of embryogenesis are totipotent, that is they retain the potential to contribute to both embryonic and extraembryonic lineages of the developing conceptus. While the embryonic lineages form the fetus proper, the extraembryonic tissues (placenta and yolk sac) provide support and nourishment to the fetus. The totipotency of blastomeres was first demonstrated by Tarkowski (1959) who showed that a single blastomere from a 2-cell embryo can develop into a fertile adult mouse when implanted into the uterus of a foster mother. Elegant work by Kelly (1977) extended these findings by showing that every individual blastomere of a 4- or 8-cell embryo maintained totipotency.

Following the morula stage, the formation of the blastocyst marks the first differentiation event during embryogenesis. At this point the embryo segregates into two distinct structures, the inner cell mass (ICM) and the trophectoderm. The trophectoderm forms the placenta, whereas the ICM gives rise to the epiblast, from which the fetus will form, and to the primitive endoderm, which contributes to the formation of the yolk sac. The first indication that the ICM contains pluripotent cells came from work by Edwards and colleagues, in which they cultured preimplantation rabbit embryos (Cole et al., 1966). They introduced the blastocysts to culture substrates and found that the trophectoderm spread out yet did not proliferate, whereas the ICM when cultured on reconstituted collagen attached and multiplied. Importantly, they found that it was capable of differentiation to several lineages including fibroblastic and epithelial cell types. The definitive experiment, however, that confirmed the pluripotency of the ICM was performed by Gardner (1968) who generated the first mouse chimeras. Donor cells extracted from the ICM were injected into recipient blastocysts and mosaicism was examined with the use of genetic markers. The resulting embryos survived to term and mosaicism was detected in

several tissues. Later work by Gardner and Rossant (1979) verified that the epiblast cells from the ICM contributed exclusively to the fetus and not to extraembryonic tissue.

Therefore, the epiblast cells of the ICM, which exist transiently during early embryogenesis, define mammalian pluripotency. As these pluripotent cells form the basis for the development of the fetus proper, they hold great potential for understanding the mechanisms of mammalian development.

1.2.2 Pluripotency in teratomas

In addition to the transient cells that appear during embryogenesis, pluripotent cells occur in gonadal tumors termed teratomas. Their name, stemming from the Greek *teratos* (monster), alludes to their appearance as the tumors are composed of heterogenous tissues and organs such as teeth, pieces of bone, muscle, skin and hair. Though the tumors are rare, their characterization allowed for the derivation of the first pluripotent stem cell lines, embryonal carcinoma (EC) cells.

The study of teratomas was significantly aided by the development of an inbred strain of mice with an incidence of spontaneous testicular teratomas (Stevens and Little, 1954). A single cell isolated from the tumor when injected intraperitoneally could produce all the cell types found in a teratoma (Kleinsmith and Pierce, 1964). This finding led to the idea that pluripotent stem cells exist within teratomas that could be isolated in culture. This idea came to fruition with the derivation of a mouse EC cell line by Martin and Evans (1974), thus marking the establishment of the first mammalian pluripotent stem cell line. This advance was followed by the isolation of an EC cell line from a human teratoma (Hogan et al., 1977).

An important contribution from research with EC cells was the establishment of specific markers that would subsequently aid in the derivation of cell lines from mouse and human embryos. The development of monoclonal antibodies in the 1970s allowed for the identification

of EC cell-specific markers. Mouse EC cells were reactive to an antibody against stage-specific embryonic antigen 1 (SSEA1), a lactoseries carbohydrate antigen (Solter and Knowles, 1978). In contrast, human EC cells reacted against globoseries antigens, stage-specific embryonic antigen 3 (SSEA3) and 4 (SSEA4), but turned on SSEA1 upon differentiation (Fenderson et al., 1987; Kannagi et al., 1983).

The derivation of EC cells was a significant advance in the study of pluripotency, however, these cells exhibited several important limitations. A key test for the verification of pluripotency is the mouse chimera experiment described above in section 1.2.1. While contribution of EC cells to most embryonic tissues was observed in the chimeras, whether there was germline transmission was unclear (Papaioannou et al., 1975). Another drawback was that many of the chimeras contained tumors of EC origin (Rossant and McBurney, 1982). Finally, it's been demonstrated that EC cells possess an abnormal karyotype (Blelloch et al., 2004). Thus, though EC cells represented an important stepping stone, the derivation of nonmalignant pluripotent cells remained necessary.

1.2.3 Isolation of mouse embryonic stem cells

The derivation of mouse embryonic stem (ES) cells ushered in a new era in stem cell biology. Aside from gleaning insights into mammalian development, mouse ES cells allowed for the development of transgenic animals. Thus, what was before a relatively niche field became at the forefront of biology and medicine. Indeed, Mario Capecchi, Sir Martin Evans, and Oliver Smithies were awarded the Nobel Prize in Physiology or Medicine in 2007 for this work.

Mouse ES cell lines were first derived from mouse blastocysts by two groups independently in 1981. The first report was by Evans and Kaufman (1981) who were able to overcome previous failed attempts by utilizing embryos from mice induced into diapause, which allowed for proliferation of epiblast cells prior to their isolation. They relied on several technological advances made during the study of EC cells. Firstly, they used the inbred strain of mice

developed by Stevens and Little (1954) (described above in section 1.2.3). Additionally, they employed a feeder layer of inactivated fibroblasts as a cell substrate (Martin and Evans, 1975)—this feeder layer was crucial for the culture of EC cells and would later also be used for the first derivation of human ES cells . The derived cell lines, which they termed “EK” cells (for Evans Kaufman) displayed a normal karyotype and formed teratomas when injected into syngeneic mice, thus demonstrating pluripotency.

While Evans and Kaufman were first to publish this advancement, the report by Martin (1981) published just a few months later employed a much more refined technique. A notable difference was that Martin avoided in vivo alteration of the blastocysts via diapause induction and instead utilized medium conditioned by EC cells to culture the isolated cells. In fact, the cell lines passaged without the conditioned medium would stop proliferating, which as Martin presciently noted suggests that it contained “a growth factor that stimulates the proliferation or inhibits the differentiation of normal pluripotent embryonic cells, or both” (Martin, 1981). Another important difference was that Martin derived clonal cell populations and tested each clone for teratoma formation, demonstrating the pluripotency of individual cells. Finally, in this report Martin coined the term “embryonic stem cells” which would endure to describe the cells isolated from the ICM of mammalian blastocysts.

Though these first reports tested the pluripotency of ES cells by teratoma formation, a formal demonstration of pluripotency was still lacking. The definitive experiment was performed by Rossant and colleagues who assessed the developmental potential of ES cells by tetraploid complementation (Nagy et al., 1990). This assay relies on the principle that extraembryonic tissues can sustain tetraploidy and develop to term, while epiblast cells do not tolerate tetraploidy (Tarkowski et al., 1977). Thus, an embryo induced to tetraploidy can be aggregated with diploid cells to test their potential for the development of the entire fetus

proper. Crucially, diploid mouse ES cells passed this rigorous test, thus verifying their pluripotency (Nagy et al., 1990).

In summary, the successful derivation of mouse ES cell lines was enabled by decades of work in classical mammalian embryology and EC cell biology. This advance laid the groundwork for the isolation of ES cells from human embryos.

1.2.4 Isolation of human embryonic stem cells

Almost two decades after the first derivation of ES cells from mouse embryos, human ES cell lines were finally successfully cultured in 1998. This advance for the field was monumental and is inspiring a revolution in regenerative medicine, the momentum of which continues through present day. Though the techniques for the derivation of human ES cells were similar to those previously utilized for mouse embryos, nonetheless, as described below, several technologies had to be integrated for the endeavor to be successful.

A critical area of research that enabled human ES cell isolation was in vitro fertilization (IVF). The first successful procedure for mammalian IVF was carried out on rabbit gametes and led to the birth of healthy young (Chang, 1959). Edwards and colleagues applied this concept in humans and grew human embryos in culture after IVF of preovulatory human oocytes (Steptoe et al., 1971). In 1978, this method led to the birth of the first human child from an embryo produced via IVF (Steptoe and Edwards, 1978). This achievement definitively demonstrated that the pluripotency of IVF-derived human embryos was uncompromised. The experience culturing human embryos that arose from IVF research led to attempts at isolating human ES cells. Initially these efforts were unsuccessful. They were further complicated by the rarity of human donor embryos as well as the underlying ethical considerations. For these reasons, the derivation of a nonhuman primate ES cell line was achieved first using blastocysts recovered from rhesus macaque uteruses (Thomson et al., 1995). Notably, the isolated cell line resembled human EC cells more so than mouse ES cells, both in morphology and marker expression. This

observation further underscored the need to produce a karyotypically normal (in contrast to EC cells) pluripotent human cell line.

Finally, the derivation of the first human ES cell lines was accomplished by Thomson et al. (1998). Strikingly, much of the methodology was similar to that used for the derivation of mouse ES cell lines. Mouse embryonic fibroblasts were used as a feeder layer, and as was the case in the report by Martin (1981), immunosurgery was performed. Immunosurgery allows for the selective isolation of the ICM from a blastocyst by exposing the outer trophectoderm cells to antiserum followed by complement (Solter and Knowles, 1975). A key innovation enabling the derivation of human ES cell lines was the development of serum-free media that allowed for prolonging the in vitro culture of human embryos through to day 5 blastocysts (Gardner et al., 1998). Thus, blastocyst-stage embryos produced by IVF gave rise to the first human ES cell lines, which displayed a normal karyotype and expressed high levels of telomerase (Thomson et al., 1998). Crucially, the cell lines maintained the potential to form derivates of all three primary germ layers in the teratoma formation assay, thus indicating their pluripotency.

In the two decades since their first derivation, there has been significant progress in human ES cell research. The original derivation relied on a number of animal-derived components including mouse feeder cells and fetal bovine serum (FBS). These xenobiotic components would make the application of human ES cells to the clinic challenging. Indeed, human ES cells derived under these conditions expressed Neu5Gc, an immunogenic nonhuman sialic acid (Martin et al., 2005). Thus, new culture conditions were developed that utilized more chemically-defined components, allowing for the derivation of human ES cell lines under xeno-free conditions (Ludwig et al., 2006). Additionally, a wide array of increasingly robust differentiation protocols have been developed for the generation of neural cells, cardiac cells, islet cells, and many others (Tabar and Studer, 2014). These developments have allowed human ES cell-derived cells to

progress to clinical trials, which are currently underway for diseases such as macular degeneration, Parkinson's, and diabetes (Trounson and DeWitt, 2016).

Human ES cells are also providing unique insight into the biology of human pluripotency. Though a rigorous verification of the pluripotency of human ES cells via intraspecies chimera formation or tetraploid complementation is not feasible due to ethical considerations, multiple lines of research indicate that these cells are indeed pluripotent. The strongest case was made by the generation of an interspecies chimera, which showed that human ES cells can colonize a mouse embryo and contribute to all three primary germ layers in the developing fetus (Mascetti and Pedersen, 2016). Furthermore, the advent of CRISPR/Cas9 genome engineering and its successful application in human ES cells (Hou et al., 2013) is facilitating the elucidation of the roles of specific genes in human pluripotency.

Earlier work investigating the potency of mouse embryos along with the derivation of mouse ES cells and human EC cells made possible the isolation of human ES cells. These embryo-derived cells together with other types of human pluripotent stem cells that have since been described are vastly improving our understanding of human development and creating new avenues for disease intervention and drug discovery.

1.2.5 Derivation of human pluripotent stem cells by reprogramming

In addition to the isolation of cells from human embryos, alternative strategies have been developed to attain human pluripotent stem (hPS) cells. Ethical considerations underlying the use of human embryos as well as the resource's limited nature fueled these efforts. Ultimately, through successful reprogramming new kinds of hPS cells were produced. This monumental achievement was indebted to the pioneering work of Sir John Gurdon and Shinya Yamanaka who were recognized for their contributions by a Nobel Prize in Physiology or Medicine in 2012.

Early experiments in the frog were the first demonstration of the power of reprogramming. The prevailing theory at the time was illustrated by Waddington's landscape model, which depicts embryonic cells during differentiation as balls rolling down a hill (Waddington, 1957). While this model continues to be influential today, its original inception assumed that differentiated cells cannot return up the hill to an embryonic state. This concept was overturned by Gurdon's work, which demonstrated that a differentiated somatic cell nucleus can be reprogrammed inside a recipient frog oocyte and thus generate a tadpole (Gurdon, 1962). Therefore, pluripotency is not limited to embryonic cells, but can also be attained through the reprogramming of differentiated cells.

Gurdon's reprogramming approach termed somatic cell nuclear transfer (SCNT) had later been successfully applied to mammalian systems resulting in the cloning of sheep and mice (Wakayama et al., 1998; Wilmut et al., 1997). Initially, however, it was not successful with human oocytes, so in the meantime a different approach for cellular reprogramming was developed. This alternate strategy relied on the finding that transcription factors can alter cellular fate. This concept was first demonstrated in seminal work by Weintraub and colleagues, in which the ectopic expression of the transcription factor MyoD in mouse fibroblasts transformed the cells into myoblasts (Davis et al., 1987). Inspired by this work as well as the work by Gurdon, Takahashi and Yamanaka (2006) applied transcription factor-based reprogramming to produce ES-cell like cells from a mouse somatic cell. By transducing mouse embryonic fibroblasts with 24 candidate genes, they were able to narrow down to 4 essential ones—*Oct4*, *Sox2*, *Klf4*, and *Myc*—that were sufficient to transform the cells into pluripotent cells they termed induced pluripotent stem (iPS) cells. Yamanaka and colleagues then demonstrated that this approach can be applied to adult human fibroblasts to generate human iPS cells (Takahashi et al., 2007), contemporaneously with a similar report by Thomson and colleagues who used a slightly different set of 4 factors (Yu et al., 2007).

Since the original generation of human iPS cells several critical advances have further highlighted the value of this alternate source of pluripotent cells. The derivation of human iPS cells from a patient with spinal muscular atrophy demonstrated the ability to model human diseases, as the resulting differentiated motor neurons displayed deficits relative to wildtype controls (Ebert et al., 2009). Additionally, human iPS cells have now been successfully generated from multiple different cell types, including from blood (Loh et al., 2009)—a cell source much easier to access from a patient. Crucially, the reprogramming methods have also been refined. Whereas previous iterations relied on retrovirus-mediated integration for delivery of reprogramming factors, inherently safer integration-free methods were introduced such as episomal vector-based (Yu et al., 2009). The pluripotency of iPS cells was rigorously validated via tetraploid complementation, demonstrating that mouse iPS cells were capable of producing viable, fertile mice (Zhao et al., 2009). Finally, though previous reports showed differences between iPS cells and ES cells, Hochedlinger and colleagues used genetically matched cell lines to confirm that they are functionally and molecularly equivalent (Choi et al., 2015).

The final major source of hPS cells arrived with the successful application of SCNT to human oocytes. Mitalipov and colleagues transferred a human fetal fibroblast into an enucleated human oocyte to produce embryos from which ES cells were isolated (Tachibana et al., 2013). These pluripotent cells resembled IVF-derived ES cells. An important advantage of SCNT is that it allows for generation of pluripotent cells with rescued metabolic function from patients with mitochondrial DNA mutations. Importantly, studies have shown functional equivalence of hPS cells derived from SCNT and transcription factor based reprogramming (Johannesson et al., 2014), as well as in comparing their differentiated progeny (Zhao et al., 2017).

In summary, in addition to IVF-derived human ES cells, hPS cells include iPS cells generated by transcription factor-based reprogramming and SCNT-derived ES cells. Human iPS cells obviate the need for using human embryos to attain hPS cells, and provide a convenient

source for generating patient-specific cells. This advantage of iPS cells is important in the application of hPS cells to the clinic as it provides a route for autologous cell generation, thus promising immunological compatibility for cell transplantation. Indeed, as is the case with human ES cells, human iPS cell-derived cells are now in clinical trials (Trounson and DeWitt, 2016).

1.2.6 Differences between human and mouse pluripotency

Though both are pluripotent, human ES cells differ significantly from cells that are designated mouse ES cells. It's now understood that the two represent developmentally distinct cell states. Therefore, caution must be used if attempting to generalize findings between rodent and human development.

Some of the differences between mouse and human ES cells are due to inherent species differences. As with EC cells discussed in section 1.2.2, mouse and human ES cells display unique cell-surface carbohydrates. Whereas undifferentiated mouse ES cells display SSEA1 and turn on SSEA3/4 upon differentiation, the reverse is the case with human ES cells, which additionally uniquely display TRA-1-60/-1-81 in the undifferentiated state (Thomson et al., 1998). The differences in these markers is not due to an in vitro artifact as the same pattern of glycan epitope display is observed for the mouse and human ICM, respectively (Henderson et al., 2002). Strikingly, gene expression analysis contrasting the roughly 2000 genes upregulated in either mouse or human ES cells found an overlap of only about 250 genes (Sato et al., 2003). Molecular differences were also detected when comparing gene expression in single epiblast cells of the mouse and human ICMs; several contrasts in the expression of some of the core pluripotency genes were identified (Blakeley et al., 2015). Notably, a recent study highlighted a stark difference for the role of the core pluripotency factor OCT4 in early embryogenesis of mouse and human embryos (Fogarty et al., 2017). CRISPR/Cas9-targeted embryos revealed that OCT4-null human embryos fail to initiate blastocyst formation and downregulate *NANOG*

expression, whereas mouse blastocysts can form from Oct4-null embryos and maintain *Nanog* expression in the ICM.

In addition to exhibiting species-specific developmental differences, mouse and human ES cells are thought to occupy distinct developmental cell states. The idea that there are different states of pluripotency gained ground with the derivation of pluripotent cells from the post-implantation mouse epiblast (Brons et al., 2007; Tesar et al., 2007). These cells termed epiblast stem (EpiS) cells express pluripotency genes and retain the ability to differentiate into the three primary germ layers. The genetic signatures of mouse EpiS cells, however, are a closer match with human ES cells than with mouse ES cells. Furthermore, like human ES cells, EpiS cells rely on FGF2/Activin A signaling instead of LIF signaling as is the case with mouse ES cells. Since mouse EpiS cells and human ES cells more closely resemble the post-implantation epiblast, whereas mouse ES cells retain an ICM-like genetic signature, it was proposed that these cells represent different cell states (Nichols and Smith, 2009). Specifically, cells in the ICM-like and epiblast-like states were deemed to exhibit naïve and primed pluripotency, respectively.

The concept of naïve and primed pluripotent states was validated experimentally by demonstrating interconversion between these states. Smith and colleagues showed that ectopic expression of *Klf4* in mouse EpiS cells cultured under naïve pluripotency conditions could revert the cells to an ES cell state (Guo et al., 2009). This naïve state was maintained after removal of the *Klf4* transgene, demonstrating the stability of the conversion. Since human ES cells resemble mouse EpiS cells more than mouse ES cells, it remained unclear whether a naïve pluripotency state was stable enough to capture in a human cell model. Therefore, an important advance came with the derivation of human naïve ES cells. Using various cocktails involving the inhibition of MAPK/ERK signaling and the addition of LIF, several groups were able to produce human naïve ES cells by either converting already established human ES cell lines or deriving the naïve cells directly from human blastocysts (Gafni et al., 2013; Takashima et al., 2014;

Theunissen et al., 2014). The human naïve ES cells relied on LIF signaling and transcriptionally and epigenetically resembled mouse ES cells. The differences and similarities between the naïve and primed states in the mouse and human are highlighted in Table 1-1.

In summary, though there are many similarities between rodent and human development, there are also important differences, including in the pluripotent state. Therefore, human ES cells present a unique model system for studying human-specific development and disease processes.

Table 1-1. Comparison between naïve and primed pluripotent cells

	Naïve pluripotency		**Primed pluripotency**	
	Mouse ES cells	**Human naïve ES cells**	**Mouse EpiS cells**	**Human ES cells**
Morphology	Domed	Domed	Flattened	Flattened
Cell surface profile	SSEA1$^+$	SSEA3$^+$, SSEA4$^+$, TRA-1-60$^+$, TRA-1-81$^+$	SSEA1$^+$	SSEA3$^+$, SSEA4$^+$, TRA-1-60$^+$, TRA-1-81$^+$
Soluble factors	LIF	LIF, FGF2 (optional), Activin A/TGFβ (optional)	FGF2, Activin A/TGFβ	FGF2, Activin A/TGFβ
X chromosome status (female cells)	X_aX_a	X_aX_a	X_aX_i	X_aX_i
Core pluripotency factors	Oct4, Sox2, higher Nanog	OCT4, SOX2, higher NANOG	Oct4, Sox2, lower Nanog	OCT4, SOX2, lower NANOG

1.3 Soluble signals that instruct human pluripotent stem cells

1.3.1 Activin/Nodal/TGF-β-induced signaling

The original derivation of human ES cells was performed on a MEF feeder layer in an FBS-containing medium (Thomson et al., 1998). These undefined, highly complex culture conditions were used initially for the propagation of human ES cells, as the factors necessary to sustain

human pluripotency were not understood. The first growth factors that were identified to be important for maintenance of human ES cells were Activin/Nodal/TGF-β.

Activin/Nodal/TGF-β are ligands of the transforming growth factor (TGF)-β superfamily of growth factors. The TGF-β superfamily comprises over 30 different ligands, which are evolutionary well conserved and are crucial for metazoan development (Wu and Hill, 2009). In general, there are two branches of TGF-β superfamily signaling pathways, which are categorized based on the activation of the downstream SMAD signaling proteins. BMP/GDF ligands activate SMAD1/5/8 via the type I receptors ALK1, ALK2, ALK3, and ALK6, whereas Activin/Nodal/TGF-β ligands activate SMAD2/3 through ALK4, ALK5, and ALK7 receptors. Once phosphorylated, the SMADs form a complex with SMAD4, and translocate to the nucleus where they bind DNA to modulate transcription (Figure 1-1).

Several early studies identified the SMAD2/3 signaling branch in contributing to the pluripotency of human ES cells. Transcriptome analysis showed gene enrichment of the Nodal signaling pathway in undifferentiated cells compared to differentiated cells (Brandenberger et al., 2004). Brivanlou and colleagues demonstrated that SMAD2/3 signaling decreased, while SMAD1/5/8 signaling increased during differentiation (James et al., 2005). Importantly, withdrawal of the MEF-conditioned medium that was necessary to sustain pluripotency, led to decrease in SMAD2/3 signaling and subsequent downregulation of OCT4 and NANOG pluripotency genes. This finding suggested that MEFs help maintain cells in a pluripotent state by secreting ligands that activate SMAD2/3 signaling. Indeed, subsequent studies showed that in absence of a feeder layer, Activin A could maintain human ES cell pluripotency (Beattie et al., 2005). In contrast, small molecule inhibition of the ALK receptors that bind Activin/Nodal/TGF-β promoted differentiation into neuroectoderm (Smith et al., 2008).

There have been several mechanistic insights into how SMAD2/3 signaling regulates human ES cell pluripotency. Chromatin immunoprecipitation (ChIP)-seq experiments showed

that SMAD2/3 binds to proximal promoter of *NANOG* (Xu et al., 2008). Mutation of SMAD2/3 binding elements in the *NANOG* promoter significantly reduced *NANOG* expression and it was no longer responsive to TGF-β signaling. Furthermore, overexpression of *NANOG* suppressed neuroectoderm differentiation (Vallier et al., 2009). Therefore, Activin/Nodal/TGF-β ligands—secreted by MEFs or supplemented into chemically defined media—help maintain human ES cells in a pluripotent state by upregulating *NANOG* expression via SMAD2/3 signaling, thus inhibiting differentiation.

This role for TGF-β family members in maintaining pluripotency was unexpected since they have well defined roles in cell fate specification during development (Wu and Hill, 2009). Indeed, Activin A was also found to promote differentiation of human ES cells into definitive endoderm when PI3K signaling was suppressed (McLean et al., 2007). The mechanism behind this apparent dual function of the SMAD2/3 pathway in influencing the cell fate of human ES cells was elucidated by Dalton and colleagues (Singh et al., 2012). They demonstrated that depending on the level of their activation, SMAD2/3 induce the expression of different sets of genes. Under self-renewal conditions PI3K signaling limits SMAD2/3 activation to a level compatible with pluripotency. Upon inhibition of PI3K signaling, SMAD2/3 phosphorylation increases which enables the proteins to activate genes involved in differentiation.

As covered above, the SMAD2/3 pathway is an important regulator of pluripotency in hPS cells and was the first of several to be implicated and characterized. Its ability to both promote self-renewal and direct differentiation highlights the complexity of cell signaling and the importance of interplay between signaling pathways.

1.3.2 FGF-induced signaling

Alongside the SMAD2/3 signaling pathway, fibroblast growth factor (FGF) signaling was also identified as an important regulator of human ES cell pluripotency. The understanding of the key contributions of these two pathways toward self-renewal paved the way for the

development of chemically-defined culture conditions for human ES cell propagation. FGF ligands and their receptor tyrosine kinases control many processes during vertebrate development (Lanner and Rossant, 2010). Signaling is initiated when an FGF ligand binds to an FGF receptor, resulting in autophosphorylation of the tyrosine resides in the intracellular domain of the receptor. The signal is further propagated in a cascade that leads to phosphorylation and activation of PI3K-AKT and MAPK/ERK pathways (Figure 1-1). These critical cell pathways control cell proliferation, differentiation, and survival.

Transcriptome analysis first identified the enrichment of the FGF pathway genes in human ES cells (Brandenberger et al., 2004). This finding supported earlier observations that human ES cells could be maintained on MEFs in serum-free conditions when supplemented with exogenous FGF2 (Amit et al., 2000). The identification of FGF2 combined with the characterization of TGF-β signaling involvement enabled the development of defined culture conditions for maintaining human ES cells. The successful formulation of the medium was based on DMEM/F12 supplemented with serum albumin, insulin, transferrin, and the key growth factors FGF2 and TGF-β1 (Ludwig et al., 2006). This medium, now referred to as mTeSR1, together with defined substrates continues to be widely used for propagation of human ES cells. The medium was later refined into a simplified, serum albumin-free formulation, resulting in a fully chemically-defined medium referred to as E8 (Chen et al., 2011). It nonetheless contained the same vital growth factors. Therefore, both FGF and TGF-β signaling are necessary to sustain human pluripotency and suppression of either pathway induces differentiation (Vallier et al., 2005). Only FGF2 supplementation was found to be necessary under MEF conditions because FGF2 signaling upregulates expression of TGF-β growth factors in MEFs (Greber et al., 2007).

FGF and TGF-β signaling cooperate to regulate human ES cell self-renewal, although the mechanism underlying the contribution of the FGF pathway is not fully understood. Small

molecule inhibition of MAPK/ERK signaling leads to differentiation, while inhibition of PI3K-AKT signaling results in loss of proliferation and cell survival (Li et al., 2007). FGF signaling, however, is also involved during differentiation to mesoderm and neural lineages (Stavridis et al., 2007; Yu et al., 2011). Therefore, the role of FGF signaling is likely context dependent. In summary, FGF signaling is a key contributor to the self-renewal of hPS cells, and illustrates the importance of cooperation between signaling pathways in influencing cell fate decisions.

1.3.4 BMP-induced signaling

Unlike the SMAD2/3 pathway, the bone morphogenetic protein (BMP) ligands of the SMAD1/5/8 branch of the TGF-β superfamily solely drive differentiation of hPS cells. BMP4 was first demonstrated to induce differentiation of human ES cells into extraembryonic lineages such as trophoblast (Xu et al., 2002). Several groups have developed BMP4- based culture conditions for producing human trophoblast cell lines, which would provide a unique tool for studying the development of human extraembryonic tissues such as the placenta (Amita et al., 2013; Li et al., 2013). However, since human ES cells are isolated from the ICM it is thought that the cells should not carry the potential for giving rise to extraembryonic lineages. Indeed, recent criteria for defining true human trophoblast suggest that the human ES cell-derived trophoblast cells do not fully meet those standards (Lee et al., 2016).

A less controversial role for BMP signaling is in inducing mesoderm differentiation of hPS cells. Short-term stimulation with BMP4 upregulates mesodermal genes such as *Brachyury/T* and *MIXL1*, with the resulting progenitor cells capable of further differentiating into cardiac and hematopoietic linages (Zhang et al., 2008). A partial mechanism underlying BMP-mediated mesoderm induction was characterized by Richter, et al. (2014). BMP4 treatment upregulated the expression of *SLUG*, with phosphorylated SMAD1/5/8 bound to its promoter. SLUG is an epithelial-mesenchymal transition-associated transcription factor; consequently, its upregulation disrupted cell interactions resulting in migration and differentiation. Depletion of

SLUG during BMP-induction blocked those changes. Thus, BMP signaling instructs hPS cells to differentiate, particularly toward mesodermal lineages. The signaling mechanism has been partially characterized, though work remains to be done. Additionally, BMP signaling intersects with other pathways such as FGF and Wnt, the latter of which is covered below in section 1.3.5.

1.3.5 Wnt-induced signaling

In addition to TGF-β, FGF, and BMP signaling, the Wnt pathway is the other key soluble factor-based signaling cascade that influences hPS cell fate. As discussed below, the role of Wnt signaling in hPS cells is complex and appears to contribute to both self-renewal and differentiation. The Wnt pathway, the name of which is a contraction of the Drosophila Wingless (Wg) gene and the murine ortholog Int, is implicated in many developmental processes (Niehrs, 2012). Wnt ligands are cysteine-rich proteins that couple to Frizzled receptors in tandem with other co-receptors. The Wnt pathway is generally classified into two branches: canonical (β-catenin-dependent) and noncanonical (β-catenin-independent). The canonical pathway is the best characterized and is initiated by the binding of Wnt ligand to Frizzled and co-receptors LRP5 or LRP6. The ensuing signaling cascade leads to the inhibition of the kinase GSK3, which normally phosphorylates the transcriptional coactivator β-catenin thereby targeting it for proteasomal degradation. Thus, activation by Wnt ligand stabilizes β-catenin, enabling it to enter the nucleus and regulate transcription of target genes (Figure 1-1).

Several studies have shown that Wnt signaling contributes to maintenance of the pluripotent state in hPS cells. Transcriptomic data in undifferentiated cells showed expression of many Wnt pathway genes, however Wnt ligands were not expressed (Brandenberger et al., 2004). In another study, small molecule inhibition of GSK3 (thus mimicking Wnt pathway activation) could maintain self-renewal and pluripotency gene expression in human ES cells cultured under feeder-free conditions (Sato et al., 2004). Withdrawal of the inhibitor led to

differentiation. Thus, Wnt signaling, at least through GSK3 inhibition, can contribute to hPS cell self-renewal.

Wnt signaling, however, appears to play a greater role in driving differentiation. In fact, a study using a β-catenin human ES cell reporter line found that β-catenin signaling is repressed in undifferentiated cells and that its activation induces mesoderm differentiation (Davidson et al., 2012). One explanation for this apparent discrepancy comes from another study that demonstrated that β-catenin possess opposite dual functions: Cytoplasmic β-catenin can promote self-renewal, whereas it induces differentiation when it translocates into the nucleus (Kim et al., 2013).

A notable aspect of Wnt signaling in hPS cells that has recently come to light, is the important role of endogenous signaling. Nusse and colleagues used a Wnt reporter line to show that human ES cells are heterogeneous for endogenous Wnt signaling activity (Blauwkamp et al., 2012). They sorted the cells into Wnt-high and Wnt-low populations and observed that the two populations exhibited different propensities for differentiation. The Wnt-high cells differentiated preferentially toward mesoderm/endoderm whereas the Wnt-low cells primarily differentiated toward neuroectoderm. Another study found that endogenous Wnt signaling mediated mesoderm induction during BMP4 treatment (Kurek et al., 2015). Cells that had high endogenous Wnt signaling differentiated to mesoderm upon BMP4 addition, whereas cells with absent endogenous Wnt signaling differentiated toward trophoblast. Therefore, endogenous Wnt signaling is an important contributor to hPS cell fate decisions. In summary, Wnt signaling is a key pathway in the differentiation of hPS cells toward all three primary germ layers, and exemplifies the importance of endogenous signaling in influencing cell fate. The Wnt pathway

together with Activin/Nodal/TGF-β, FGF, and BMP signaling illustrate how soluble factors direct hPS cell fate decisions.

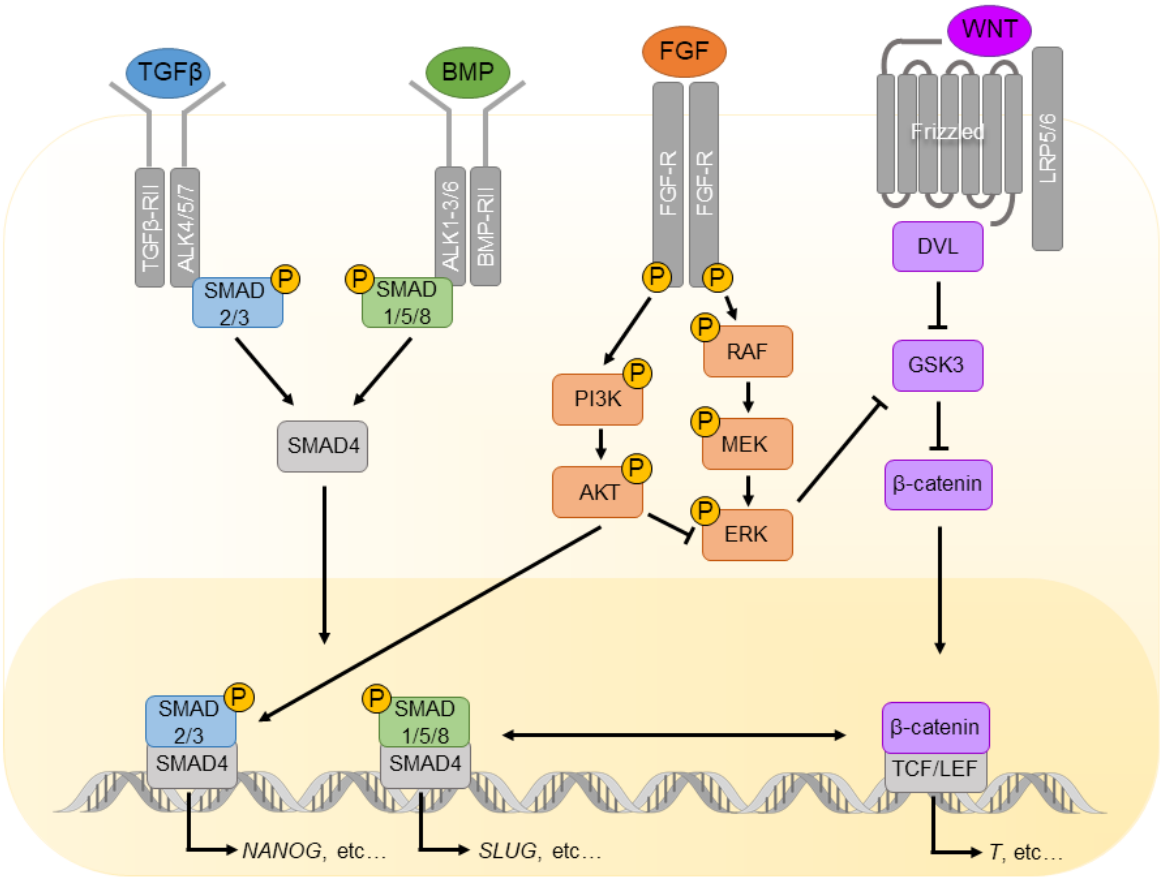

Figure 1-1. The main soluble factor signaling pathways that influence hPS cell fate decisions are Activin/Nodal/TGF-β (TGFβ), BMP, FGF, and Wnt. Through intricate interactions with each other, these pathways induce the transcription of genes that promote either self-renewal (e.g., *NANOG* expression) or differentiation (e.g., *SLUG, T* expression), depending on the context.

1.4 Insoluble signals that instruct human pluripotent stem cells

1.4.1 Cell-cell interactions between pluripotent cells

In addition to signals initiated by soluble factors (discussed in section 1.3), hPS cells receive insoluble cues that also influence their cell fate. The characterization of the roles of insoluble signals has contributed greatly to our ability to control the fate of hPS cells. One such key signal

is communicated via cell-cell interactions between individual hPS cells. When human ES cells were first derived, it was noted that they had very low cloning efficiency (Thomson et al., 1998). Upon complete dissociation, the cells underwent massive cell death, thus hindering experiments like genetic modification that require clonal derivation. Therefore, a crucial advance was the discovery that a small molecule inhibitor of Rho-associated kinase (ROCK) could prevent dissociation-induced apoptosis of human ES cells (Watanabe et al., 2007). Shortly after, a molecular mechanism underlying the ROCK-dependent cell death of human ES cells was characterized. Loss of E-cadherin-dependent cell-cell interactions was found to be responsible for the blebbing and apoptosis (Ohgushi et al., 2010). Apoptosis was induced by actomyosin hyperactivation, which was triggered by ROCK activation during the loss of intercellular contacts. ROCK inhibition suppressed phosphorylation of myosin light chain, thereby reducing actomyosin contraction (Chen et al., 2010). Additionally, E-cadherin has also been found to contribute to the self-renewal of hPS cells (Li et al., 2012). Thus, intercellular contacts in hPS cells help mediate cell survival and pluripotency.

Another notable influence of cell-cell interactions is illustrated by the ability of hPS cells to self-organize into three-dimensional tissues termed organoids. Generation of hPS-cell derived organoids was described in seminal work by Sasai and colleagues, initially using mouse (Eiraku et al., 2011) and later human ES cells (Nakano et al., 2012). They developed serum-free and growth factor-reduced culture conditions that enabled spontaneous aggregation of human ES cells. The aggregated cells recapitulated optic cup morphogenesis during eye development. An earlier version of this technique was used with human ES cells induced toward a neuroepithelial lineage, which went on to form polarized cortical tissues with distinct regions in a pattern mimicking in vivo brain development (Eiraku et al., 2008). In a further advance, a similar method was used to generate cerebral organoids (Lancaster et al., 2013). Notably, when using human iPS cells derived from microcephaly patients, the resulting organoids phenocopied microcephaly-associated pathologies.

In summary, cell-cell interactions between hPS cells can exert profound influence over cell fate. These contacts regulate cell survival, self-renewal, and differentiation. Taking advantage of the ability of hPS cells to self-organize has paved the way for the generation of organoids. These three-dimensional structures serve as unique tools for studying human organ development and disease.

1.4.2 Cell-cell interactions between pluripotent cells and other cells

Aside from intercellular contacts between individual hPS cells, signals exchanged between an hPS cell and another cell type can also influence cell fate decisions. Depending on the cell type and microenvironment, heterotypic co-culture can promote either self-renewal or differentiation. As covered earlier, the original derivation of human ES cells, as with mouse ES cells, was carried out on a MEF feeder layer (Thomson et al., 1998). In fact, in the absence of MEFs the cells spontaneously differentiated. In addition to secreting self-renewal factors like Activin A, the cells provided extracellular matrix support (covered in section 1.4.3). As culture conditions became better interrogated and characterized, MEFs were not needed to maintain pluripotency. However, in the conversion of primed to naïve human pluripotent stem cells, MEFs are generally still employed (Warrier et al., 2017). Therefore, the contribution of MEF co-culture to pluripotency remains to be fully understood.

Co-culture during differentiation of hPS cells can also provide invaluable signals. Neuronal maturation is greatly accelerated when the differentiation takes place in the presence of a glial co-culture (Johnson et al., 2007). Synaptic transmission was enhanced by the co-culture with astrocytes, and moreover, the improvement was cell-contact dependent: Addition of astrocyte-conditioned medium could not recapitulate the effect. In another study, the successful production of blood-brain barrier endothelial cells from hPS cells required co-culture with astrocytes (Lippmann et al., 2012). In an important advance, co-culture of hPS-cell derived endothelial and mesenchymal precursor cells enabled the generation of functional blood vessels

(Samuel et al., 2013). Finally, a landmark feat was the creation of the first vascularized organoid. Taniguchi and colleagues were able to generate human liver buds by leveraging the self-organization of hPS-cell derived hepatic cells in co-culture with human endothelial and mesenchymal stem cells (Takebe et al., 2013). In summary, cell-cell interactions with other cell types present unique signals to hPS cells, thus facilitating cell maturation and the generation of more complex tissues and organoids.

1.4.3 Cell interactions with extracellular matrix ligands

In addition to cell-cell interactions, another important source of insoluble cues is the extracellular matrix (ECM). The ECM is a hydrated network of proteins and polysaccharides to which cells are anchored in their microenvironment. Cells adhere to the ECM via transmembrane receptors known as integrins or through the anionic carbohydrate chains of proteoglycans termed glycosaminoglycans (GAGs). Leveraging the differential engagement of cell-surface molecules to ECM proteins and synthetic mimics offers additional control over hPS cell fate.

Substantial progress has been made in identifying and generating defined surfaces for hPS cell propagation. Initially, human ES cells were derived and cultured on MEF feeder layers that although were capable of sustaining pluripotency presented several challenges. The inherent complexity of this culture system hindered elucidation of relevant signaling cues and suffered from issues of batch-to-batch variability and immunogenicity. Thus, an important advance was the development of a feeder-free system for hPS cell culture. Instead of MEFs, human ES cells could be cultured on Matrigel or laminin, though originally still requiring MEF-condition medium (Xu et al., 2001). Matrigel is a gelatinous protein mixture secreted by mouse sarcoma cells and remains a popular substrate for hPS cell propagation as its easier and cheaper to produce than a purified ECM protein. Matrigel, however, though an improvement over MEF feeder layers, suffers from some of the same drawbacks in terms of variability and

immunogenicity. It is also highly complex—proteomic studies have revealed it contains as many as 1800 different proteins including ECM proteins and growth factors (Hughes et al., 2010). Due to these drawbacks, fully defined surfaces were developed. These include recombinant proteins such as vitronectin and laminin-511 (Braam et al., 2008; Rodin et al., 2010), recombinant protein fragments such as laminin E8 (Miyazaki et al., 2012), synthetic polymers such as PMEDSAH (Villa-Diaz et al., 2010), and peptide-presenting surfaces for engaging cell-surface integrins or GAGs (Klim et al., 2010; Melkoumian et al., 2010). These surfaces combined with chemically defined media (discussed in section 1.3.2) allowed for the propagation of hPS cells under a fully controlled culture system.

With defined culture conditions finally available, it's becoming possible to begin to understand the contribution of ECM adhesion to hPS cell fate decisions. For example, laminin was found to enhance neuronal differentiation (Ma et al., 2008), whereas vitronectin promoted generation of oligodendrocytes (Gil et al., 2009). Using an ECM protein array, vitronectin and fibronectin were identified as conducive to differentiation toward definitive endoderm (Brafman et al., 2013). A combination surface composed of laminin-521 and E-cadherin allowed for the derivation and clonal culture of hPS cells without the need for ROCK inhibitor (Rodin et al., 2014), suggesting that the engagement of both the laminin-specific integrin α6β1 and E-cadherin is required to prevent dissociation-induced apoptosis. Using peptides specific for either cell-surface integrins or GAGs, Wrighton, et al. (2014) dissected their individual contributions to hPS cell fate. Engagement of both integrins and GAGs supported ectoderm and neuronal differentiation, whereas selective engagement of GAGs enhanced differentiation to mesoderm and definitive endoderm. Integrin-activating surfaces were antagonistic to endoderm differentiation due to integrin-linked kinase-mediated stimulation of AKT signaling.

In summary, adhesion to the ECM is an additional insoluble cue that influences hPS cell fate. ECM proteins and synthetic surfaces signal via differential engagement of hPS cell-surface

molecules such as integrins and GAGs, and thereby provide a valuable strategy for controlling cell fate.

1.4.4 Cell interactions with extracellular matrix mechanics

Once cells adhere to the ECM they form complexes called focal adhesions, which connect the ECM to the intracellular actin cytoskeleton (Figure 1-2). The idea that through this coupling cells can sense and respond to changes in the mechanical properties of the ECM arose following an observation from over a century ago. In 1892, anatomist Julius Wolff discovered that bone can remodel following loading, suggesting that the cells in the bone tissue were transducing the mechanical cues and responding by altering their microenvironment (Wolff, 1986). In the 1980-90s, several lines of research emerged in support of this idea. Culture of chick fibroblasts on sheets of polydimethylsiloxane (PDMS) revealed wrinkles and deformations in the elastic substrate that were the result of traction forces exerted by the cells (Harris et al., 1980). To systemically test whether cells can probe and respond to changes in the mechanical properties, Pelham and Wang (1997) developed tunable polyacrylamide-based hydrogels. Hydrogels are water-swollen synthetic polymers that exhibit tissue-like properties and are biocompatible (Murphy et al., 2014). Their elasticity, as measured by the Young's modulus, could be easily tuned during synthesis by controlling the amount of cross-linking reagent (Pelham and Wang, 1997). Rat epithelial and fibroblastic cells introduced onto the hydrogels responded in a substrate elasticity-dependent manner: Cells on rigid substrates showed increased spreading and reduced motility compared to those on soft substrates. Together, these results demonstrated that cells sense and respond to changes in substrate elasticity.

Since terminally differentiated cells were initially used to probe the effects of matrix mechanics, it was unknown if mechanical cues can influence cell fate until stem cells were examined. Thus, Discher and colleagues showed that human bone marrow-derived mesenchymal stem (hMS) cells differentiated toward different lineages depending on the

elasticity of the substrate they were on (Engler et al., 2006). This landmark discovery drove efforts to understand the underlying mechanical mechanisms. In seminal work, Piccolo and colleagues identified Yes-associated protein (YAP) and transcriptional coactivator with PDZ-binding motif (TAZ) as key transducers of mechanical cues in hMS cells (Dupont et al., 2011). These paralogous transcriptional coactivators changed their subcellular localization in response to changes in matrix elasticity, and their absence or presence in the nucleus dictated differentiation. These findings showed that substrate elasticity influences the cell fate of multipotent stem cells, but it remained unclear if pluripotent cells, which possess a much greater differential potential, were also sensitive to mechanical cues.

Examining the effects of substrate elasticity on hMS cells laid the groundwork for investigating the role of mechanical cues on pluripotent stem cell fate. Soft substrates were shown to enable the self-renewal of mouse ES cells in the absence of LIF supplementation, which is normally required on stiff substrates (Chowdhury et al., 2010). Consistent with the differences between mouse and human pluripotency described in section 1.2.6, hPS cells required stiffer substrates to support self-renewal. Using chemically-defined polyacrylamide hydrogels, Musah, et al. (2012) showed that stiff substrates modified with a GAG-binding peptide enabled the self-renewal of hPS cells, while softer hydrogels did not support cell proliferation. Cells cultured on the stiff hydrogels, in contrast to those on the soft, displayed robust F-actin structures and retained nuclear localization of Yes-associated protein (YAP) and transcriptional coactivator with PDZ-binding motif (TAZ). These findings indicated that hPS cells, like hMS cells, can sense and respond to changes in matrix elasticity, and implicated YAP/TAZ in hPS cell mechanotransduction.

YAP/TAZ were originally identified to be part of the Hippo signaling pathway, which controls organ size in animals (Pan, 2007), but are now known to control a multitude of biological processes including proliferation, cancer, and tissue homeostasis (Piccolo et al.,

2014). Importantly, they've also been implicated in maintaining the pluripotency of hPS cells. Together with their transcriptional enhancer activator domain (TEAD) transcription factor partners, they form a regulatory complex with SMAD2/3 and OCT4, which modulates the expression of core pluripotency genes in hPS cells (Beyer et al., 2013). The nuclear localization of YAP/TAZ in hPS cells is promoted by a Rho-mediated survival pathway, which is driven by the Rho activator AKAP-Lbc (Ohgushi et al., 2015). Thus, on stiff substrates Rho/F-actin signaling induces nuclear localization of YAP/TAZ, which mediate expression of genes associated with hPS cell self-renewal (Figure 1-2).

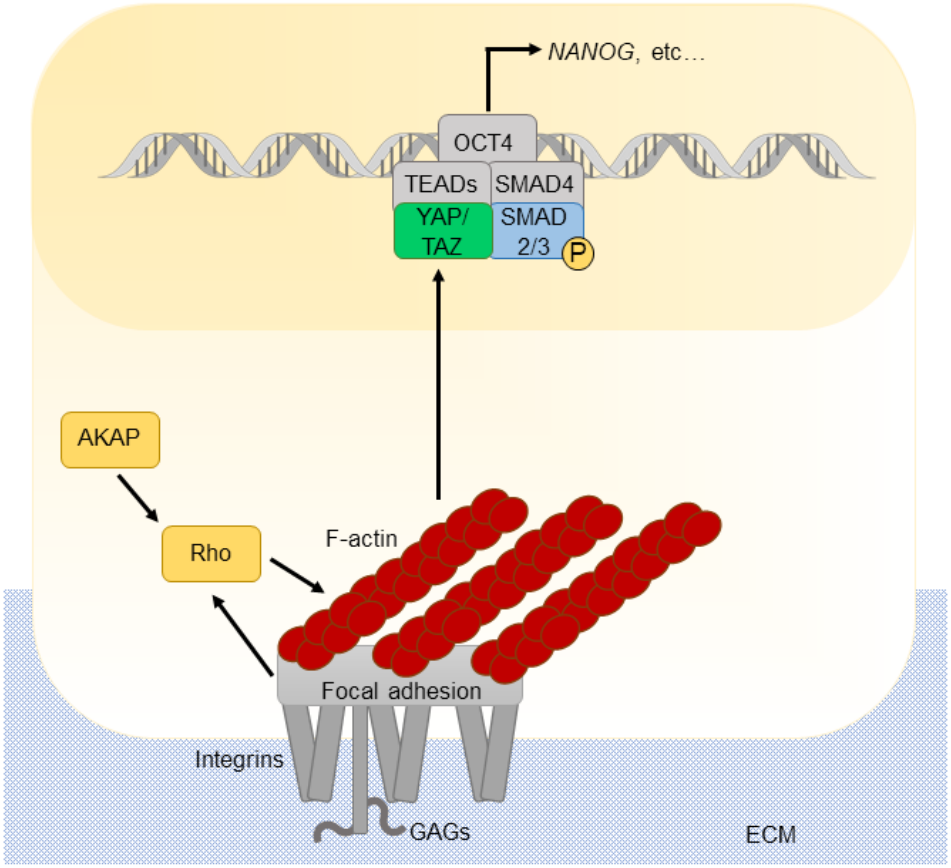

Figure 1-2. Matrix mechanics modulate YAP/TAZ activity in hPS cells. Integrins and the GAG chains of proteoglycans mediate adhesion to the ECM. Stiff substrates induce clustering of these cell adhesion molecules into focal adhesion complexes, which connect to the F-actin cytoskeleton. Focal adhesion signaling activates Rho GTPase whose activity is also sustained by

the Rho activator AKAP. Activated Rho GTPase promotes F-actin growth and stability, which in turn promotes YAP/TAZ nuclear localization. In the nucleus, YAP/TAZ join in with TEADs, SMADs, and OCT4 to form a regulatory complex that drives transcription of pluripotency genes.

Consistent with the observed YAP/TAZ nuclear exclusion, soft substrates promote hPS cell differentiation. We and others found that hydrogels with an elastic modulus similar to human brain tissue induced neuronal differentiation (Musah et al., 2014; Sun et al., 2014). The underlying mechanism was dependent on both F-actin and YAP, as inhibition of F-actin polymerization or depletion of YAP in hPS cells on stiff surfaces phenocopied the differentiation on the soft hydrogels (Musah et al., 2014). While soft surfaces promote neuronal differentiation, another study found that cardiomyocyte differentiation was enhanced by stiffer surfaces (Hazeltine et al., 2014). Together these studies demonstrate that altering matrix elasticity can profoundly influence hPS cell fate.

In summary, the ECM can influence hPS cell fate through either differential engagement of cell-surface molecules or through bulk mechanical properties. Together with cell-cell interactions, these insoluble cues along with soluble factors direct hPS cell fate decisions (Figure 1-3). Our increased understanding of the contributions of these individual cues, enabled by the development of chemically-defined culture systems, is facilitating more efficient and specific differentiation of hPS cells to desired cell types.

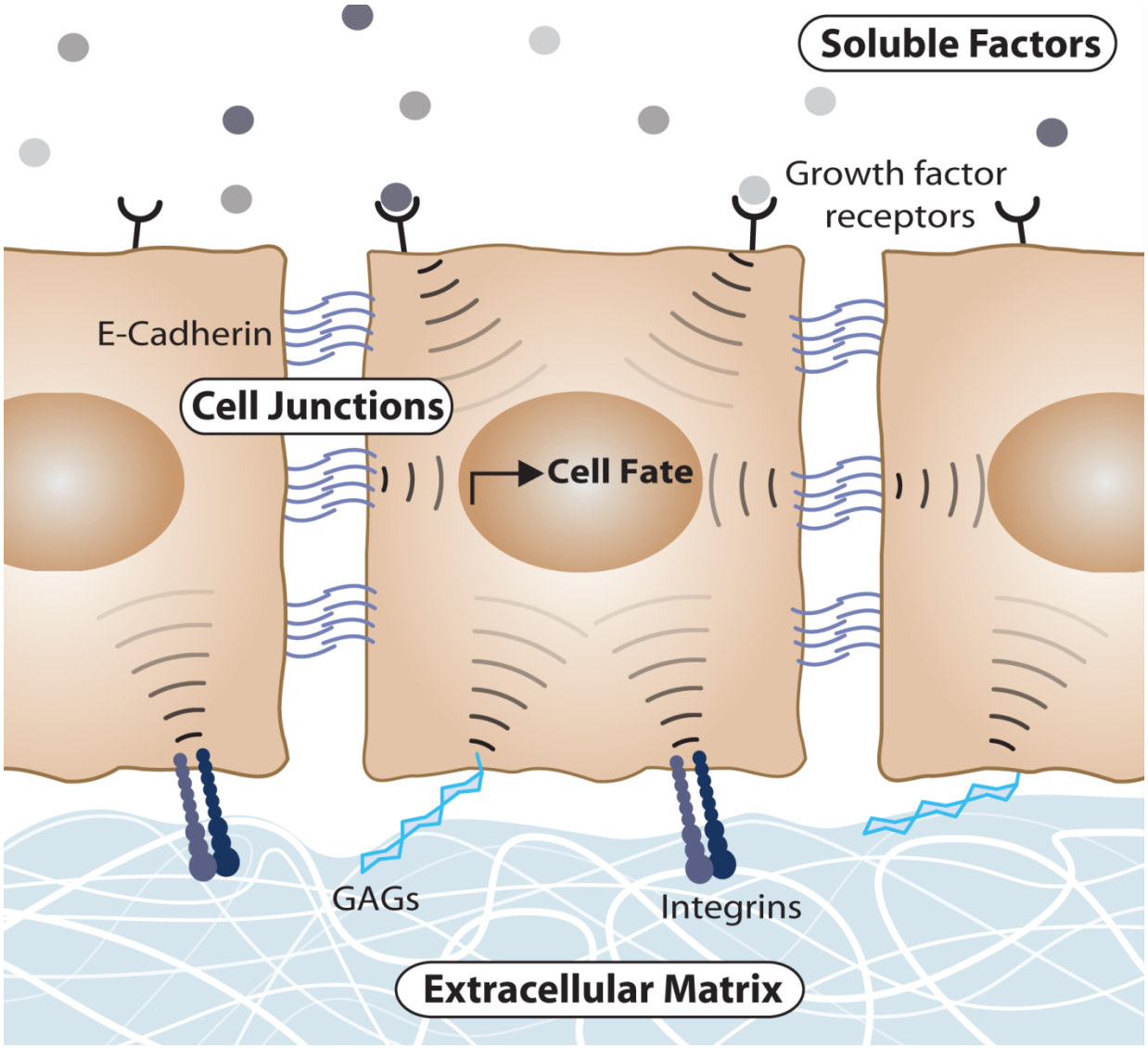

Figure 1-3. Soluble factor signal inputs converge with insoluble signal inputs in the hPS cell microenvironment. Insoluble cues include cell-cell interactions, extracellular matrix adhesion, and the mechanical properties of the matrix. Together these signals instruct hPS cells to either self-renew or differentiate.

1.5 References

Amit, M., Carpenter, M.K., Inokuma, M.S., Chiu, C.P., Harris, C.P., Waknitz, M.A., Itskovitz-Eldor, J., and Thomson, J.A. (2000). Clonally derived human embryonic stem cell lines maintain pluripotency and proliferative potential for prolonged periods of culture. Dev Biol *227*, 271-278.

Amita, M., Adachi, K., Alexenko, A.P., Sinha, S., Schust, D.J., Schulz, L.C., Roberts, R.M., and Ezashi, T. (2013). Complete and unidirectional conversion of human embryonic stem cells to trophoblast by BMP4. Proc Natl Acad Sci U S A *110*, E1212-1221.

Beattie, G.M., Lopez, A.D., Bucay, N., Hinton, A., Firpo, M.T., King, C.C., and Hayek, A. (2005). Activin A maintains pluripotency of human embryonic stem cells in the absence of feeder layers. Stem Cells *23*, 489-495.

Beyer, T.A., Weiss, A., Khomchuk, Y., Huang, K., Ogunjimi, A.A., Varelas, X., and Wrana, J.L. (2013). Switch enhancers interpret TGF-beta and Hippo signaling to control cell fate in human embryonic stem cells. Cell Rep *5*, 1611-1624.

Blakeley, P., Fogarty, N.M., del Valle, I., Wamaitha, S.E., Hu, T.X., Elder, K., Snell, P., Christie, L., Robson, P., and Niakan, K.K. (2015). Defining the three cell lineages of the human blastocyst by single-cell RNA-seq. Development *142*, 3151-3165.

Blauwkamp, T.A., Nigam, S., Ardehali, R., Weissman, I.L., and Nusse, R. (2012). Endogenous Wnt signalling in human embryonic stem cells generates an equilibrium of distinct lineage-specified progenitors. Nat Commun *3*, 1070.

Blelloch, R.H., Hochedlinger, K., Yamada, Y., Brennan, C., Kim, M., Mintz, B., Chin, L., and Jaenisch, R. (2004). Nuclear cloning of embryonal carcinoma cells. Proc Natl Acad Sci U S A *101*, 13985-13990.

Braam, S.R., Zeinstra, L., Litjens, S., Ward-van Oostwaard, D., van den Brink, S., van Laake, L., Lebrin, F., Kats, P., Hochstenbach, R., Passier, R.*, et al.* (2008). Recombinant vitronectin is a functionally defined substrate that supports human embryonic stem cell self-renewal via alphavbeta5 integrin. Stem Cells *26*, 2257-2265.

Brafman, D.A., Phung, C., Kumar, N., and Willert, K. (2013). Regulation of endodermal differentiation of human embryonic stem cells through integrin-ECM interactions. Cell Death Differ *20*, 369-381.

Brandenberger, R., Wei, H., Zhang, S., Lei, S., Murage, J., Fisk, G.J., Li, Y., Xu, C., Fang, R., Guegler, K.*, et al.* (2004). Transcriptome characterization elucidates signaling networks that control human ES cell growth and differentiation. Nat Biotechnol *22*, 707-716.

Brons, I.G., Smithers, L.E., Trotter, M.W., Rugg-Gunn, P., Sun, B., Chuva de Sousa Lopes, S.M., Howlett, S.K., Clarkson, A., Ahrlund-Richter, L., Pedersen, R.A.*, et al.* (2007). Derivation of pluripotent epiblast stem cells from mammalian embryos. Nature *448*, 191-195.

Chang, M.C. (1959). Fertilization of rabbit ova in vitro. Nature *184(Suppl 7)*, 466-467.

Chen, G., Gulbranson, D.R., Hou, Z., Bolin, J.M., Ruotti, V., Probasco, M.D., Smuga-Otto, K., Howden, S.E., Diol, N.R., Propson, N.E., *et al.* (2011). Chemically defined conditions for human iPSC derivation and culture. Nat Methods *8*, 424-429.

Chen, G., Hou, Z., Gulbranson, D.R., and Thomson, J.A. (2010). Actin-myosin contractility is responsible for the reduced viability of dissociated human embryonic stem cells. Cell Stem Cell *7*, 240-248.

Choi, J., Lee, S., Mallard, W., Clement, K., Tagliazucchi, G.M., Lim, H., Choi, I.Y., Ferrari, F., Tsankov, A.M., Pop, R., *et al.* (2015). A comparison of genetically matched cell lines reveals the equivalence of human iPSCs and ESCs. Nat Biotechnol *33*, 1173-1181.

Chowdhury, F., Li, Y., Poh, Y.C., Yokohama-Tamaki, T., Wang, N., and Tanaka, T.S. (2010). Soft substrates promote homogeneous self-renewal of embryonic stem cells via downregulating cell-matrix tractions. PLoS One *5*, e15655.

Cole, R.J., Edwards, R.G., and Paul, J. (1966). Cytodifferentiation and embryogenesis in cell colonies and tissue cultures derived from ova and blastocysts of the rabbit. Dev Biol *13*, 385-407.

Davidson, K.C., Adams, A.M., Goodson, J.M., McDonald, C.E., Potter, J.C., Berndt, J.D., Biechele, T.L., Taylor, R.J., and Moon, R.T. (2012). Wnt/beta-catenin signaling promotes differentiation, not self-renewal, of human embryonic stem cells and is repressed by Oct4. Proc Natl Acad Sci U S A *109*, 4485-4490.

Davis, R.L., Weintraub, H., and Lassar, A.B. (1987). Expression of a single transfected cDNA converts fibroblasts to myoblasts. Cell *51*, 987-1000.

Dupont, S., Morsut, L., Aragona, M., Enzo, E., Giulitti, S., Cordenonsi, M., Zanconato, F., Le Digabel, J., Forcato, M., Bicciato, S., *et al.* (2011). Role of YAP/TAZ in mechanotransduction. Nature *474*, 179-183.

Ebert, A.D., Yu, J., Rose, F.F., Jr., Mattis, V.B., Lorson, C.L., Thomson, J.A., and Svendsen, C.N. (2009). Induced pluripotent stem cells from a spinal muscular atrophy patient. Nature *457*, 277-280.

Eiraku, M., Takata, N., Ishibashi, H., Kawada, M., Sakakura, E., Okuda, S., Sekiguchi, K., Adachi, T., and Sasai, Y. (2011). Self-organizing optic-cup morphogenesis in three-dimensional culture. Nature *472*, 51-56.

Eiraku, M., Watanabe, K., Matsuo-Takasaki, M., Kawada, M., Yonemura, S., Matsumura, M., Wataya, T., Nishiyama, A., Muguruma, K., and Sasai, Y. (2008). Self-organized formation of polarized cortical tissues from ESCs and its active manipulation by extrinsic signals. Cell Stem Cell *3*, 519-532.

Engler, A.J., Sen, S., Sweeney, H.L., and Discher, D.E. (2006). Matrix elasticity directs stem cell lineage specification. Cell *126*, 677-689.

Evans, M.J., and Kaufman, M.H. (1981). Establishment in culture of pluripotential cells from mouse embryos. Nature *292*, 154-156.

Fenderson, B.A., Andrews, P.W., Nudelman, E., Clausen, H., and Hakomori, S. (1987). Glycolipid core structure switching from globo- to lacto- and ganglio-series during retinoic acid-

induced differentiation of TERA-2-derived human embryonal carcinoma cells. Dev Biol *122*, 21-34.

Fogarty, N.M.E., McCarthy, A., Snijders, K.E., Powell, B.E., Kubikova, N., Blakeley, P., Lea, R., Elder, K., Wamaitha, S.E., Kim, D.*, et al.* (2017). Genome editing reveals a role for OCT4 in human embryogenesis. Nature *550*, 67-73.

Gafni, O., Weinberger, L., Mansour, A.A., Manor, Y.S., Chomsky, E., Ben-Yosef, D., Kalma, Y., Viukov, S., Maza, I., Zviran, A.*, et al.* (2013). Derivation of novel human ground state naive pluripotent stem cells. Nature *504*, 282-286.

Gardner, D.K., Vella, P., Lane, M., Wagley, L., Schlenker, T., and Schoolcraft, W.B. (1998). Culture and transfer of human blastocysts increases implantation rates and reduces the need for multiple embryo transfers. Fertil Steril *69*, 84-88.

Gardner, R.L. (1968). Mouse chimeras obtained by the injection of cells into the blastocyst. Nature *220*, 596-597.

Gardner, R.L., and Rossant, J. (1979). Investigation of the fate of 4-5 day post-coitum mouse inner cell mass cells by blastocyst injection. J Embryol Exp Morphol *52*, 141-152.

Gil, J.E., Woo, D.H., Shim, J.H., Kim, S.E., You, H.J., Park, S.H., Paek, S.H., Kim, S.K., and Kim, J.H. (2009). Vitronectin promotes oligodendrocyte differentiation during neurogenesis of human embryonic stem cells. FEBS Lett *583*, 561-567.

Greber, B., Lehrach, H., and Adjaye, J. (2007). Fibroblast growth factor 2 modulates transforming growth factor beta signaling in mouse embryonic fibroblasts and human ESCs (hESCs) to support hESC self-renewal. Stem Cells *25*, 455-464.

Guo, G., Yang, J., Nichols, J., Hall, J.S., Eyres, I., Mansfield, W., and Smith, A. (2009). Klf4 reverts developmentally programmed restriction of ground state pluripotency. Development *136*, 1063-1069.

Gurdon, J.B. (1962). The developmental capacity of nuclei taken from intestinal epithelium cells of feeding tadpoles. J Embryol Exp Morphol *10*, 622-640.

Harris, A.K., Wild, P., and Stopak, D. (1980). Silicone rubber substrata: a new wrinkle in the study of cell locomotion. Science *208*, 177-179.

Hazeltine, L.B., Badur, M.G., Lian, X., Das, A., Han, W., and Palecek, S.P. (2014). Temporal impact of substrate mechanics on differentiation of human embryonic stem cells to cardiomyocytes. Acta Biomater *10*, 604-612.

Henderson, J.K., Draper, J.S., Baillie, H.S., Fishel, S., Thomson, J.A., Moore, H., and Andrews, P.W. (2002). Preimplantation human embryos and embryonic stem cells show comparable expression of stage-specific embryonic antigens. Stem Cells *20*, 329-337.

Hogan, B., Fellous, M., Avner, P., and Jacob, F. (1977). Isolation of a human teratoma cell line which expresses F9 antigen. Nature *270*, 515-518.

Hou, Z., Zhang, Y., Propson, N.E., Howden, S.E., Chu, L.F., Sontheimer, E.J., and Thomson, J.A. (2013). Efficient genome engineering in human pluripotent stem cells using Cas9 from Neisseria meningitidis. Proc Natl Acad Sci U S A *110*, 15644-15649.

Hughes, C.S., Postovit, L.M., and Lajoie, G.A. (2010). Matrigel: a complex protein mixture required for optimal growth of cell culture. Proteomics *10*, 1886-1890.

James, D., Levine, A.J., Besser, D., and Hemmati-Brivanlou, A. (2005). TGFbeta/activin/nodal signaling is necessary for the maintenance of pluripotency in human embryonic stem cells. Development *132*, 1273-1282.

Johannesson, B., Sagi, I., Gore, A., Paull, D., Yamada, M., Golan-Lev, T., Li, Z., LeDuc, C., Shen, Y., Stern, S.*, et al.* (2014). Comparable frequencies of coding mutations and loss of imprinting in human pluripotent cells derived by nuclear transfer and defined factors. Cell Stem Cell *15*, 634-642.

Johnson, M.A., Weick, J.P., Pearce, R.A., and Zhang, S.C. (2007). Functional neural development from human embryonic stem cells: accelerated synaptic activity via astrocyte coculture. J Neurosci *27*, 3069-3077.

Kannagi, R., Cochran, N.A., Ishigami, F., Hakomori, S., Andrews, P.W., Knowles, B.B., and Solter, D. (1983). Stage-specific embryonic antigens (SSEA-3 and -4) are epitopes of a unique globo-series ganglioside isolated from human teratocarcinoma cells. EMBO J *2*, 2355-2361.

Kelly, S.J. (1977). Studies of the developmental potential of 4- and 8-cell stage mouse blastomeres. J Exp Zool *200*, 365-376.

Kim, H., Wu, J., Ye, S., Tai, C.I., Zhou, X., Yan, H., Li, P., Pera, M., and Ying, Q.L. (2013). Modulation of beta-catenin function maintains mouse epiblast stem cell and human embryonic stem cell self-renewal. Nat Commun *4*, 2403.

Kleinsmith, L.J., and Pierce, G.B., Jr. (1964). Multipotentiality of Single Embryonal Carcinoma Cells. Cancer Res *24*, 1544-1551.

Klim, J.R., Li, L., Wrighton, P.J., Piekarczyk, M.S., and Kiessling, L.L. (2010). A defined glycosaminoglycan-binding substratum for human pluripotent stem cells. Nat Methods *7*, 989-994.

Kurek, D., Neagu, A., Tastemel, M., Tuysuz, N., Lehmann, J., van de Werken, H.J., Philipsen, S., van der Linden, R., Maas, A., van, I.W.F.*, et al.* (2015). Endogenous WNT signals mediate BMP-induced and spontaneous differentiation of epiblast stem cells and human embryonic stem cells. Stem Cell Reports *4*, 114-128.

Lancaster, M.A., Renner, M., Martin, C.A., Wenzel, D., Bicknell, L.S., Hurles, M.E., Homfray, T., Penninger, J.M., Jackson, A.P., and Knoblich, J.A. (2013). Cerebral organoids model human brain development and microcephaly. Nature *501*, 373-379.

Lanner, F., and Rossant, J. (2010). The role of FGF/Erk signaling in pluripotent cells. Development *137*, 3351-3360.

Lee, C.Q., Gardner, L., Turco, M., Zhao, N., Murray, M.J., Coleman, N., Rossant, J., Hemberger, M., and Moffett, A. (2016). What Is Trophoblast? A Combination of Criteria Define Human First-Trimester Trophoblast. Stem Cell Reports *6*, 257-272.

Li, J., Wang, G., Wang, C., Zhao, Y., Zhang, H., Tan, Z., Song, Z., Ding, M., and Deng, H. (2007). MEK/ERK signaling contributes to the maintenance of human embryonic stem cell self-renewal. Differentiation *75*, 299-307.

Li, L., Bennett, S.A., and Wang, L. (2012). Role of E-cadherin and other cell adhesion molecules in survival and differentiation of human pluripotent stem cells. Cell Adh Migr *6*, 59-70.

Li, Y., Moretto-Zita, M., Soncin, F., Wakeland, A., Wolfe, L., Leon-Garcia, S., Pandian, R., Pizzo, D., Cui, L., Nazor, K., *et al.* (2013). BMP4-directed trophoblast differentiation of human embryonic stem cells is mediated through a DeltaNp63+ cytotrophoblast stem cell state. Development *140*, 3965-3976.

Lippmann, E.S., Azarin, S.M., Kay, J.E., Nessler, R.A., Wilson, H.K., Al-Ahmad, A., Palecek, S.P., and Shusta, E.V. (2012). Derivation of blood-brain barrier endothelial cells from human pluripotent stem cells. Nat Biotechnol *30*, 783-791.

Loh, Y.H., Agarwal, S., Park, I.H., Urbach, A., Huo, H., Heffner, G.C., Kim, K., Miller, J.D., Ng, K., and Daley, G.Q. (2009). Generation of induced pluripotent stem cells from human blood. Blood *113*, 5476-5479.

Ludwig, T.E., Levenstein, M.E., Jones, J.M., Berggren, W.T., Mitchen, E.R., Frane, J.L., Crandall, L.J., Daigh, C.A., Conard, K.R., Piekarczyk, M.S., *et al.* (2006). Derivation of human embryonic stem cells in defined conditions. Nat Biotechnol *24*, 185-187.

Ma, W., Tavakoli, T., Derby, E., Serebryakova, Y., Rao, M.S., and Mattson, M.P. (2008). Cell-extracellular matrix interactions regulate neural differentiation of human embryonic stem cells. BMC Dev Biol *8*, 90.

Martin, G.R. (1981). Isolation of a pluripotent cell line from early mouse embryos cultured in medium conditioned by teratocarcinoma stem cells. Proceedings of the National Academy of Sciences *78*, 7634-7638.

Martin, G.R., and Evans, M.J. (1974). The morphology and growth of a pluripotent teratocarcinoma cell line and its derivatives in tissue culture. Cell *2*, 163-172.

Martin, G.R., and Evans, M.J. (1975). Differentiation of clonal lines of teratocarcinoma cells: formation of embryoid bodies in vitro. Proc Natl Acad Sci U S A *72*, 1441-1445.

Martin, M.J., Muotri, A., Gage, F., and Varki, A. (2005). Human embryonic stem cells express an immunogenic nonhuman sialic acid. Nat Med *11*, 228-232.

Mascetti, V.L., and Pedersen, R.A. (2016). Human-Mouse Chimerism Validates Human Stem Cell Pluripotency. Cell Stem Cell *18*, 67-72.

McLean, A.B., D'Amour, K.A., Jones, K.L., Krishnamoorthy, M., Kulik, M.J., Reynolds, D.M., Sheppard, A.M., Liu, H., Xu, Y., Baetge, E.E., *et al.* (2007). Activin a efficiently specifies definitive endoderm from human embryonic stem cells only when phosphatidylinositol 3-kinase signaling is suppressed. Stem Cells *25*, 29-38.

Melkoumian, Z., Weber, J.L., Weber, D.M., Fadeev, A.G., Zhou, Y., Dolley-Sonneville, P., Yang, J., Qiu, L., Priest, C.A., Shogbon, C., *et al.* (2010). Synthetic peptide-acrylate surfaces for long-term self-renewal and cardiomyocyte differentiation of human embryonic stem cells. Nat Biotechnol *28*, 606-610.

Miyazaki, T., Futaki, S., Suemori, H., Taniguchi, Y., Yamada, M., Kawasaki, M., Hayashi, M., Kumagai, H., Nakatsuji, N., Sekiguchi, K., *et al.* (2012). Laminin E8 fragments support efficient adhesion and expansion of dissociated human pluripotent stem cells. Nat Commun *3*, 1236.

Murphy, W.L., McDevitt, T.C., and Engler, A.J. (2014). Materials as stem cell regulators. Nat Mater *13*, 547-557.

Musah, S., Morin, S.A., Wrighton, P.J., Zwick, D.B., Jin, S., and Kiessling, L.L. (2012). Glycosaminoglycan-binding hydrogels enable mechanical control of human pluripotent stem cell self-renewal. ACS Nano *6*, 10168-10177.

Musah, S., Wrighton, P.J., Zaltsman, Y., Zhong, X., Zorn, S., Parlato, M.B., Hsiao, C., Palecek, S.P., Chang, Q., Murphy, W.L., *et al.* (2014). Substratum-induced differentiation of human pluripotent stem cells reveals the coactivator YAP is a potent regulator of neuronal specification. Proc Natl Acad Sci U S A *111*, 13805-13810.

Nagy, A., Gocza, E., Diaz, E.M., Prideaux, V.R., Ivanyi, E., Markkula, M., and Rossant, J. (1990). Embryonic stem cells alone are able to support fetal development in the mouse. Development *110*, 815-821.

Nakano, T., Ando, S., Takata, N., Kawada, M., Muguruma, K., Sekiguchi, K., Saito, K., Yonemura, S., Eiraku, M., and Sasai, Y. (2012). Self-formation of optic cups and storable stratified neural retina from human ESCs. Cell Stem Cell *10*, 771-785.

Nichols, J., and Smith, A. (2009). Naive and primed pluripotent states. Cell Stem Cell *4*, 487-492.

Niehrs, C. (2012). The complex world of WNT receptor signalling. Nat Rev Mol Cell Biol *13*, 767-779.

Ohgushi, M., Matsumura, M., Eiraku, M., Murakami, K., Aramaki, T., Nishiyama, A., Muguruma, K., Nakano, T., Suga, H., Ueno, M., *et al.* (2010). Molecular pathway and cell state responsible for dissociation-induced apoptosis in human pluripotent stem cells. Cell Stem Cell *7*, 225-239.

Ohgushi, M., Minaguchi, M., and Sasai, Y. (2015). Rho-Signaling-Directed YAP/TAZ Activity Underlies the Long-Term Survival and Expansion of Human Embryonic Stem Cells. Cell Stem Cell *17*, 448-461.

Pan, D. (2007). Hippo signaling in organ size control. Genes Dev *21*, 886-897.

Papaioannou, V.E., McBurney, M.W., Gardner, R.L., and Evans, M.J. (1975). Fate of teratocarcinoma cells injected into early mouse embryos. Nature *258*, 70-73.

Pelham, R.J., Jr., and Wang, Y. (1997). Cell locomotion and focal adhesions are regulated by substrate flexibility. Proc Natl Acad Sci U S A *94*, 13661-13665.

Piccolo, S., Dupont, S., and Cordenonsi, M. (2014). The biology of YAP/TAZ: hippo signaling and beyond. Physiol Rev *94*, 1287-1312.

Richter, A., Valdimarsdottir, L., Hrafnkelsdottir, H.E., Runarsson, J.F., Omarsdottir, A.R., Ward-van Oostwaard, D., Mummery, C., and Valdimarsdottir, G. (2014). BMP4 promotes EMT and mesodermal commitment in human embryonic stem cells via SLUG and MSX2. Stem Cells *32*, 636-648.

Rodin, S., Antonsson, L., Niaudet, C., Simonson, O.E., Salmela, E., Hansson, E.M., Domogatskaya, A., Xiao, Z., Damdimopoulou, P., Sheikhi, M.*, et al.* (2014). Clonal culturing of human embryonic stem cells on laminin-521/E-cadherin matrix in defined and xeno-free environment. Nat Commun *5*, 3195.

Rodin, S., Domogatskaya, A., Strom, S., Hansson, E.M., Chien, K.R., Inzunza, J., Hovatta, O., and Tryggvason, K. (2010). Long-term self-renewal of human pluripotent stem cells on human recombinant laminin-511. Nat Biotechnol *28*, 611-615.

Rossant, J., and McBurney, M.W. (1982). The developmental potential of a euploid male teratocarcinoma cell line after blastocyst injection. J Embryol Exp Morphol *70*, 99-112.

Samuel, R., Daheron, L., Liao, S., Vardam, T., Kamoun, W.S., Batista, A., Buecker, C., Schafer, R., Han, X., Au, P.*, et al.* (2013). Generation of functionally competent and durable engineered blood vessels from human induced pluripotent stem cells. Proc Natl Acad Sci U S A *110*, 12774-12779.

Sato, N., Meijer, L., Skaltsounis, L., Greengard, P., and Brivanlou, A.H. (2004). Maintenance of pluripotency in human and mouse embryonic stem cells through activation of Wnt signaling by a pharmacological GSK-3-specific inhibitor. Nat Med *10*, 55-63.

Sato, N., Sanjuan, I.M., Heke, M., Uchida, M., Naef, F., and Brivanlou, A.H. (2003). Molecular signature of human embryonic stem cells and its comparison with the mouse. Dev Biol *260*, 404-413.

Singh, A.M., Reynolds, D., Cliff, T., Ohtsuka, S., Mattheyses, A.L., Sun, Y., Menendez, L., Kulik, M., and Dalton, S. (2012). Signaling network crosstalk in human pluripotent cells: a Smad2/3-regulated switch that controls the balance between self-renewal and differentiation. Cell Stem Cell *10*, 312-326.

Smith, J.R., Vallier, L., Lupo, G., Alexander, M., Harris, W.A., and Pedersen, R.A. (2008). Inhibition of Activin/Nodal signaling promotes specification of human embryonic stem cells into neuroectoderm. Dev Biol *313*, 107-117.

Solter, D., and Knowles, B.B. (1975). Immunosurgery of mouse blastocyst. Proc Natl Acad Sci U S A *72*, 5099-5102.

Solter, D., and Knowles, B.B. (1978). Monoclonal antibody defining a stage-specific mouse embryonic antigen (SSEA-1). Proc Natl Acad Sci U S A *75*, 5565-5569.

Stavridis, M.P., Lunn, J.S., Collins, B.J., and Storey, K.G. (2007). A discrete period of FGF-induced Erk1/2 signalling is required for vertebrate neural specification. Development *134*, 2889-2894.

Steptoe, P.C., and Edwards, R.G. (1978). Birth after the reimplantation of a human embryo. Lancet *2*, 366.

Steptoe, P.C., Edwards, R.G., and Purdy, J.M. (1971). Human blastocysts grown in culture. Nature *229*, 132-133.

Stevens, L.C., and Little, C.C. (1954). Spontaneous Testicular Teratomas in an Inbred Strain of Mice. Proc Natl Acad Sci U S A *40*, 1080-1087.

Sun, Y., Yong, K.M., Villa-Diaz, L.G., Zhang, X., Chen, W., Philson, R., Weng, S., Xu, H., Krebsbach, P.H., and Fu, J. (2014). Hippo/YAP-mediated rigidity-dependent motor neuron differentiation of human pluripotent stem cells. Nat Mater *13*, 599-604.

Tabar, V., and Studer, L. (2014). Pluripotent stem cells in regenerative medicine: challenges and recent progress. Nat Rev Genet *15*, 82-92.

Tachibana, M., Amato, P., Sparman, M., Gutierrez, N.M., Tippner-Hedges, R., Ma, H., Kang, E., Fulati, A., Lee, H.S., Sritanaudomchai, H.*, et al.* (2013). Human embryonic stem cells derived by somatic cell nuclear transfer. Cell *153*, 1228-1238.

Takahashi, K., Tanabe, K., Ohnuki, M., Narita, M., Ichisaka, T., Tomoda, K., and Yamanaka, S. (2007). Induction of pluripotent stem cells from adult human fibroblasts by defined factors. Cell *131*, 861-872.

Takahashi, K., and Yamanaka, S. (2006). Induction of pluripotent stem cells from mouse embryonic and adult fibroblast cultures by defined factors. Cell *126*, 663-676.

Takashima, Y., Guo, G., Loos, R., Nichols, J., Ficz, G., Krueger, F., Oxley, D., Santos, F., Clarke, J., Mansfield, W.*, et al.* (2014). Resetting transcription factor control circuitry toward ground-state pluripotency in human. Cell *158*, 1254-1269.

Takebe, T., Sekine, K., Enomura, M., Koike, H., Kimura, M., Ogaeri, T., Zhang, R.R., Ueno, Y., Zheng, Y.W., Koike, N.*, et al.* (2013). Vascularized and functional human liver from an iPSC-derived organ bud transplant. Nature *499*, 481-484.

Tarkowski, A.K. (1959). Experiments on the Development of Isolated Blastomeres of Mouse Eggs. Nature *184*, 1286-1287.

Tarkowski, A.K., Witkowska, A., and Opas, J. (1977). Development of cytochalasin in B-induced tetraploid and diploid/tetraploid mosaic mouse embryos. J Embryol Exp Morphol *41*, 47-64.

Tesar, P.J., Chenoweth, J.G., Brook, F.A., Davies, T.J., Evans, E.P., Mack, D.L., Gardner, R.L., and McKay, R.D. (2007). New cell lines from mouse epiblast share defining features with human embryonic stem cells. Nature *448*, 196-199.

Theunissen, T.W., Powell, B.E., Wang, H., Mitalipova, M., Faddah, D.A., Reddy, J., Fan, Z.P., Maetzel, D., Ganz, K., Shi, L.*, et al.* (2014). Systematic identification of culture conditions for induction and maintenance of naive human pluripotency. Cell Stem Cell *15*, 471-487.

Thomson, J.A., Itskovitz-Eldor, J., Shapiro, S.S., Waknitz, M.A., Swiergiel, J.J., Marshall, V.S., and Jones, J.M. (1998). Embryonic Stem Cell Lines Derived from Human Blastocysts. Science *282*, 1145-1147.

Thomson, J.A., Kalishman, J., Golos, T.G., Durning, M., Harris, C.P., Becker, R.A., and Hearn, J.P. (1995). Isolation of a primate embryonic stem cell line. Proc Natl Acad Sci U S A *92*, 7844-7848.

Trounson, A., and DeWitt, N.D. (2016). Pluripotent stem cells progressing to the clinic. Nat Rev Mol Cell Biol *17*, 194-200.

Vallier, L., Alexander, M., and Pedersen, R.A. (2005). Activin/Nodal and FGF pathways cooperate to maintain pluripotency of human embryonic stem cells. J Cell Sci *118*, 4495-4509.

Vallier, L., Mendjan, S., Brown, S., Chng, Z., Teo, A., Smithers, L.E., Trotter, M.W., Cho, C.H., Martinez, A., Rugg-Gunn, P.*, et al.* (2009). Activin/Nodal signalling maintains pluripotency by controlling Nanog expression. Development *136*, 1339-1349.

Villa-Diaz, L.G., Nandivada, H., Ding, J., Nogueira-de-Souza, N.C., Krebsbach, P.H., O'Shea, K.S., Lahann, J., and Smith, G.D. (2010). Synthetic polymer coatings for long-term growth of human embryonic stem cells. Nat Biotechnol *28*, 581-583.

Waddington, C.H. (1957). The strategy of the genes; a discussion of some aspects of theoretical biology (London,: Allen & Unwin).

Wakayama, T., Perry, A.C., Zuccotti, M., Johnson, K.R., and Yanagimachi, R. (1998). Full-term development of mice from enucleated oocytes injected with cumulus cell nuclei. Nature *394*, 369-374.

Warrier, S., Van der Jeught, M., Duggal, G., Tilleman, L., Sutherland, E., Taelman, J., Popovic, M., Lierman, S., Chuva De Sousa Lopes, S., Van Soom, A.*, et al.* (2017). Direct comparison of distinct naive pluripotent states in human embryonic stem cells. Nat Commun *8*, 15055.

Watanabe, K., Ueno, M., Kamiya, D., Nishiyama, A., Matsumura, M., Wataya, T., Takahashi, J.B., Nishikawa, S., Nishikawa, S., Muguruma, K.*, et al.* (2007). A ROCK inhibitor permits survival of dissociated human embryonic stem cells. Nat Biotechnol *25*, 681-686.

Wilmut, I., Schnieke, A.E., McWhir, J., Kind, A.J., and Campbell, K.H. (1997). Viable offspring derived from fetal and adult mammalian cells. Nature *385*, 810-813.

Wolff, J. (1986). The law of bone remodelling (Berlin ; New York: Springer-Verlag).

Wrighton, P.J., Klim, J.R., Hernandez, B.A., Koonce, C.H., Kamp, T.J., and Kiessling, L.L. (2014). Signals from the surface modulate differentiation of human pluripotent stem cells through glycosaminoglycans and integrins. Proc Natl Acad Sci U S A *111*, 18126-18131.

Wu, M.Y., and Hill, C.S. (2009). Tgf-beta superfamily signaling in embryonic development and homeostasis. Dev Cell *16*, 329-343.

Xu, C., Inokuma, M.S., Denham, J., Golds, K., Kundu, P., Gold, J.D., and Carpenter, M.K. (2001). Feeder-free growth of undifferentiated human embryonic stem cells. Nat Biotechnol *19*, 971-974.

Xu, R.H., Chen, X., Li, D.S., Li, R., Addicks, G.C., Glennon, C., Zwaka, T.P., and Thomson, J.A. (2002). BMP4 initiates human embryonic stem cell differentiation to trophoblast. Nat Biotechnol *20*, 1261-1264.

Xu, R.H., Sampsell-Barron, T.L., Gu, F., Root, S., Peck, R.M., Pan, G., Yu, J., Antosiewicz-Bourget, J., Tian, S., Stewart, R.*, et al.* (2008). NANOG is a direct target of TGFbeta/activin-mediated SMAD signaling in human ESCs. Cell Stem Cell *3*, 196-206.

Yu, J., Hu, K., Smuga-Otto, K., Tian, S., Stewart, R., Slukvin, II, and Thomson, J.A. (2009). Human induced pluripotent stem cells free of vector and transgene sequences. Science *324*, 797-801.

Yu, J., Vodyanik, M.A., Smuga-Otto, K., Antosiewicz-Bourget, J., Frane, J.L., Tian, S., Nie, J., Jonsdottir, G.A., Ruotti, V., Stewart, R.*, et al.* (2007). Induced pluripotent stem cell lines derived from human somatic cells. Science *318*, 1917-1920.

Yu, P., Pan, G., Yu, J., and Thomson, J.A. (2011). FGF2 sustains NANOG and switches the outcome of BMP4-induced human embryonic stem cell differentiation. Cell Stem Cell *8*, 326-334.

Zhang, P., Li, J., Tan, Z., Wang, C., Liu, T., Chen, L., Yong, J., Jiang, W., Sun, X., Du, L.*, et al.* (2008). Short-term BMP-4 treatment initiates mesoderm induction in human embryonic stem cells. Blood *111*, 1933-1941.

Zhao, M.T., Chen, H., Liu, Q., Shao, N.Y., Sayed, N., Wo, H.T., Zhang, J.Z., Ong, S.G., Liu, C., Kim, Y.*, et al.* (2017). Molecular and functional resemblance of differentiated cells derived from isogenic human iPSCs and SCNT-derived ESCs. Proc Natl Acad Sci U S A.

Zhao, X.Y., Li, W., Lv, Z., Liu, L., Tong, M., Hai, T., Hao, J., Guo, C.L., Ma, Q.W., Wang, L.*, et al.* (2009). iPS cells produce viable mice through tetraploid complementation. Nature *461*, 86-90.

Chapter 2

Substrate-induced neuronal differentiation of human pluripotent stem cells

Portions of this work have been published in:

Musah, S., Wrighton, P.J., **Zaltsman, Y.,** Zhong, X., Zorn, S., Parlato, M.B., Hsiao, C., Palecek, S.P., Chang, Q., Murphy, W.L., et al. (2014). Substratum-induced differentiation of human pluripotent stem cells reveals the coactivator YAP is a potent regulator of neuronal specification. Proc Natl Acad Sci U S A *111*, 13805-13810.

2.1 Abstract

Physical stimuli can act in either a synergistic or antagonistic manner to regulate cell fate decisions, but it is less clear whether insoluble signals alone can direct human pluripotent stem (hPS) cell differentiation into specialized cell types. We previously reported that stiff materials promote nuclear localization of the YAP transcriptional coactivator and support long-term self-renewal of hPS cells. Here, we show that even in the presence of soluble pluripotency factors, compliant substrates inhibit the nuclear localization of YAP and promote highly efficient differentiation of hPS cells into post-mitotic neurons. The neurons derived from substrate induction alone express mature markers and possess action potentials. The hPS cell differentiation observed on compliant surfaces could be recapitulated on stiff surfaces by adding small molecule inhibitors of F-actin polymerization or by depleting YAP. These studies reveal that the matrix alone can mediate differentiation of hPS cells into a mature cell type, independent of soluble inductive factors. That mechanical cues can override soluble signals suggests that their contributions to early tissue development and lineage commitment are significant.

2.2 Introduction

Human pluripotent stem (hPS) cells, which include human embryonic (hES) and induced pluripotent stem cells, possess the remarkable capacity to self-renew indefinitely and differentiate into almost any specialized cell type (Takahashi et al., 2007; Thomson et al., 1998). They represent a potentially unlimited supply of cells for regenerative medicine, drug screening, and studies of human development. These applications require efficient and reproducible conditions to direct hPS cell differentiation into specialized cell types, including neuronal cells. To date, focus has been on identifying soluble factors, such as growth factors and small molecules, that can influence hPS cell differentiation. The ability of insoluble signals to promote hPS cell lineage specification remains less clear.

Studies in murine embryonic stem cells (Chowdhury et al., 2010a; Chowdhury et al., 2010b) and tissue-specific stem cells (Engler et al., 2006; Holst et al., 2010; Li et al., 2014; Mammoto and Ingber, 2010; Moore and Sheetz, 2011; Yang et al., 2014) indicate that the adhesive and mechanical properties of the substrate employed can influence cell fate decisions. For example, human mesenchymal stem (hMS) cells are sensitive to changes in substrate elasticity and respond by differentiating toward distinct cell lineages depending on the stiffness of the matrix (Engler et al., 2006). HMS cells, however, tend to exist in heterogeneous cell populations and lack a specific and unique cell characterization marker (Neirinckx et al., 2013). Their differentiation capacity is restricted to a few tissues that arise from the mesoderm lineage, such as bone, fat and cartilage. Indeed, there are questions about whether these cells undergo transdifferentiation to cell types such as neurons (Krabbe et al., 2005; Lu et al., 2004; Neirinckx et al., 2013). With the unique ability to differentiate into almost any cell type, hPS cells serve as an excellent model for understanding the roles of extracellular signals on lineage specification and tissue morphogenesis.

In examining the influence of substrate mechanics on hPS cell propagation, we found that stiff surfaces facilitate hPS cell expansion (Musah et al., 2012). Key to this activity is their ability to promote the nuclear localization of the paralogous transcriptional coactivators Yes-associated protein (YAP) and transcriptional coactivator with PDZ-binding domain (TAZ) (Dupont et al., 2011; Musah et al., 2012), which are critical for pluripotency (Lian et al., 2010; Musah et al., 2012). Alternatively, compliant matrices inhibit nuclear localization of YAP and are unable to support hPS cell self-renewal (Musah et al., 2012). YAP acts with TEAD transcription factors to drive cell cycle progression (Cao et al., 2008), and YAP depletion or inhibition of YAP-TEAD interactions can promote neuronal differentiation (Cao et al., 2008; Zhang et al., 2012). Fu and colleagues reported that PDMS micropost arrays that inhibit Hippo/YAP signaling can improve neuronal differentiation of hPS cells induced by soluble neurogenic factors (Sun et al., 2014). We postulated that the mechanical properties of the substrate alone would be powerful enough to poise cells for neuronal differentiation. Using synthetic hydrogels as a tunable platform (Gauvin et al., 2012), we tested this hypothesis by evaluating the differentiation of hPS cells on the surfaces of different stiffness. These investigations revealed that compliant hydrogels induce rapid and efficient differentiation of hPS cells into neurons that express mature neuronal markers and possess action potentials. The molecular mechanism underlying the substrate-induced differentiation is through modulation of the subcellular localization of YAP. Our results indicate that mechanical properties of the extracellular matrix can be a principle factor in directing the lineage specific differentiation of hPS cells.

2.3 Results and Discussion

2.3.1 Substrate-induced neuronal differentiation of hPS cells

Exploiting the chemoselective synthesis of peptide-bearing hydrogels, we previously found that stiff hydrogels (elastic modulus ~10 kPa) displaying the glycosaminoglycan (GAG) binding peptide CGKKQRFRHRNRKG derived from the vitronectin heparin-binding domain (VHBD) can support long-term self-renewal of hPS cells, but the corresponding compliant hydrogels (~0.7 kPa) do not (Musah et al., 2012). The inability of compliant hydrogels to support hPS cell expansion suggests they might facilitate hPS cell differentiation. To test this possibility, we cultured hES cells on compliant polyacrylamide (PA) hydrogels (~0.7 kPa) functionalized with the aforementioned VHBD peptide (Klim et al., 2010; Musah et al., 2012). For initial experiments, we employed a defined hPS cell culture medium used for hPS cell self-renewal, mTeSR (Ludwig et al., 2006) supplemented with Y27632, a small molecule inhibitor of Rho-associated protein kinase (ROCK)(Watanabe et al., 2007). The ROCK inhibitor was added to facilitate hPS cell survival. After approximately 14 days of culture on the compliant hydrogels, hES cells differentiated selectively. The cells' loss of expression of key pluripotency marker OCT4 was accompanied by their adoption of a cell morphology consistent with neurons and expression of neuronal marker TUJ1 (neuron-specific class III beta-tubulin) (Figure 2-1A, B). Given that the mTeSR culture medium is designed to promote pluripotency and lacks the soluble signaling factors used to induce neuronal differentiation, these observations were notable.

The effect of the compliant hydrogels prompted us to evaluate the efficiency of this differentiation protocol. We primed hES cells for differentiation to facilitate their adhesion to the compliant hydrogels and then cultured them with defined media. This media tested consisted of mTeSR or mTeSR lacking key soluble signaling components FGF2, TGFß, or

gamma-aminobutyric acid (GABA). We found that the cells exhibited neuronal morphology and stained positive for TUJ1 neuronal marker, irrespective of the medium composition (Figure 2-1*C*). The differentiation timeframe was conspicuous. The cells rapidly (within 5 to 10 days) adopted neuronal morphology and expressed TUJ1, and they did so more efficiently in defined media lacking the self-renewal factor FGF2. None of the media components were required to induce differentiation. The primed cells developed neuronal characteristics in defined medium depleted of all three soluble factors (FGF2, TGFß, and GABA) (referred to as "depleted medium"). Together, these results indicate that the appearance of neuronal traits by the hPS cells was not triggered by soluble inductive factors.

To determine whether the primed hES cells undergo selective differentiation on stiffer hydrogels, we tested PA hydrogels of varying elasticity (0.7, 3 and 10 kPa) and functionalized them with the VHBD peptide (Klim et al., 2010; Musah et al., 2012). Primed hES cells were cultured on the hydrogels in depleted medium. After 10 days, only the compliant hydrogel (0.7 kPa) promoted efficient and reproducible neuronal differentiation. Although the majority of cells on the stiff hydrogels differentiated (indicated by loss of OCT4 expression), only a small population (~ 5%) expressed the neuronal marker TUJ1 (Figure 2-1D, E). These results indicate that compliant hydrogels are robust substrates for inducing neuronal differentiation.

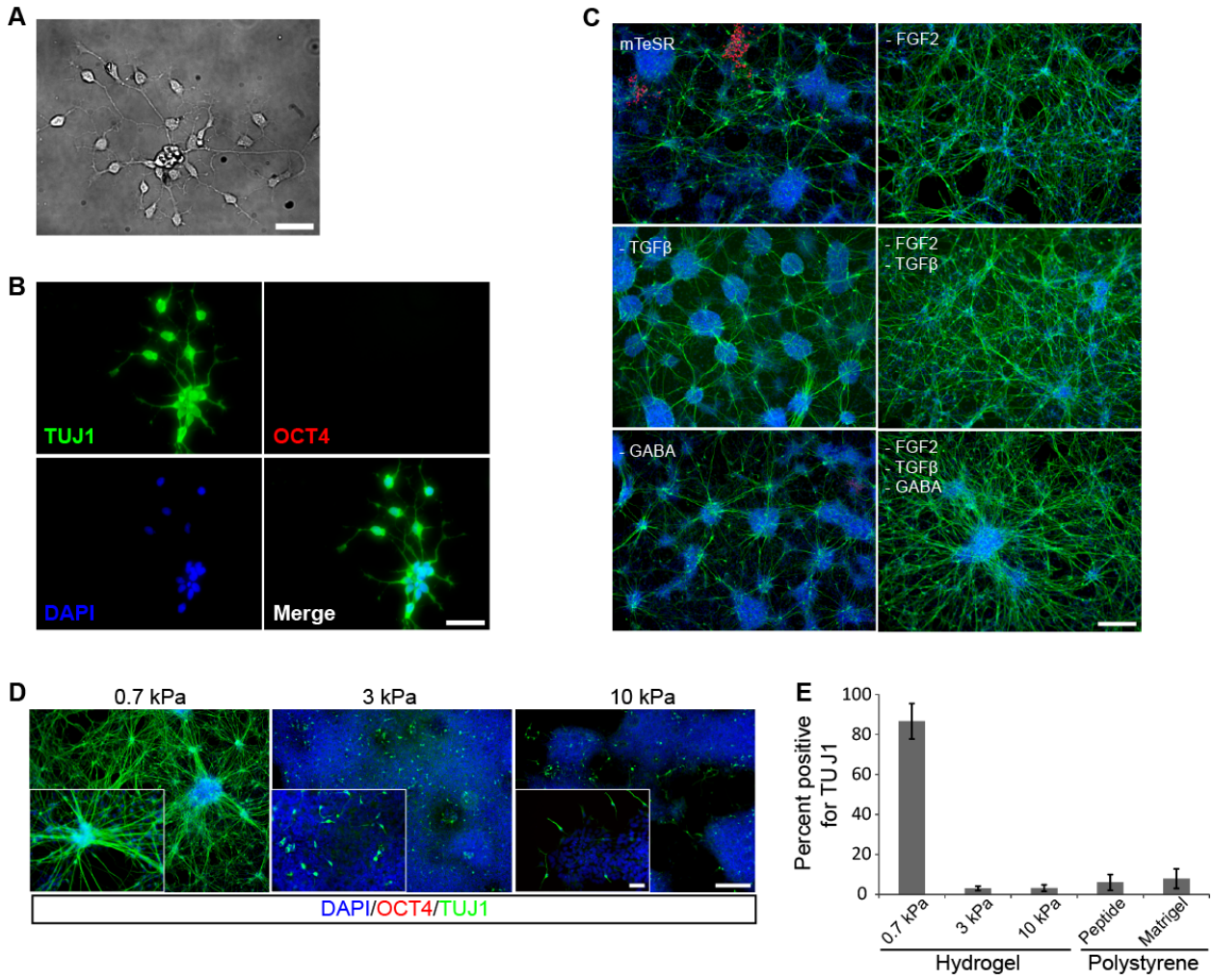

Figure 2-1: Neuronal differentiation of hES cells on compliant (0.7 kPa) PA hydrogels.

(A-B) Bright-field (A) and immunofluorescence (B) images of naive hES cells (SA02 line) cultured for 14 d on the hydrogels with defined mTeSR medium. Scale bars: 50 μm

(C) Primed hES cells (SA02 line) differentiated for 5 d on compliant hydrogels with defined mTeSR medium or mTeSR lacking the indicated soluble signaling factors. Cells were immunostained for TUJ1 (green) and OCT4 (red), and counterstained with DAPI (blue). Scale bar: 250 μm.

(D-E) H9 hES cells differentiated for 10 d on PA hydrogels that vary in elasticity. Cells were immunostained for the pluripotency marker OCT4 (red) and neuronal marker TUJ1 (green), and counterstained with DAPI (blue). (E) Quantification of neuronal induction efficiency (H9 cell

line) on hydrogels of varying elasticity, or on polystyrene functionalized with either the VHBD peptide or Matrigel. Error bars represent SD of the mean (n = 4).

2.3.2 Characterization of substrate-derived neurons

To evaluate the developmental status of the substrate-differentiated cells, we first examined their proliferative capacity, as neurons are post-mitotic. After 2 weeks of differentiation on compliant hydrogels, the majority of the resulting cells ceased proliferation (Figure 2-2A, B). Therefore, substrate-derived neurons are post-mitotic.

We analyzed the gene expression profile of the hydrogel-differentiated cells by assessing lineage identification gene markers specific for pluripotent stem cells, progenitor cells from all three embryonic germ layers (ectoderm, mesoderm, and endoderm), and terminally differentiated cells such as astrocytes, neurons, cardiomyocytes, and beta cells (see Table S2-1 for functional gene grouping). After 2 weeks of differentiation on the compliant hydrogels, pluripotency genes (*POU5F1*, *ZFP42*, *PODXL*, and *LEFTY1*) were significantly down-regulated (Figure 2-2C and Table S2-2). Additionally, expression levels were decreased for the genes encoding endoderm markers *KRT19* and *ITGB4*, and the mesoderm marker *T* (Brachyury). Ectoderm and neuroectoderm markers *ZIC1* and *NEUROG2* were highly upregulated, as were neuronal genes including *NEUROD1*, *DCX*, *HES5*, *FABP7* (Figure 2-2C Table S2-2). These results are consistent with the morphological and immunocytochemical findings that the compliant substrate facilitates neuronal differentiation of hPS cells.

Most of the hydrogel-derived neurons exhibit bipolar projections (Fig. 2*D*), a morphological feature of interneurons (Maxwell et al., 2007). To determine whether the differentiated cells express markers of glutamatergic (excitatory) or GABAergic (inhibitory) interneurons, we evaluated their gene expression profile and immunoreactivity. Immunocytochemistry analyses confirmed expression of the proteins vGAT (vesicular GABA transporter, encoded by *SLC32A1*)

and GAD67 (glutamate decarboxylase 67, encoded by *GAD1*) (Fig. 2*E* and Fig. S8). These results indicate that the compliant hydrogel can function without soluble inductive factors to rapidly and efficiently induce hPS cell differentiation into a specific neuronal subtype. Standard protocols for hES cell differentiation into GABAergic neurons involve multiple phases of treatment with soluble signaling factors and require a timeline of 45 days or longer (Liu and Zhang, 2011a). Using our defined substrate, hES cell differentiated into cells characteristic of GABAergic neurons within 2 weeks.

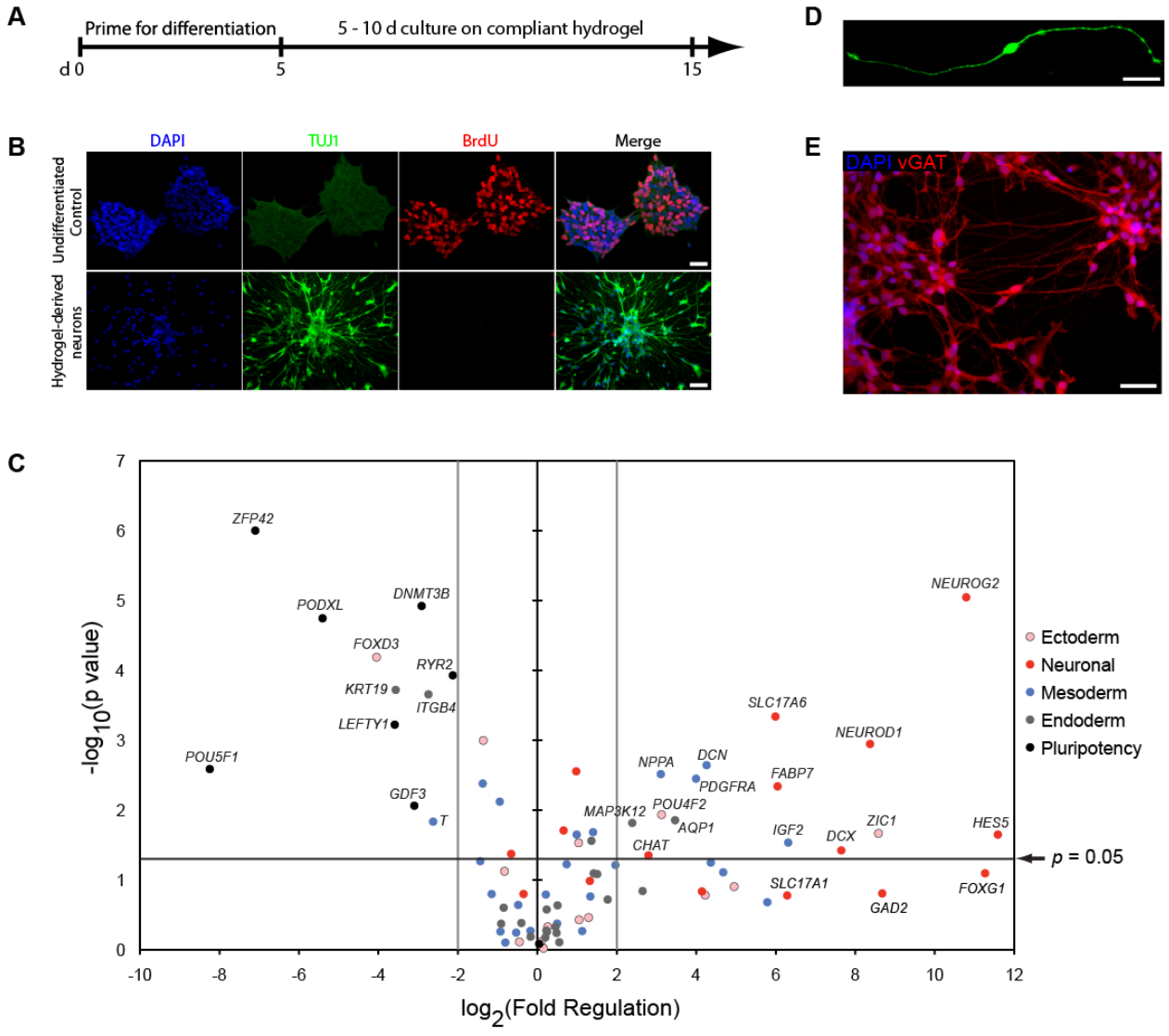

Figure 2-2: Characterization of substrate-derived neurons.

(A) Schematic representation of the procedure for neuronal induction of hES cells on a

compliant hydrogel.

(B) BrdU labeling analysis of hES cells (H9 line) that were undifferentiated or differentiated for 2 wk on a compliant hydrogel. Cells were immunostained for TUJ1 (green) and BrdU (red), and counterstained with DAPI (blue).

(C) Gene expression analysis of substrate-derived neurons. The hES cells (H9 line) were cultured for 2 wk on compliant PA hydrogels, and their levels of neuronal, pluripotency, and germ layer markers were examined relative to undifferentiated cells. Values shown are log2 of mean fold regulation (x axis) and the statistical significance [y axis: $-\log_{10}$ (P value)] for n = 3 biological replicates.

(D) Representative image of a TUJ1-positive (green) cell showing dual axon morphology of the substrate-derived neurons.

(E) Microscopy image of substrate-derived neurons expressing vesicular GABA transporter (vGAT). Cells were counterstained with DAPI (blue). (Scale bars: 50 μm.)

We next assessed the functional attributes of the substrate-derived neurons using electrophysiology. After 2 weeks of differentiation on the compliant hydrogel, whole-cell patch clamp recordings indicated that the differentiated cells express large inward and outward currents indicative of neurons (Figure 2-3A). The substrate-derived cells also display spontaneous postsynaptic currents (Figure 2-3B), and a subset (3 of 21) of the tested cells had spontaneous action potentials (Figure 2-3C). Thus, the substrate-derived neurons are electrophysiologically functional and are electrochemically similar to those derived by standard hES cell differentiation protocols that require a differentiation timeline of 4 weeks (Johnson et al., 2007). To ascertain if the substrate-derived neurons are capable of further maturation, we allowed the cells to differentiate for 12 days on the compliant hydrogels in depleted medium and then switched to N2B27 neuronal maintenance medium. Using a transgenic hES cell line (Du et al., 2009), engineered with a GFP reporter for synapsin, we found that the differentiated cells

express synapsis, a marker of synaptic vesicles in mature neurons (Figure 2-3D). Together, these results indicate that the substrate-differentiated cells are post-mitotic and possess molecular markers indicative of mature neuronal cells.

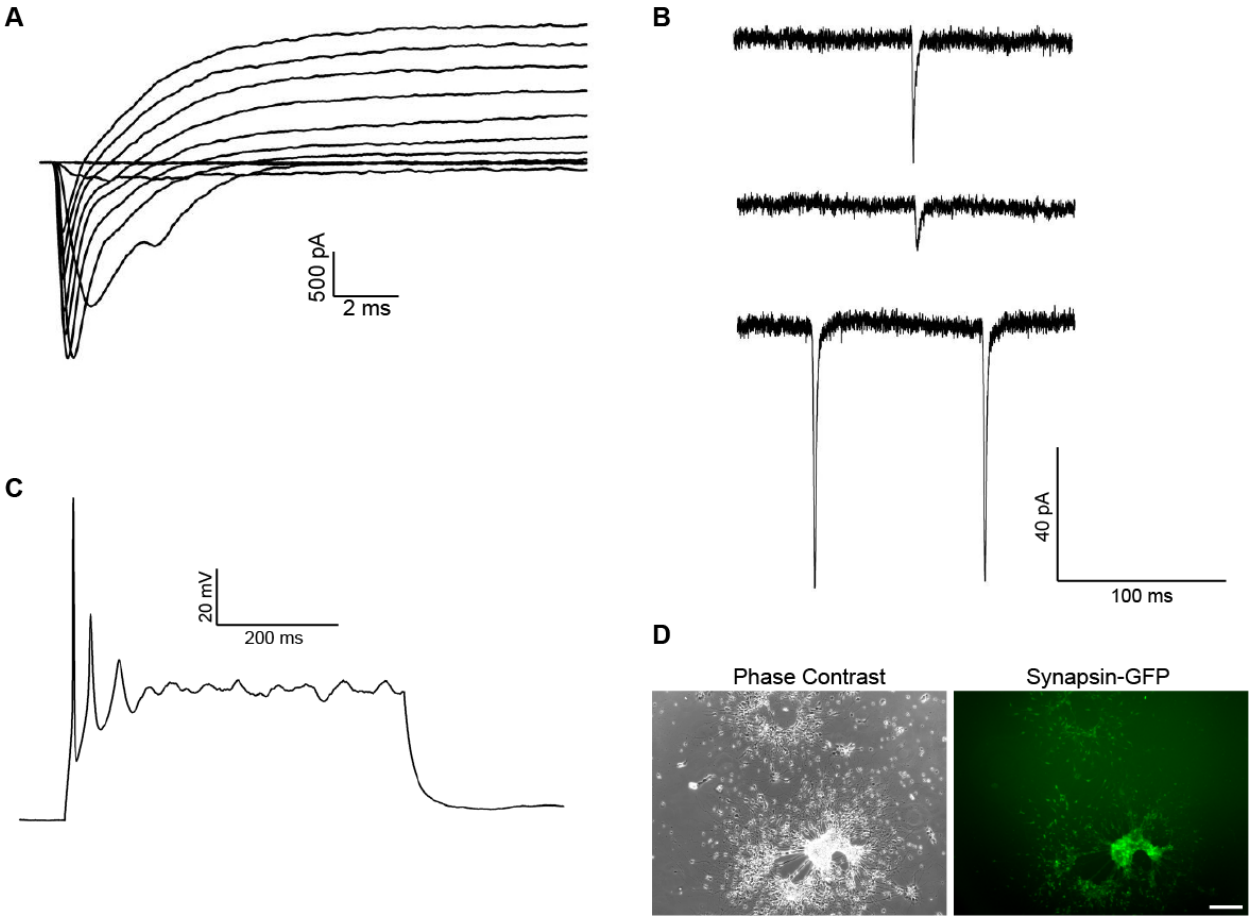

Figure 2-3: Functional characterization of substrate-derived neurons.

(A-C) hES cells (H9 line) were differentiated for 2 wk on compliant PA hydrogels and analyzed by electrophysiology Step-induced currents revealed large, rapidly inactivating inward currents followed by sustained outward currents. Traces of spontaneous postsynaptic currents (B) and action potentials (C) detected in substrate-derived neurons.

(D) Expression of mature neuronal markers in prolonged culture of substrate-derived neurons. H9 synapsin-GFP hES cell line was cultured on 0.7 kPa hydrogels that were functionalized with

VHBD peptide using depleted medium. After 12 days the medium was switched to N2B27 medium and cultured for an additional 2 weeks. Cells were visualized by phase contrast and fluorescent illumination for GFP expression. Scale bar: 200 μm.

2.3.3 Soft substrates enhance motor neuron differentiation

Next, we examined if culture on compliant hydrogels would enhance the neuronal differentiation of an existing soluble factor-based protocol. We focused on motor neurons due to their promise in providing treatments for neurodegenerative disorders such as amyotrophic lateral sclerosis and spinal muscular atrophy (Davis-Dusenbery et al., 2014). By measuring neural cell adhesion molecule 1 (NCAM1) expression, a cell-surface neuronal marker, we detected an increase in NCAM1 expression by flow cytometry in hES cells differentiated to motor neurons on compliant hydrogels relative to stiff Matrigel-coated polystyrene (Figure 2-4A). About 70% of the resulting neurons expressed Islet1, a marker of motor neuron fate (Figure 2-4B). These results indicate that substrate signaling can augment soluble cues during hPS cell differentiation.

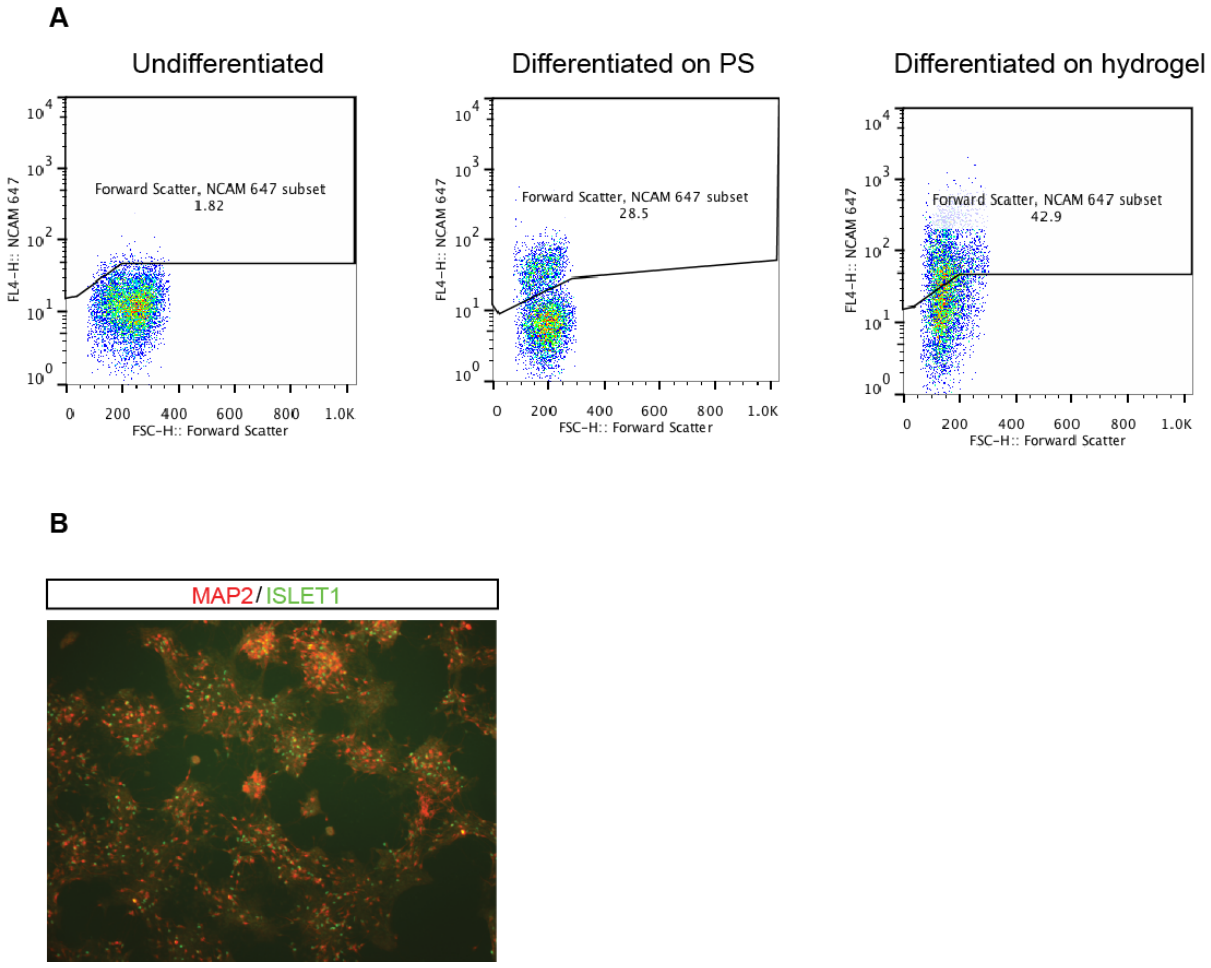

Figure 2-4: Motor neuron differentiation is enhanced on compliant substrates.

(A) Dot plots of NCAM fluorescence intensity in undifferentiated H9 cells (left) or H9 cells differentiated to motor neurons on either polystyrene presenting the VHBD peptide (middle) or a compliant substrate modified with the VHBD peptide (right).

(B) Protein levels of MAP2 and Islet1 in H9 cells differentiated to motor neurons on compliant substrate modified with the VHBD peptide. ~70% of MAP2^{+} neurons co-express Islet1.

2.3.4 Molecular mechanism of substrate-induced neuronal differentiation of hPS cells

As we previously reported, hPS cells localize YAP/TAZ to the nucleus on stiff surfaces whereas the proteins are excluded from the nucleus in cells cultured on soft surfaces (Musah et al., 2012) (Figure 2-5A). Since we also observed low YAP/TAZ abundance in the cytoplasm on soft surfaces, we hypothesized that the proteins were degraded as both YAP and TAZ are known to undergo proteasomal degradation (Liu et al., 2010; Zhao et al., 2010). If YAP/TAZ are being proteosomally degraded in the cytoplasm of hPS cells on soft surfaces, then proteasomal inhibition should rescue cytoplasmic staining. Indeed, incubation with MG-132, a small molecule proteasomal inhibitor, rescues YAP and TAZ detection in the cytoplasm (Figure 2-5B). Therefore, soft surfaces induce YAP/TAZ nuclear exclusion and proteasomal degradation.

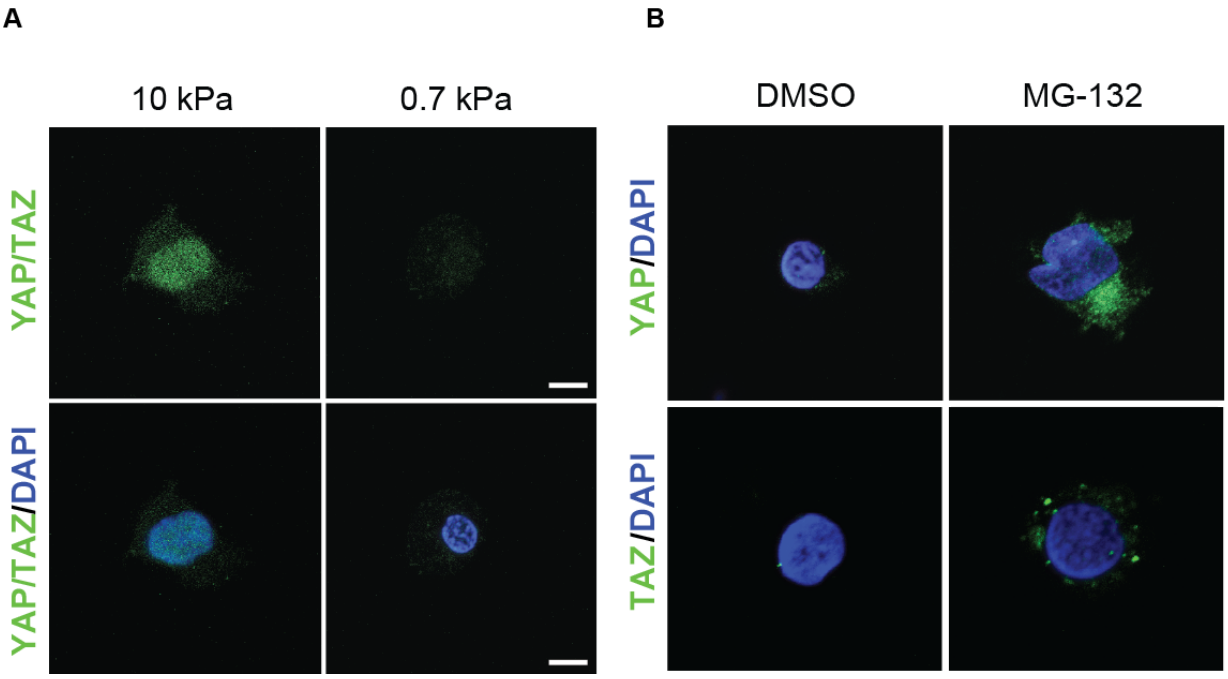

Figure 2-5: YAP and TAZ are excluded from cell nuclei and proteasomally degraded in cells on soft substrates.

(A) YAP/TAZ subcellular localization in H9 cells on stiff (left) or compliant substrates (right). (B) YAP (top) and TAZ (bottom) subcellular localization in H9 cells on compliant substrates treated with DMSO (right) or 62.5 nM MG-132 (left) for 24 hours.

If absence of YAP or TAZ is important for substrate-induced differentiation, then depleting the transcriptional coactivator on a stiff substrate could result in neuronal differentiation. We knocked down *WWTR1* (TAZ) in hPS cells using lentiviral-mediated RNA interference, but did not detect differentiation (Figure 2-6A-C). In contrast, knockdown of *YAP* resulted in a decrease of *CTGF* expression (an indicator of YAP activity), and neuronal differentiation of hES cells cultured on a rigid polystyrene surface (Figure 2-6D-F). This lineage restriction occurred even in the presence of mTeSR medium. Thus, by preventing nuclear localization of YAP, compliant substrates override soluble signals and robustly induce neuronal differentiation of hPS cells. The activity of the compliant surfaces indicates that the substrates can be as powerful as soluble factors in influencing hPS cell lineage specification.

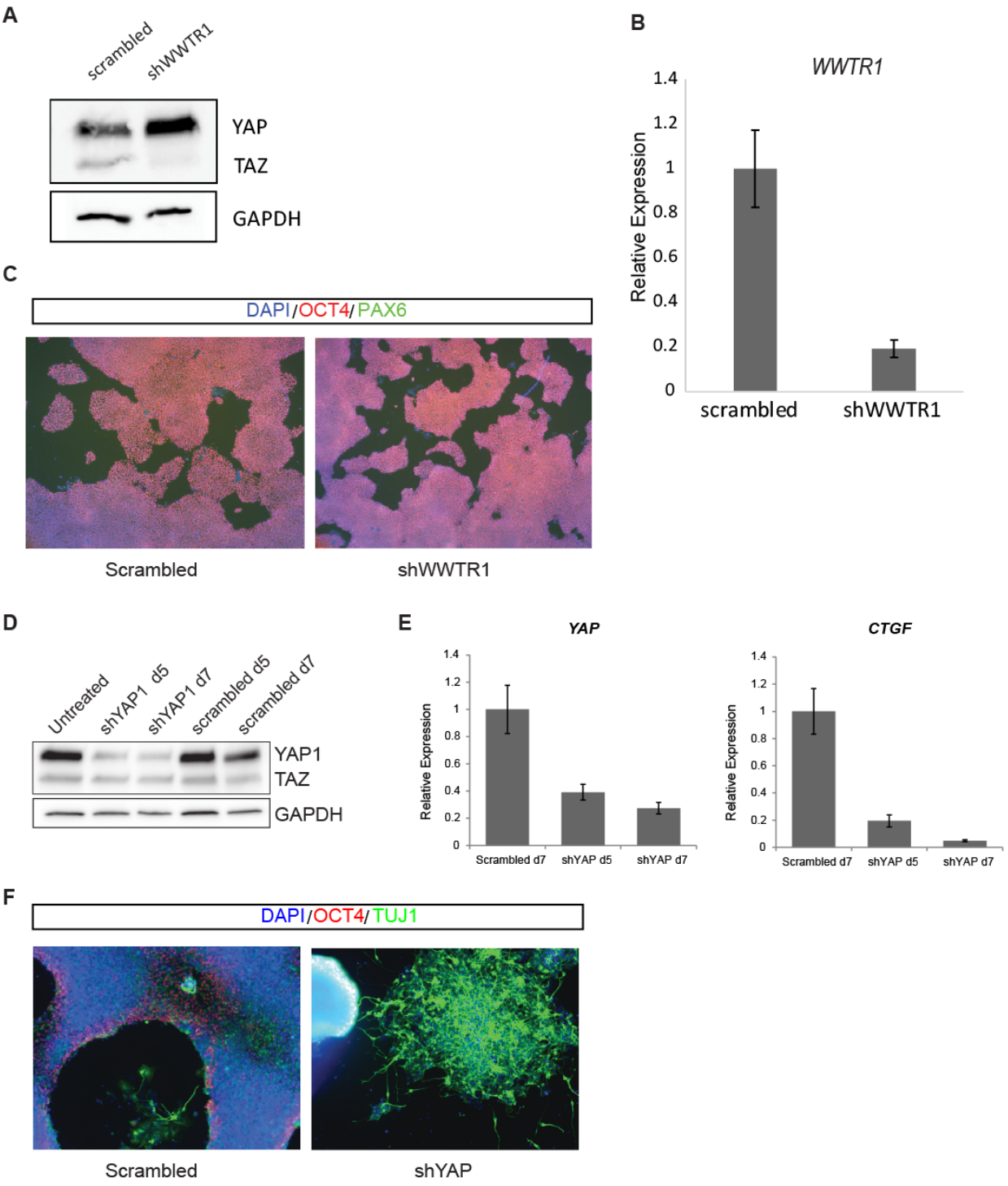

Figure 2-6: YAP, but not TAZ, depletion in cells on a stiff surface induces neuronal differentiation

(A) Protein levels of YAP and TAZ in scrambled and shWWTR1 H9 cells

(B) *WWTR1* expression in scrambled and shWWTR1 H9 cells

(C) Microscopy image of scrambled and shWWTR1 H9 cells stained for OCT4 (red) and PAX6 (green) and counterstained with DAPI (blue).

(D) Protein levels of YAP and TAZ in scrambled and shYAP H9 cells

(E) *YAP* and *CTGF* expression in scrambled and shYAP H9 cells

(F) Microscopy image of scrambled and shYAP H9 cells stained for OCT4 (red) and TUJ1 (green) and counterstained with DAPI (blue).

Cells bound to compliant surfaces can exhibit cytoskeletal changes, including a decrease in F-actin polymerization (Discher et al., 2009; Dupont et al., 2011; Musah et al., 2012). A decrease in F-actin polymerization and stress fiber formation has been linked to YAP nuclear exclusion in hMS cells (Dupont et al., 2011). To examine if the hPS cell cytoskeleton is influencing YAP subcellular localization, we cultured hES cells on a stiff substrate (polystyrene functionalized with Matrigel) in depleted medium supplemented with small molecule cytoskeletal inhibitors. Unlike in hMS cells, inhibition of stress fiber formation in hPS cells with small molecule inhibitors of Rho-associated kinase (ROCK) or non-muscle myosin II (NMII) did not influence YAP subcellular localization (Figure 2-7A). In contrast, inhibition of F-actin polymerization or Rho, a GTPase that regulates F-actin polymerization, resulted in YAP nuclear exclusion and downregulation of *CTGF* (Figure 2-7A, B). Accordingly, this change in YAP subcellular localization was accompanied by an increase in phosphorylation of YAP on S127, a post-translation modification of YAP that occurs in the cytoplasm (Figure 2-C). If these cytoskeletal changes are important for eliciting neuronal differentiation of hES cells, F-actin inhibition should promote neuronal differentiation even on stiff surfaces. Indeed, treatment with F-actin inhibitor promoted neuronal differentiation of hES cells on a stiff substrate (Figure 2-7D). Together, these results indicate that F-actin-mediated regulation of YAP subcellular localization underlies substrate-induced neuronal differentiation of hPS cells.

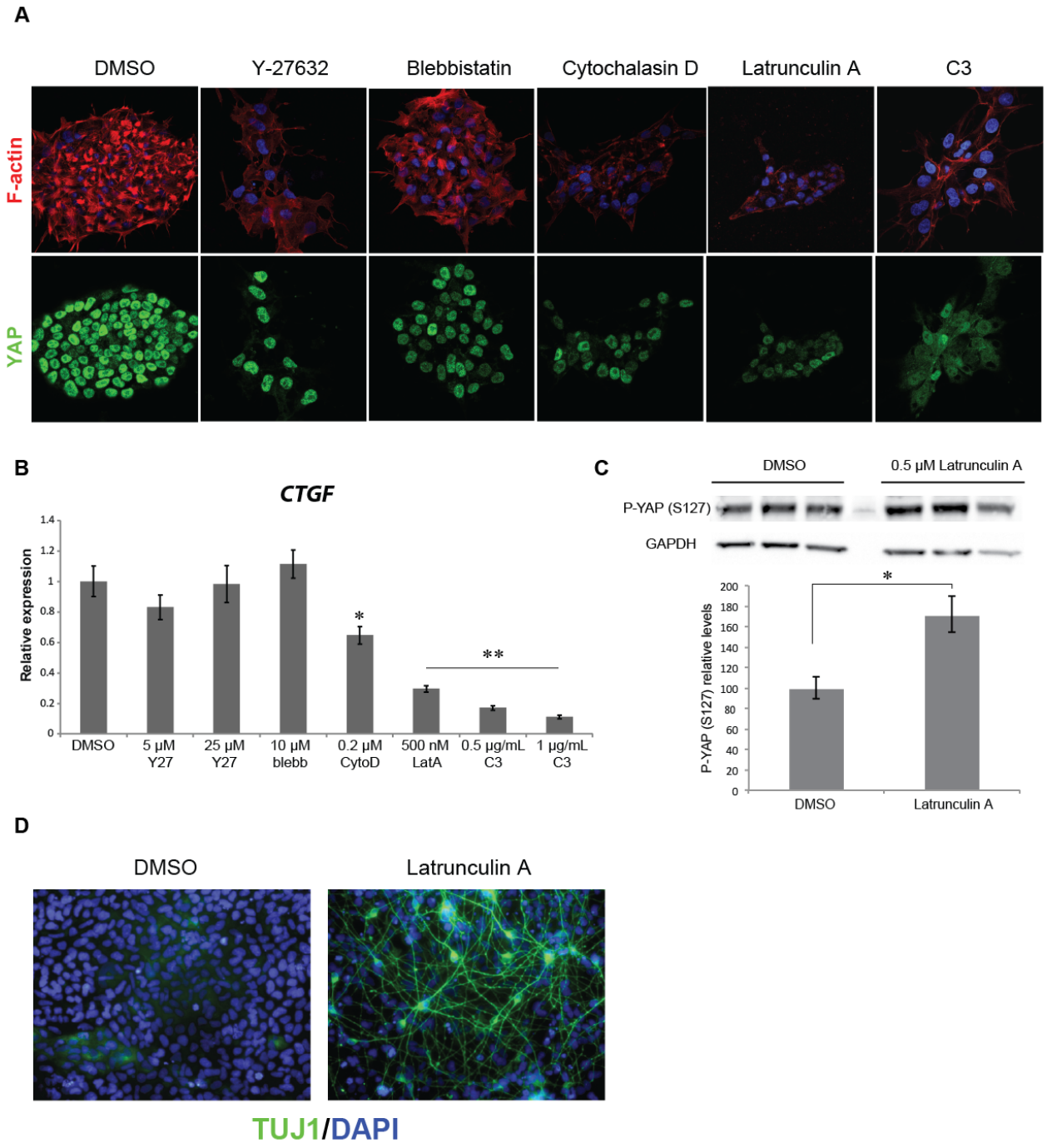

Figure 2-7: Inhibition of F-actin polymerization leads to YAP nuclear exclusion and neuronal differentiation.

(A-B) F-actin levels and YAP subcellular localization (A) or *CTGF* expression (B) in H9 cells on Matrigel-coated tissue culture polystyrene following treatment for 24 hours with DMSO, 25 µM Y-27632 (ROCK inhibitor), 10 µM blebbistatin (NM II inhibitor), 200 nM cytochalasin D, 500

nM latrunculin A (F-actin inhibitors), or 1 μg/mL C3 (Rho inhibitor). *p-value < 0.007, **p-value < 0.0004.

(C) Quantification of phosphorylated YAP levels after small molecule inhibition of F-actin polymerization. H9 hES cells were cultured on polystyrene coated with Matrigel. The cells were treated with 0.5 μm Latrunculin A or DMSO control for 24h. Levels of phosphorylated YAP were assayed quantified relative to GAPDH reference gene (n=3). *p-value < 0.02.

(D) TUJ1 protein levels in H9 cells cultured for 9 days on Matrigel-coated tissue culture polystyrene in depleted medium supplemented with DMSO (left) or 0.5 μM latrunculin A (right).

2.4 Conclusions

In summary, our data indicate that insoluble signals from cell culture substrates can significantly impact hPS cell lineage specification. Compliant substrates (~1 kPa) rapidly and efficiently direct terminal differentiation of hPS cells into neurons. Thus, neuronal specification of hPS cells need not depend only on soluble inductive factors, but rather also on substrate features. Our data highlight the profound influence of the substrate and underscore the benefits of exploiting substrate features in design of protocols to guide hPS cell differentiation.

Although our efforts are aimed at devising effective protocols for in vitro differentiation, it is intriguing that the hydrogels with elasticity similar to brain tissue are the most effective at inducing neuronal differentiation. We propose that substrate elasticity controls neuronal differentiation of hPS cells by regulating the subcellular localization of YAP (Figure 2-8). Intriguingly, YAP activity is decreased during mammalian neurogenesis (Cao et al., 2008; Fernandez et al., 2009; Lin et al., 2012) in conjunction with Hedgehog (Fernandez et al., 2009; Lin et al., 2012) and SMAD (Alarcon et al., 2009) signaling pathways, which are ubiquitous targets of soluble factors used to promote neuronal differentiation of hES cells (Chambers et al.,

2009; Chambers et al., 2012; LaVaute et al., 2009; Liu and Zhang, 2011b; Ma et al., 2012; Neely et al., 2012; Shimada et al., 2012; Surmacz et al., 2012).

Efforts to differentiate hPS cells to neurons have focused on two key proneural basic helix-loop-helix (bHLH) transcription factors—NEUROD1 and NEUROG2. Lentiviral-mediated overexpression of either of these genes induces neuronal differentiation in hPS cells (Zhang, 2013). Intriguingly, *NEUROG2* and *NEUROD1*, master regulators of neuronal development (Zhang et al., 2012; Zhang et al., 2013), are upregulated in cells cultured on the compliant hydrogels. As YAP is excluded from the nucleus in cells cultured on the compliant hydrogels and knock down of YAP is sufficient to induce neurogenesis, it is possible that YAP represses the production of these master regulators. Therefore, our findings suggest that modulating YAP localization via substrate elasticity can circumvent the need for overexpression of exogenous transcription factors in driving neuronal differentiation. Another bHLH factor likely regulated by YAP in hPS cells is NEUROD4 (also known as NEUROM), which is repressed by YAP overexpression in the chick neural tube (Cao, 2008). *NEUROD4* is transiently expressed in cells approaching the post-mitotic phase, and persists in bipolar neurons until terminal differentiation (Roztocil et al., 1997). The substrate-induced neurons possess bipolar projections, a characteristic morphology of interneurons (Maxwell et al., 2007). It is therefore possible that YAP inhibition by the compliant hydrogels promotes *NEUROG2* expression along with continuous activation of *NEUROD4*, which subsequently guides hPS cell differentiation into interneurons. Given the importance of YAP signaling in organ development and function (Boggiano and Fehon, 2012; Zhao et al., 2011), our results suggest that synthetic materials could mimic the inductive power of the embryo and drive hPS cells to specialize.

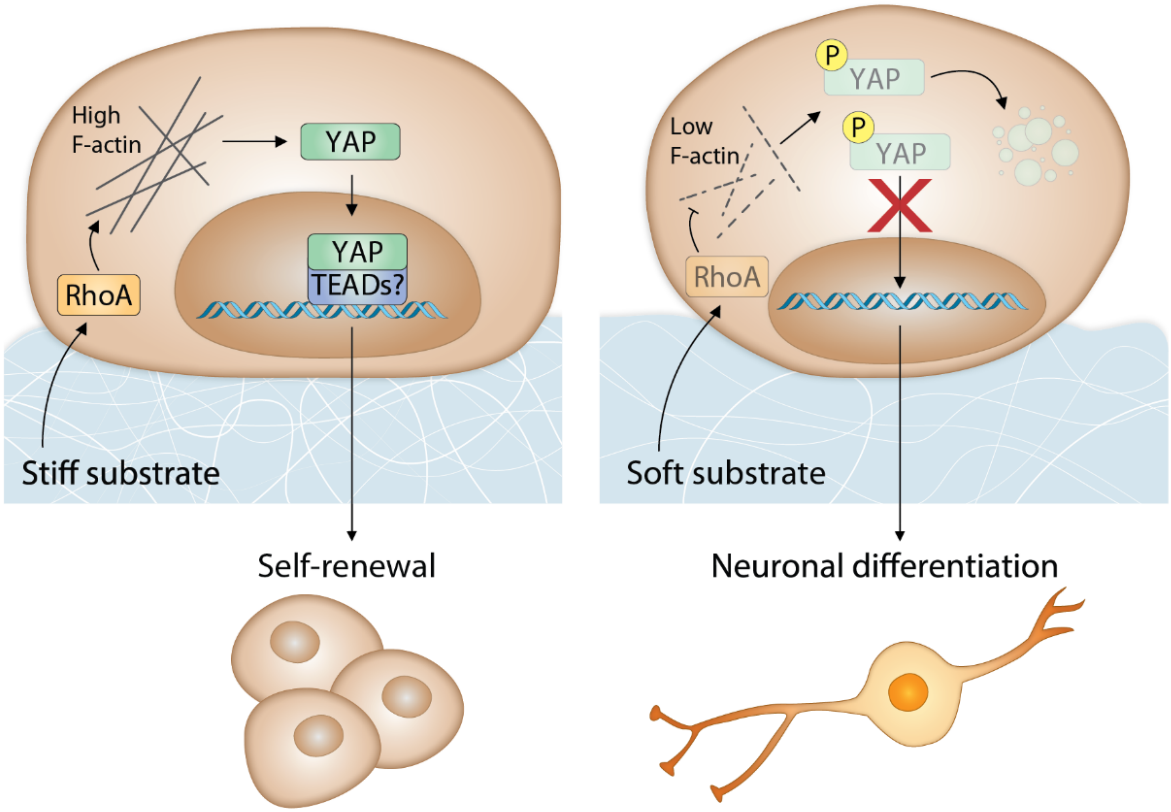

Figure 2-8: Proposed model for substrate-induced neuronal differentiation of hPS cells. Stiff substrates promote F-actin polymerization and stress fiber formation, which results in the translocation of YAP to the nucleus, where it regulates gene expression to support self-renewal of hPS cells. Compliant substrates decrease F-actin polymerization, afford increased phosphorylation of YAP, and result in YAP localization in the cytoplasm. Inhibition of YAP coactivator function induces neurogenesis in hPS cells. P: phosphorylation.

2.5 Methods

2.5.1 Polyacrylamide hydrogel synthesis

Polyacrylamide hydrogels were synthesized as previously described (Musah et al., 2012) with a minor modification in the generation of reactive coverslips. Reactive coverslips were prepared by first rinsing either 12, 18, or 22 mm No. 1 cover glass (Corning Inc.) with ethanol, and the rinsed glass was allowed to air dry. The coverslips were etched by treatment with 0.1 M NaOH for 5 min, followed by a 5 min exposure to 3-aminopropyltriethoxysilane (Sigma). The coverslips were washed several times with distilled water and air-dried before use. Siliconized coverslips of corresponding size (12, 18, or 22 mm) were also generated using a known protocol (Klein et al., 2007; Musah et al., 2012). For hydrogel synthesis, the following stock solutions were freshly prepared: 40% w/v acrylamide (Sigma), 2% w/v bisacrylamide (Promega Corp.), 10% w/v ammonium persulfate (APS) (Aldrich Chemical Co. Inc), saturated solution of acrylic acid *N*-hydroxysuccinimidyl ester (acrylic-NHS) from Aldrich Chemical Co. Inc., and *N,N,N',N'*-tetramethylenediamine (TEMED)(Sigma). For compliant (~0.7 kPa) hydrogels, a precursor solution was prepared from the stock solutions by mixing 75 μL of acrylamide, 10 μL of bisacrylamide, 193 μL of H_2O, 0.3 μL of TEMED, 4 μL of APS, and 118 μL of acrylic-NHS. To synthesize the stiffer hydrogels, 60 μL (~3 kPa) or 120 μL (~10 kPa) of bisacrylamide was used, and the prepolymer solution was adjusted to a final volume of 400 μL with water. The prepolymer solution mixture was briefly vortexed, and a fixed volume of 35, 75, or 120 μL was added to the 12, 18, or 22 mm reactive coverslip, respectively. A siliconized coverslip of equal size was gently placed on top of the hydrogel solution. Once polymerization was complete, after about 10 min, the siliconized coverslips were removed and hydrogels were transferred to a 24-, 12-, or 6-well plates. The hydrogels were washed three times with phosphate buffered saline (PBS) for 5 min each.

For functionalization with VHBD peptide (Biomatik), the electrophilic succinimidyl ester groups on the hydrogels were converted to amides by exposure for two hours to a solution (5

mM, pH 7.5) consisting of a 1:1 ratio of *N*-methyl-D-glucamine (Aldrich) to *N*-(2-aminoethyl)maleimide trifluoroacetate (Fluka) at a final volume of 400 μL, 0.5 mL, or 1.5 mL per well of a 24-, 12-, or 6-well plates, respectively. The hydrogels were washed three times with PBS for 10 min, and a solution of 0.1 mM of the indicated peptide in PBS (pH 7.5) was added to hydrogels and the resulting mixture was allowed to undergo reaction overnight at room temperature. Under sterile conditions, the hydrogels were washed several times with PBS, sterilized with 60% ethanol, and washed with DMEM/F12. Hydrogels were used for cell culture or stored at 4 ^{o}C in DMEM/F12 until needed. All hydrogels were used within a week after their synthesis.

2.5.2 Cell culture and differentiation

Human ES cells (H9, H9 Syn-GFP, and SA02, all from WiCell) were propagated on plates coated with Matrigel (BD Biosciences) using mTeSR medium (Stem Cell Technologies). Cells were incubated at 37 ^{o}C in 5% CO_2, and passaged every 5–7 days by treatment with dispase (2 mg/mL). For spontaneous differentiation, cells were cultured for a minimum of 25 days with embryoid body (EB) medium consisting IMDM (Gibco), 15% heat-inactivated fetal bovine serum (FBS) from Gibco, 1% MEM non-essential amino acids (Gibco), and 200 μL/100 mL of 2-mercaptoethanol.

For differentiation on hydrogels, hES cells at ~60% confluence were first primed (unless indicated otherwise) by treatment with EB medium for 5 days. The cells (~80% confluence) were then detached from Matrigel-coated plates by treatment with Accutase (Gibco) for 3 min. The cells were washed once with mTeSR medium by centrifugation at 1200 rpm for 5 min. The supernatant was removed and cells were resuspended in depleted medium (mTeSR medium lacking signaling components FGF2, TGFβ, and GABA; and supplemented with 5 μM Y27632), and centrifuged again at 1200 rpm for 5 min. Supernatant was removed and cells were plated onto hydrogels at 1:4 splitting density in depleted medium at final volume of 400 μL, 0.5 mL, or

2 mL per well of a 24-, 12-, or 6-well plate. To examine the effects of any of the three signaling components (FGF2, TGFβ, and GABA) or their combinations, mTeSR medium lacking the indicated component(s) was employed. Cells were incubated at 37 ^{o}C in 5% CO_2 and medium was refreshed daily. For all the cell lines examined in this study (H9, H9 Syn-GFP and SA02), neuronal differentiation occurred within 10 days of culture on the compliant PA. For prolonged culture of the substrate-derived neurons, the cells were first differentiated on the hydrogels for 12 days using depleted medium, then the medium was switched to N2B27 medium (1:1 mixture of DMEM/F12 and Neurobasal media supplemented with 1:100 of GlutaMAX, B27, and N2, all from Gibco). The substrate-derived neurons remained viable in N2B27 medium for at least an additional 2 weeks of culture.

2.5.3 BrdU labeling assay

H9 hES cells were primed and differentiated into neurons (as described above) by culturing on the complaint hydrogels for a maximum of 14 days. As a positive control, standard H9 cultures on Matrigel-coated plates were used. Cells were incubated for 5 h with BrdU labeling reagent (Invitrogen) diluted at 1:100 in depleted medium (1 mL per well of 12-well plate). The cells were fixed by treatment with 4% paraformaldehyde in PBS for 20 min at room temperature, and then washed three times with PBS (10 min per wash). The cells were permeabilized by incubating with 0.125% Triton X-100 (in PBS) for 5 min, followed by denaturation by treatment with 1.5 M hydrochloric acid for 1 h at room temperature with gentle rocking. The cells were washed three times with PBS (5 min per wash) and once with permeabilize buffer. Cells were blocked and immunostained for BrdU and TUJ1 as described below.

2.5.4 Small molecule inhibition of F-actin polymerization

Human ES cells were detached from Matrigel-coated plate by treatment with Accutase for 3 min. Cells were washed twice in mTeSR medium by centrifugation at 1200 rpm for 5 min each. Supernatant was removed and cells were resuspendend in mTeSR medium, followed by plating on newly prepared Matrigel-coated polystyrene surfaces (12-well tissue culture plates) at ~$2x10^5$ cells/well. Cells were incubated at 37 ^oC for 24 h. Spent medium was removed and cells were rinsed twice with DMEM/F12. The cells were then cultured for 9 days with depleted medium only (blank), or depleted medium supplemented with 0.5 μM latrunculin A (Santa Cruz Biotech. Inc.) diluted from a 5 mM stock solution in DMSO (final DMSO concentration of 0.01%). As an additional control, depleted medium supplemented with DMSO (0.01%) was also employed. Cells were incubated at 37 ^oC and medium was refreshed daily. After 9 days (10 days total culture period), bright field images were captured, and cells were fixed and stained or immunostained for YAP/TAZ, TUJ1, and phalloidin as described below. To examine the levels of phosphorylated YAP protein, cells were harvested after 24 h culture for Western blot analysis.

2.5.5 Immunostaining and microscopy analysis

Cells were fixed with 4% paraformaldehyde (in PBS) for 20 min at room temperature, and permeabilized for 5 min with 0.125% Triton X-100 (in PBS). Cells were then blocked with 1% BSA (in permeabilization buffer) for 30 min at room temperature, followed by three washes (5 min each) with permeabilization buffer. Cells were incubated overnight at 4 ^oC with primary antibodies at indicated dilutions in permeabilization buffer. Cells were exposed to secondary antibodies at 1:1000 dilution in permeabilization buffer (1:100 for BrdU labeling) for 1 h at room temperature, and then washed three times with permeabilization buffer (10 min per wash). The primary antibodies used in this study include OCT4 (R&D Systems, 1:400), TUJ1 (neuron-specific β-III tubulin) (Sigma, 1:400), YAP/TAZ (Sc-101199, Santa Cruz Biotech., 1:300), vesicular GABA transporter (vGAT) (Sigma, 1:300), GAD67 (Millipore, 1:400), and BrdU

(Invitrogen, 1:100). Alexa Fluor 488- and 594-conjugated antibodies (Invitrogen) were used as secondary antibodies. For F-actin staining, cells were incubated with Alexa Fluor 594-conjugated phalloidin (Invitrogen, 1:40) in PBS for 20 min at room temperature. Cells were counterstained by incubating for 5 min with 4,6-diamidino-2-phenylindole (DAPI, from Invitrogen) at 1:1000 dilution in water. Cells were visualized with Olympus IX81 microscope equipped with Hamamatsu digital camera. Images were colored and overlaid in Adobe Photoshop CS3.

Neuronal differentiation efficiency was determined by the total number of TUJ1-positive cells with neuronal morphology, defined as cells with three-dimensional appearance and extending a thin process of at least three times longer than the cell body(Pang et al., 2011). Calculations were performed using randomly selected images from biological replicates at 40X magnification with 120 mm^2 visual area. The number of TUJ1-positive cells was divided by the number of cell nuclei (DAPI) to obtain the percentage of neuronal TUJ1-positive cells. Data are presented as the mean ± s. d.

2.5.6 Immunoblotting

Cells were washed with PBS and lysed on ice in RIPA buffer supplemented with Halt Protease Inhibitor Cocktail (Thermo) and Halt Phosphoprotease Inhibitor Cocktail (Thermo). Protein samples were separated by SDS-PAGE and transferred onto a PVDF membrane. Membranes were blocked with 5% milk in Tris-buffered saline with Tween 20 (TBST), and immunoblotting was carried out according to standard procedure. Primary antibodies were diluted in TBST supplemented with 5% BSA. Primary antibodies used for Western blot were mouse anti-YAP/TAZ (Sc-101199, Santa Cruz Biotech., 1:500), rabbit anti-phospho-YAP (Ser 127) (4911, Cell Signaling Tech., 1:1000), and rabbit anti-GAPDH (5174, Cell Signaling Tech., 1:10000). Secondary antibodies were HRP-conjugated goat anti-mouse and HRP-conjugated goat anti-rabbit (Jackson ImmunoResearch). Chemoluminescence was detected using

Amersham ECL Prime (GE Healthcare Life Sciences) and ImageQuant LAS 400 (GE Healthcare Life Sciences). Signal intensities were quantified using ImageJ software (NIH).

2.5.7 Gene expression analysis

Human ES cells were primed and then differentiated on the compliant polyacrylamide hydrogels for 2 weeks with depleted medium. Cells were detached from the hydrogels by treatment with 0.05% trypsin-EDTA (Gibco) for about 3 min. Primed and undifferentiated hES cell controls were also detached from Matrigel-coated plates by treatment with 0.05% trypsin-EDTA. Trypsin activity was quenched with EB medium and centrifuged for 5 min at 1200 rpm. The cells were resuspended in sterile PBS and centrifuged again at 1200 rpm for 5 min. Supernatant was removed and cell pellets were stored at -80 ^{o}C. Total RNA was isolated from cell pellets using RNeasy Plus Kit (Qiagen). For each sample, 800 ng of RNA was reverse transcribed into cDNA libraries using the iScript QPCR cDNA Synthesis Kit (BioRAD). Cell Lineage Identification RT^{2} Profiler PCR Arrays (SABiosciences: PAHS – 508ZC) were performed for each sample according to the manufacture's protocol using a 7500 Fast Block instrument (Applied Biosystems). Data were compiled and analyzed with SABiosciences data analysis web client. Volcano plots depict fold regulation and statistical significance (p) calculated from the mean (n = 3 biological replicates) for primed or hydrogel-differentiated samples internally normalized to β-actin and GAPDH reference genes, and compared to the mean (n = 3 biological replicates) for undifferentiated cells. Genes up- or down-regulated greater than fourfold with $p <$ 0.05 were considered significant.

2.5.8 Lentivirus-mediated RNA interference

HEK293FT cells (Invitrogen) were co-transfected using Lipofectamine-2000 (Invitrogen) with packaging plasmids psPAX2 (Addgene plasmid 12260) and pMD2.6 (Addgene plasmid 12259) and lentiviral vectors (pLKO.1) containing shRNA sequences targeting YAP (Addgene plasmid 27368)(Zhao et al., 2008) or a non-targeting control (Addgene plasmid

1864)(Sarbassov et al., 2005). Medium containing viral particles was collected over four days and then concentrated using the Lenti-X concentrator (Clontech) according to the manufacturer's instructions. H9 cells were cultured in mTeSR on Matrigel-coated polystyrene plates until 30% confluent then treated with 25 µL concentrated viral particles containing shYAP or the non-targeting control overnight (day 0). The viral particle-containing medium was removed and cells were allowed to recover (day 1) before selecting with 1 µg mL^{-1} puromycin (day 2). Cells were cultured continuously in mTeSR with puromycin for 14 days total. Cell samples were either harvested for qPCR and Western blot analysis to monitor YAP knockdown at day 5 and day 7 or fixed at day 14 for immunocytochemical analysis.

qPCR Primers:

Target	Forward Primer (5'-3')	Reverse Primer (5'-3')
ACTB	TCAGAAGGATTCCTATGTGGGCGA	TTTCTCCATGTCGTCCCAGTTGGT
YAP1	GCTGCCACCAAGCTAGATAA	GTGCATGTGTCTCCTTAGATCC
WWTR1	GAGGGTGTATGGTGGAGATAAA	CCAACTGTAGCAAACAGGATTAG
CTGF	AGGAGTGGGTGTGTGACGA	CCAGGCAGTTGGCTCTAATC

2.5.9 Flow cytometry

For analysis of NCAM1 cell surface levels, undifferentiated and differentiated H9 were detached with 1 mM EDTA, centrifuged, and resuspended in 1 mL cold PBS containing 1 µL LIVE/DEAD fixable green dead cell stain. Cells were then centrifuged and resuspended in PBS containing 2% BSA (w/v) supplemented with Alexa Fluor 647-conjugated anti-mouse CD56 for 1 hour on ice. Antibody exposure was followed by two washes. Data were obtained using a FACSCalibur instrument (BD) and analyzed using FlowJo software (Tree Star, Inc.).

2.5.10 Electrophysiology analysis

Human ES cells (H9) were differentiated on compliant polyacrylamide hydrogels (on 12 mm coverslips) as described above. For electrophysiology analysis, the differentiated cells (adhered to hydrogels on 12 mm coverslips) were transferred to a recording chamber and superfused with extracellular solution with the following composition: 140 mM NaCl, 3 mM KCl, 1 mM $MgCl_2$, 2 mM $CaCl_2$, 20 mM glucose, and 15 mM Hepes at 300 ± 5 mOsm, and pH7.4. The patch pipette (3 to 5 Ω) solution contained 121 mM K-gluconate, 20 mM KCl, 10 mM Hepes-Na^+ and 5 mM EGTA at 290 ± 5 mOsm, and pH7.4. The substrate-derived neurons were visualized using an Olympus Optical BX51WI microscope (Tokyo, Japan). Patch clamp was performed in either voltage clamp or current clamp mode using a MultiClamp 700B (Molecular Devices). Signals were filtered at 2 kHz and sampled at 10 kHz by using a Digidata 1440A (Molecular Devices). Data were acquired and analyzed using pClamp 10.2 software (Molecular Devices). Series resistance ranged from 10 to 25 MΩ. The holding potential was -70 mV in voltage clamp mode. There was no holding during membrane potential recording. Postsynaptic currents were analyzed using the Template search tool in Clampfit 10.2 software and the events were manually accepted.

2.6 Supplementary Information

Table S2-1: Functional grouping of the genes examined in quantitative PCR analyses.

Pluripotency Markers: POU5F1 (OCT4), NANOG, PODXL, ZFP42, LEFTY1, GDF3, DNMT3B	
Germ Layers	
Ectoderm: OTX2, ZIC1, FGF5, FOXD3	
Neuroectoderm: NEUROG2, GBX2	
Mesoderm: PDGFRA, IGF2, RUNX1 (AML1), T (Brachyury), MIXL1, HAND1, CD34, GATA2, BMP4, DCN	
Endoderm: SOX17, SOX7, GATA1, GATA6, HNF4A, FOXA1	
Progenitors	
Ectoderm	
	Neuronal: HES5, SOX2, FABP7, PROM1
	Immature neuron: DCX
	Immature GABA neuron: GAD2, SLC32A1
	Motor neuron: FOXG1, OLIG2
	Oligodendrocyte: NKX2-2, OLIG2
	Limbal progenitors: ENO1, MSLN
Mesoderm	
	Early cardiomyocyte: HAND2
	Muscle stem cell: CD34
	Early B cell: CD79A
	Early T cell: PTCRA, CD3E
Endoderm	
	Pancreatic islet cells: KRT19
	Hepatic stem cells: MAP3K12, DPP4, APOH
Terminal Differentiation Markers	
Ectoderm	
	Mature neuron: NEUROD1
	cholinergic neuron: CHAT
	GABA neuron: GAD1
	Glutamatergic neuron: SLC17A6, SLC17A7
	Astrocyte: GFAP, GALC
	Keratinocytes: KRT10, KRT14
	Ganglion cell: POU4F2
	Melanocyte: TYR
	Photoreceptor cell: RCVRN
Mesoderm	
	Osteoblast: IBSP
	Osteoclast: CTSK
	Cardiomyocyte: MYL3, NPPA, RYR2, MYH7
	Smooth muscle cell: SMTN, MYH11
	Skeletal muscle cell: MYH1
	Macrophage: CCR5
	Chondrocyte: COMP, COL10A1
Endoderm	
	Hepatocyte: TAT, ALB, G6PC
	Lung cell: SFTPB, SFTPD
	Beta cell: SLC2A2, INS
	Exocrine cell: CPA1
	cholangiocyte: ITGB4
	Proximal tubule cell: AQP1, MIOX

Table S2. Quantitative gene expression profile of substrate-derived neurons. Gene expression levels and statistical signficance of hES cells (H9) differentiated for 2 weeks on compliant polyacrylamide hydrogels relative to undifferentiated cells. Gene are grouped based on (*A*) upregulation and (*B*) downregulation by at least two-fold, or genes that remain relatively (*C*) unchanged between the two conditions. Fold change values represent the mean of three biological replicates. Significant *p*-values are in red ($p < 0.05$).

A

Gene Name	Fold Change	*p* value
HES5	3081.62	0.022501
FOXG1	2465.19	0.080571
NEUROG2	1773.26	0.000009
GAD2	409.92	0.156463
ZIC1	383.67	0.021611
NEUROD1	331.35	0.001134
DCX	200.62	0.037891
IGF2	79.50	0.029259
SLC32A1	78.10	0.167306
FABP7	66.05	0.004586
SLC17A6	63.61	0.000459
HAND2	55.25	0.20892
TYR	30.93	0.125056
MYH7	25.58	0.077902
COMP	20.59	0.056626
DCN	19.14	0.002282
FGF5	18.70	0.165651
GAD1	17.66	0.146575
PDGFRA	15.93	0.003559
AQP1	11.05	0.01401
POU4F2	8.73	0.011651
NPPA	8.61	0.003066
CHAT	6.94	0.044684
FOXA1	6.27	0.144498
MAP3K12	5.23	0.015338
HAND1	3.90	0.061423
CPA1	3.41	0.191426
SFTPB	2.84	0.08273
GATA1	2.67	0.080812
MYH1	2.64	0.020785
ALB	2.57	0.027627
GATA2	2.52	0.173305
GBX2	2.50	0.103694
RCVRN	2.44	0.346687
CCR5	2.19	0.541648
KRT10	2.07	0.372877
GALC	2.05	0.029548

B

Gene Name	Fold Change	*p* value
IBSP	-2.22	0.159629
ENO1	-2.57	0.001011
CD3E	-2.59	0.004184
MYH11	-2.71	0.054074
RYR2	-4.37	0.000118
T	-6.16	0.014692
ITGB4	-6.68	0.000221
DNMT3B	-7.53	0.000012
GDF3	-8.55	0.008674
KRT19	-11.84	0.000191
LEFTY1	-12.03	0.000601
FOXD3	-16.53	0.000065
PODXL	-42.38	0.000018
ZFP42	-136.34	0.000001
POU5F1	-303.77	0.002593

C

Gene Name	Fold Change	*p* value
CD79A	1.99	0.022528
SLC17A7	1.97	0.002798
BMP4	1.67	0.059754
SOX2	1.58	0.019642
TAT	1.47	0.78318
INS	1.42	0.232414
MYL3	1.41	0.422749
SOX17	1.40	0.575613
MIOX	1.37	0.471216
OTX2	1.20	0.469141
SOX7	1.18	0.55661
SFTPD	1.18	0.266013
G6PC	1.17	0.531028
SMTN	1.16	0.162489
HNF4A	1.15	0.667638
KRT14	1.11	0.956552
NKX2-2	1.07	0.765152
NANOG	1.03	0.82499
APOH	-1.13	0.652103
RUNX1	-1.13	0.536628
PROM1	-1.27	0.159485
SLC2A2	-1.32	0.415588
GFAP	-1.37	0.774104
CTSK	-1.40	0.229118
COL10A1	-1.45	0.570151
OLIG2	-1.58	0.042478
PTCRA	-1.75	0.790578
MSLN	-1.77	0.075378
DPP4	-1.80	0.250476
GATA6	-1.88	0.425538
CD34	-1.90	0.550257

2.7 Acknowledgments

I thank Dr. Samira Musah for spearheading this project, including developing the GAG-binding hydrogels and the characterizing the neuronal differentiation in the absence and presence of soluble pluripotency factors. I thank Dr. Paul Wrighton for help with the qPCR array and analysis. I thank Xiaofen Zhong and Dr. Qiang Chang for electrophysiology analysis. I hank Cheston Hsiao, Dr. Lance Lian, and Dr. Sean Palecek for help with lentivirus generation.

2.8 References

Alarcon, C., Zaromytidou, A.I., Xi, Q., Gao, S., Yu, J., Fujisawa, S., Barlas, A., Miller, A.N., Manova-Todorova, K., Macias, M.J., *et al.* (2009). Nuclear CDKs drive Smad transcriptional activation and turnover in BMP and TGF-beta pathways. Cell *139*, 757-769.

Boggiano, J.C., and Fehon, R.G. (2012). Growth control by committee: intercellular junctions, cell polarity, and the cytoskeleton regulate Hippo signaling. Dev Cell *22*, 695-702.

Cao, X., Pfaff, S.L., and Gage, F.H. (2008). YAP regulates neural progenitor cell number via the TEA domain transcription factor. Genes Dev *22*, 3320-3334.

Chambers, S.M., Fasano, C.A., Papapetrou, E.P., Tomishima, M., Sadelain, M., and Studer, L. (2009). Highly efficient neural conversion of human ES and iPS cells by dual inhibition of SMAD signaling. Nat Biotech *27*, 275-280.

Chambers, S.M., Qi, Y., Mica, Y., Lee, G., Zhang, X.-J., Niu, L., Bilsland, J., Cao, L., Stevens, E., Whiting, P., *et al.* (2012). Combined small-molecule inhibition accelerates developmental timing and converts human pluripotent stem cells into nociceptors. Nat Biotech *30*, 715-720.

Chowdhury, F., Li, Y., Poh, Y.C., Yokohama-Tamaki, T., Wang, N., and Tanaka, T.S. (2010a). Soft substrates promote homogeneous self-renewal of embryonic stem cells via downregulating cell-matrix tractions. PLoS One *5*, e15655.

Chowdhury, F., Na, S., Li, D., Poh, Y.C., Tanaka, T.S., Wang, F., and Wang, N. (2010b). Material properties of the cell dictate stress-induced spreading and differentiation in embryonic stem cells. Nat Mater *9*, 82-88.

Davis-Dusenbery, B.N., Williams, L.A., Klim, J.R., and Eggan, K. (2014). How to make spinal motor neurons. Development *141*, 491-501.

Discher, D.E., Mooney, D.J., and Zandstra, P.W. (2009). Growth factors, matrices, and forces combine and control stem cells. Science *324*, 1673-1677.

Du, Z.W., Hu, B.Y., Ayala, M., Sauer, B., and Zhang, S.C. (2009). Cre recombination-mediated cassette exchange for building versatile transgenic human embryonic stem cells lines. Stem Cells *27*, 1032-1041.

Dupont, S., Morsut, L., Aragona, M., Enzo, E., Giulitti, S., Cordenonsi, M., Zanconato, F., Le Digabel, J., Forcato, M., Bicciato, S., *et al.* (2011). Role of YAP/TAZ in mechanotransduction. Nature *474*, 179-183.

Engler, A.J., Sen, S., Sweeney, H.L., and Discher, D.E. (2006). Matrix elasticity directs stem cell lineage specification. Cell *126*, 677-689.

Fernandez, L.A., Northcott, P.A., Dalton, J., Fraga, C., Ellison, D., Angers, S., Taylor, M.D., and Kenney, A.M. (2009). YAP1 is amplified and up-regulated in hedgehog-associated medulloblastomas and mediates Sonic hedgehog-driven neural precursor proliferation. Genes Dev *23*, 2729-2741.

Gauvin, R., Parenteau-Bareil, R., Dokmeci, M.R., Merryman, W.D., and Khademhosseini, A. (2012). Hydrogels and microtechnologies for engineering the cellular microenvironment. Wiley Interdiscip Rev-Nanomed Nanobiotechnol *4*, 235-246.

Holst, J., Watson, S., Lord, M.S., Eamegdool, S.S., Bax, D.V., Nivison-Smith, L.B., Kondyurin, A., Ma, L., Oberhauser, A.F., Weiss, A.S.*, et al.* (2010). Substrate elasticity provides mechanical signals for the expansion of hemopoietic stem and progenitor cells. Nat Biotechnol *28*, 1123-1128.

Johnson, M.A., Weick, J.P., Pearce, R.A., and Zhang, S.-C. (2007). Functional Neural Development from Human Embryonic Stem Cells: Accelerated Synaptic Activity via Astrocyte Coculture. The Journal of Neuroscience *27*, 3069-3077.

Klein, E.A., Yung, Y., Castagnino, P., Kothapalli, D., and Assoian, R.K. (2007). Cell adhesion, cellular tension, and cell cycle control. In Integrins (San Diego: Elsevier Academic Press Inc), pp. 155-175.

Klim, J.R., Li, L., Wrighton, P.J., Piekarczyk, M.S., and Kiessling, L.L. (2010). A defined glycosaminoglycan-binding substratum for human pluripotent stem cells. Nat Methods *7*, 989-994.

Krabbe, C., Zimmer, J., and Meyer, M. (2005). Neural transdifferentiation of mesenchymal stem cells--a critical review. APMIS *113*, 831-844.

LaVaute, T.M., Yoo, Y.D., Pankratz, M.T., Weick, J.P., Gerstner, J.R., and Zhang, S.C. (2009). Regulation of neural specification from human embryonic stem cells by BMP and FGF. Stem Cells *27*, 1741-1749.

Li, J., Han, D., and Zhao, Y.-P. (2014). Kinetic behaviour of the cells touching substrate: the interfacial stiffness guides cell spreading. Sci Rep *4*.

Lian, I., Kim, J., Okazawa, H., Zhao, J., Zhao, B., Yu, J., Chinnaiyan, A., Israel, M.A., Goldstein, L.S.B., Abujarour, R.*, et al.* (2010). The role of YAP transcription coactivator in regulating stem cell self-renewal and differentiation. Genes and Development *24*, 1106-1118.

Lin, Y.T., Ding, J.Y., Li, M.Y., Yeh, T.S., Wang, T.W., and Yu, J.Y. (2012). YAP regulates neuronal differentiation through Sonic hedgehog signaling pathway. Exp Cell Res *318*, 1877-1888.

Liu, C.Y., Zha, Z.Y., Zhou, X., Zhang, H., Huang, W., Zhao, D., Li, T., Chan, S.W., Lim, C.J., Hong, W.*, et al.* (2010). The hippo tumor pathway promotes TAZ degradation by phosphorylating a phosphodegron and recruiting the SCF{beta}-TrCP E3 ligase. J Biol Chem *285*, 37159-37169.

Liu, H., and Zhang, S.C. (2011a). Specification of neuronal and glial subtypes from human pluripotent stem cells. Cell Mol Life Sci, 1-14.

Liu, H.S., and Zhang, S.C. (2011b). Specification of neuronal and glial subtypes from human pluripotent stem cells. Cell Mol Life Sci *68*, 3995-4008.

Lu, P., Blesch, A., and Tuszynski, M.H. (2004). Induction of bone marrow stromal cells to neurons: differentiation, transdifferentiation, or artifact? J Neurosci Res *77*, 174-191.

Ludwig, T.E., Levenstein, M.E., Jones, J.M., Berggren, W.T., Mitchen, E.R., Frane, J.L., Crandall, L.J., Daigh, C.A., Conard, K.R., Piekarczyk, M.S., *et al.* (2006). Derivation of human embryonic stem cells in defined conditions. Nat Biotechnol *24*, 185-187.

Ma, L., Hu, B., Liu, Y., Vermilyea, Scott C., Liu, H., Gao, L., Sun, Y., Zhang, X., and Zhang, S.-C. (2012). Human Embryonic Stem Cell-Derived GABA Neurons Correct Locomotion Deficits in Quinolinic Acid-Lesioned Mice. Cell Stem Cell *10*, 455-464.

Mammoto, T., and Ingber, D.E. (2010). Mechanical control of tissue and organ development. Development *137*, 1407-1420.

Maxwell, D.J., Belle, M.D., Cheunsuang, O., Stewart, A., and Morris, R. (2007). Morphology of inhibitory and excitatory interneurons in superficial laminae of the rat dorsal horn. J Physiol *584*, 521-533.

Moore, S.W., and Sheetz, M.P. (2011). Biophysics of Substrate Interaction: Influence on Neural Motility, Differentiation, and Repair. Developmental Neurobiology *71*, 1090-1101.

Musah, S., Morin, S.A., Wrighton, P.J., Zwick, D.B., Jin, S., and Kiessling, L.L. (2012). Glycosaminoglycan-binding hydrogels enable mechanical control of human pluripotent stem cell self-renewal. ACS Nano *6*, 10168-10177.

Neely, M.D., Litt, M.J., Tidball, A.M., Li, G.G., Aboud, A.A., Hopkins, C.R., Chamberlin, R., Hong, C.C., Ess, K.C., and Bowman, A.B. (2012). DMH1, a Highly Selective Small Molecule BMP Inhibitor Promotes Neurogenesis of hiPSCs: Comparison of PAX6 and SOX1 Expression during Neural Induction. ACS Chem Neurosci *3*, 482-491.

Neirinckx, V., Coste, C., Rogister, B., and Wislet-Gendebien, S. (2013). Concise review: adult mesenchymal stem cells, adult neural crest stem cells, and therapy of neurological pathologies: a state of play. Stem Cells Transl Med *2*, 284-296.

Pang, Z.P., Yang, N., Vierbuchen, T., Ostermeier, A., Fuentes, D.R., Yang, T.Q., Citri, A., Sebastiano, V., Marro, S., Sudhof, T.C., *et al.* (2011). Induction of human neuronal cells by defined transcription factors. Nature *476*, 220-223.

Roztocil, T., Matter-Sadzinski, L., Alliod, C., Ballivet, M., and Matter, J.M. (1997). NeuroM, a neural helix-loop-helix transcription factor, defines a new transition stage in neurogenesis. Development *124*, 3263-3272.

Sarbassov, D.D., Guertin, D.A., Ali, S.M., and Sabatini, D.M. (2005). Phosphorylation and regulation of Akt/PKB by the rictor-mTOR complex. Science *307*, 1098-1101.

Shimada, T., Takai, Y., Shinohara, K., Yamasaki, A., Tominaga-Yoshino, K., Ogura, A., Toi, A., Asano, K., Shintani, N., Hayata-Takano, A., *et al.* (2012). A simplified method to generate serotonergic neurons from mouse embryonic stem and induced pluripotent stem cells. J Neurochem *122*, 81-93.

Sun, Y., Yong, K.M., Villa-Diaz, L.G., Zhang, X., Chen, W., Philson, R., Weng, S., Xu, H., Krebsbach, P.H., and Fu, J. (2014). Hippo/YAP-mediated rigidity-dependent motor neuron differentiation of human pluripotent stem cells. Nat Mater *13*, 599-604.

Surmacz, B., Fox, H., Gutteridge, A., Lubitz, S., and Whiting, P. (2012). Directing Differentiation of Human Embryonic Stem Cells Toward Anterior Neural Ectoderm Using Small Molecules. Stem Cells *30*, 1875-1884.

Takahashi, K., Tanabe, K., Ohnuki, M., Narita, M., Ichisaka, T., Tomoda, K., and Yamanaka, S. (2007). Induction of pluripotent stem cells from adult human fibroblasts by defined factors. Cell *131*, 861-872.

Thomson, J.A., Itskovitz-Eldor, J., Shapiro, S.S., Waknitz, M.A., Swiergiel, J.J., Marshall, V.S., and Jones, J.M. (1998). Embryonic stem cell lines derived from human blastocysts. Science *282*, 1145-1147.

Watanabe, K., Ueno, M., Kamiya, D., Nishiyama, A., Matsumura, M., Wataya, T., Takahashi, J.B., Nishikawa, S., Muguruma, K., and Sasai, Y. (2007). A ROCK inhibitor permits survival of dissociated human embryonic stem cells. Nat Biotechnol *25*, 681-686.

Yang, C., Tibbitt, M.W., Basta, L., and Anseth, K.S. (2014). Mechanical memory and dosing influence stem cell fate. Nat Mater *advance online publication*.

Zhang, H., Deo, M., Thompson, R.C., Uhler, M.D., and Turner, D.L. (2012). Negative regulation of Yap during neuronal differentiation. Dev Biol *361*, 103-115.

Zhang, Y., Pak, C., Han, Y., Ahlenius, H., Zhang, Z., Chanda, S., Marro, S., Patzke, C., Acuna, C., Covy, J.*, et al.* (2013). Rapid single-step induction of functional neurons from human pluripotent stem cells. Neuron *78*, 785-798.

Zhao, B., Li, L., Tumaneng, K., Wang, C.Y., and Guan, K.L. (2010). A coordinated phosphorylation by Lats and CK1 regulates YAP stability through SCF(beta-TRCP). Genes Dev *24*, 72-85.

Zhao, B., Tumaneng, K., and Guan, K.L. (2011). The Hippo pathway in organ size control, tissue regeneration and stem cell self-renewal. Nat Cell Biol *13*, 877-883.

Zhao, B., Ye, X., Yu, J., Li, L., Li, W., Li, S., Lin, J.D., Wang, C.Y., Chinnaiyan, A.M., Lai, Z.C.*, et al.* (2008). TEAD mediates YAP-dependent gene induction and growth control. Genes & development *22*, 1962-1971.

Chapter 3

Angiomotin regulates YAP localization during neuronal differentiation

3.1 Abstract

Fully leveraging the extraordinary potential of human pluripotent stem (hPS) cells requires a thorough understanding of the signal inputs that influence their cell fate decisions. A key developmental signal is substrate elasticity, a signal that can be transduced in hPS cells via Yes-associated protein (YAP), as we previously described. Cells introduced onto surfaces mimicking brain elasticity exclude YAP from their nuclei and differentiate to neurons. How YAP localization is controlled during neuronal differentiation, however, has been elusive. Here, I employed CRISPR/Cas9 to tag endogenous YAP in hPS cells, and used this fusion protein to analyze YAP's interaction partners during differentiation. The data reveal that angiomotin (AMOT) regulates YAP localization during differentiation. AMOT expression increases during neuronal differentiation, and overexpression of AMOT in hPS cells leads to nuclear exclusion of YAP. Our findings indicate that AMOT-dependent regulation of YAP helps direct hPS cell fate. Thus, they further reveal the molecular mechanisms by which pliable microenvironments induce neuronal differentiation.

3.2 Introduction

As described in Chapter 1, hPS cells integrate a variety of signal inputs that govern their decision to either self-renew or differentiate. These signals include soluble factors, such as growth factors and small molecules (Chen et al., 2014), neighboring cells (Li et al., 2012), and insoluble cues, such as the extracellular matrix composition and rigidity (Klim et al., 2010; Murphy et al., 2014; Wrighton et al., 2014). Matrix rigidity influences the cell fate of adult stem cells (Dupont et al., 2011; Engler et al., 2006; Saha et al., 2008; Yang et al., 2014), and the elasticity (or rigidity) of an hPS cell's microenvironment can serve as a potent signal to self-renew or differentiate (Musah et al., 2012; Musah et al., 2014; Sun et al., 2014). As was described in Chapter 2 when hPS cells are introduced to microenvironments with elasticities comparable to human brain tissue, they efficiently differentiate to neurons—without requiring the addition of soluble neurogenic factors (Musah et al., 2014). The transcriptional coactivator Yes-associated protein (YAP) can mediate responses to substrate stiffness in mesenchymal stem cells (Dupont et al., 2011), and YAP is also a key mediator of mechanotransduction in hPS cells. When hPS cells are cultured on a rigid surface, such as polystyrene or glass, YAP localizes to the nucleus and hPS cells self-renew (Musah et al., 2012). In contrast, when cells are cultured on soft substrates or with small molecule inhibitors of F-actin polymerization, YAP translocates out of the nucleus and the cells differentiate to neurons (Musah et al., 2014). Knockdown of YAP in cells on rigid surfaces induces neuronal differentiation, phenocopying the cells grown on soft surfaces or cells with disrupted F-actin polymerization.

In addition to its role in mechanotransduction, YAP participates in an array of cellular processes including Hippo signaling, tissue homeostasis, cancer stem cell reprogramming, and growth factor signaling (Piccolo et al., 2014). While there has been substantial progress in characterizing the regulation of YAP in the aforementioned contexts, YAP regulation in the context of hPS cell fate remains unclear. This knowledge gap is notable given that YAP helps

maintain the pluripotency of mammalian pluripotent stem cells. In mouse embryonic stem cells, knockdown of YAP led to loss of pluripotency factors OCT4 and SOX2 and consequent differentiation (Lian et al., 2010). In hPS cells, YAP/TAZ-SMAD2/3 complexes engage with TEAD transcription factors and OCT4 to help maintain pluripotency (Beyer et al., 2013). YAP is additionally involved in promoting self-renewal of neural stem cells (NSCs), though its regulation in these cells is also not well understood. In the developing chick neural tube, YAP gain of function significantly expanded the neural progenitor pool in a TEAD-dependent manner (Cao et al., 2008). Repression of YAP/TEAD target genes led to cell cycle exit and premature neuronal differentiation. Similar results were observed for NSCs in the mouse embryonic brain (Han et al., 2015). YAP induction has also been shown to reprogram terminally differentiated neurons into NSCs (Panciera et al., 2016). Transient expression of YAP in the neurons was sufficient to induce NSCs, in which self-renewal was autonomously maintained.

Given YAP's many fundamental roles in development and disease, I sought to better understand the molecular mechanisms regulating YAP subcellular localization in hPS cells during self-renewal or differentiation. To identify proteins that interact with YAP in hPS cells, I employed CRISPR/Cas9 to generate an hPS cell line in which YAP is tagged, thus facilitating affinity purification of endogenous-level YAP complexes for analysis. This strategy uncovered proteins that interact with YAP during self-renewal and differentiation, and pointed to angiomotin (AMOT) as a key regulator of YAP localization during neuronal differentiation.

3.3 Results

3.3.1 CRISPR/Cas9 generation of an hPS cell line with tagged YAP

We employed CRISPR/Cas9 and took advantage of homology-directed repair to engineer the H9 human embryonic stem cell line to produce a C-terminal 3xFLAG-tagged YAP (Figure 3-1A). After puromycin selection and clone screening, we isolated a clone in which the introduced tag was present in both alleles (Figure S3-1A). In this YAP-FLAG cell line, the FLAG tag was

universally expressed and fully coincident with YAP staining (Figure 3-1B). The fusion protein also retained proper localization in response to mechanical cues: YAP-FLAG was present in the nucleus on rigid surfaces; the fusion protein was detected in the cytoplasm on soft surfaces (Figure S3-1B). The addition of latrunculin A, an F-actin polymerization inhibitor which mimics the mechanoresponse to soft surfaces, also resulted in YAP-FLAG detection in the cytoplasm (Figure S3-1B). The YAP-FLAG cell line allowed for highly specific affinity purification of YAP with anti-FLAG magnetic beads (Figure 3-1C). Moreover, YAP co-purified with well characterized binding partners, including the TEAD transcription factors and 14-3-3 adaptor proteins (Figure 3-1C). Therefore, application of CRISPR/Cas9 afforded an hPS cell line in which a tagged YAP is produced from its endogenous genomic locus, and thus facilitating affinity purification of endogenous-level YAP complexes.

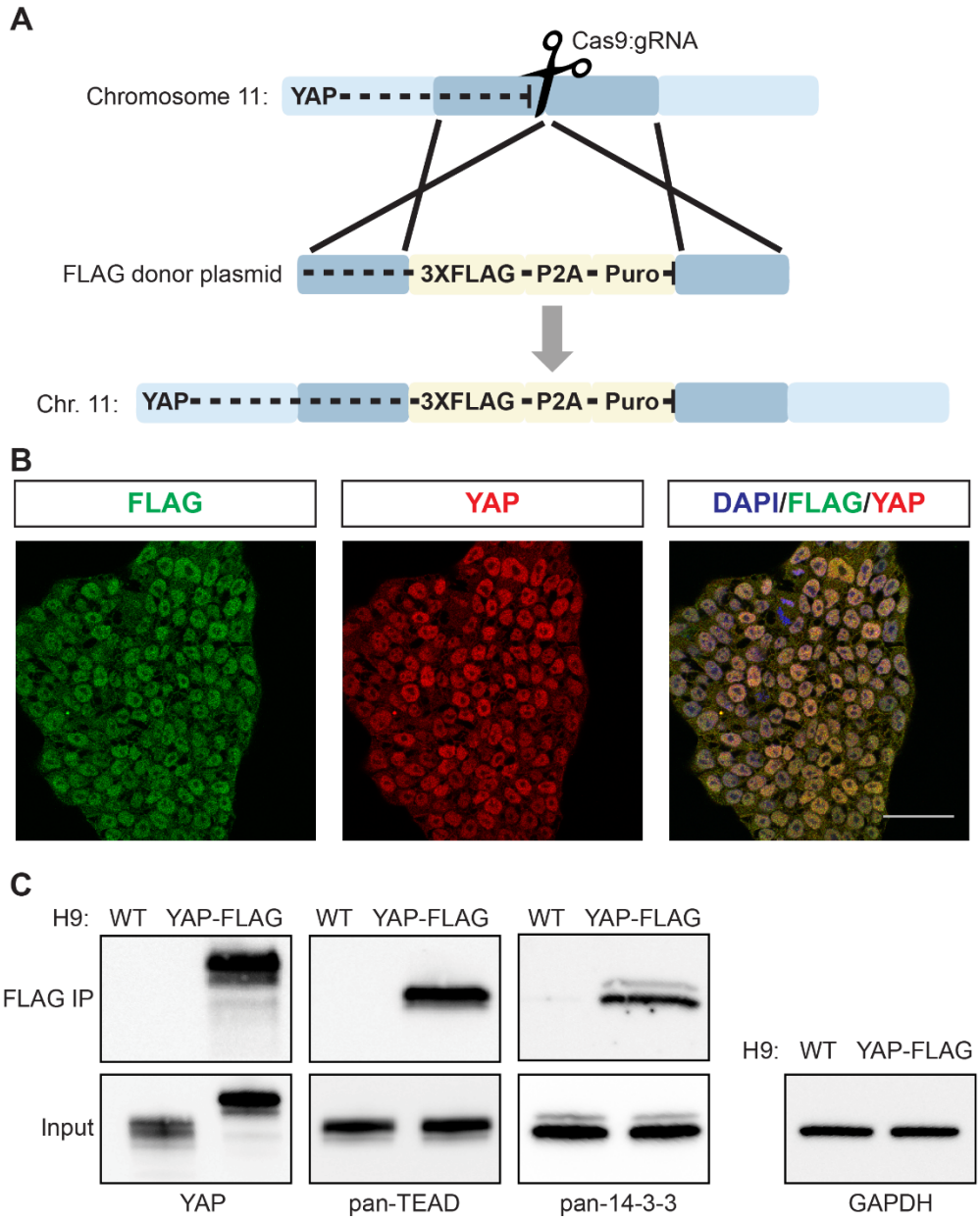

Figure 3-1: CRISPR/Cas9-mediated editing enables generation of an hPS cell line in which FLAG-tagged YAP is produced from its native chromosomal locus.

(A) Scheme for the generation of the 3xFLAG-tagged YAP hPS cell line (H9) using CRISPR/Cas9 and homology-directed repair.

(B) YAP subcellular localization in H9 YAP-FLAG cell line. Scale bar, 50 μm.

(C) Top: Immunoblots from FLAG co-immunoprecipitation with H9 WT and H9 YAP-FLAG cell lines. Bottom: IP input.

3.3.2 YAP-AMOT interaction is enhanced during neuronal differentiation

The YAP-FLAG cell line was used for affinity purification-mass spectrometry (AP-MS) to characterize the proteins YAP interacts with in hPS cells during self-renewal and neuronal differentiation (Figure 3-2A). As expected, immunoprecipitation from undifferentiated H9 cells with anti-FLAG magnetic beads afforded YAP as the most highly enriched protein in YAP-FLAG cells relative to wildtype cells (Table S3-1). Other enriched proteins included both previously characterized YAP binding partners (e.g., PTPN14, TEAD1-4, and 14-3-3 proteins) (Yu and Guan, 2013), as well as novel interactors (e.g., ARID3B and SALL4) (Figure 3-2B and Table S3-1). To determine the interactors regulating YAP localization during neuronal differentiation, we examined which interacting partners change as cells differentiate. As YAP is expressed in NSCs but not in neurons, we monitored cells at the initial stages of a small molecule-based neuronal differentiation protocol (Davis-Dusenbery et al., 2014) for NSC markers. After 6 days of dual inhibition of the SMAD signaling pathways, the majority of the cells expressed PAX6 and/or SOX1, markers of NSC state (Figure 3-2C). We then used AP-MS to compare YAP's binding partners in differentiated cells with those in undifferentiated cells. During the differentiation, the most significant increase among YAP's protein interaction network was with AMOT (Figure 3-2D and Table S3-2). These results suggest that AMOT is involved in regulating YAP during neuronal differentiation.

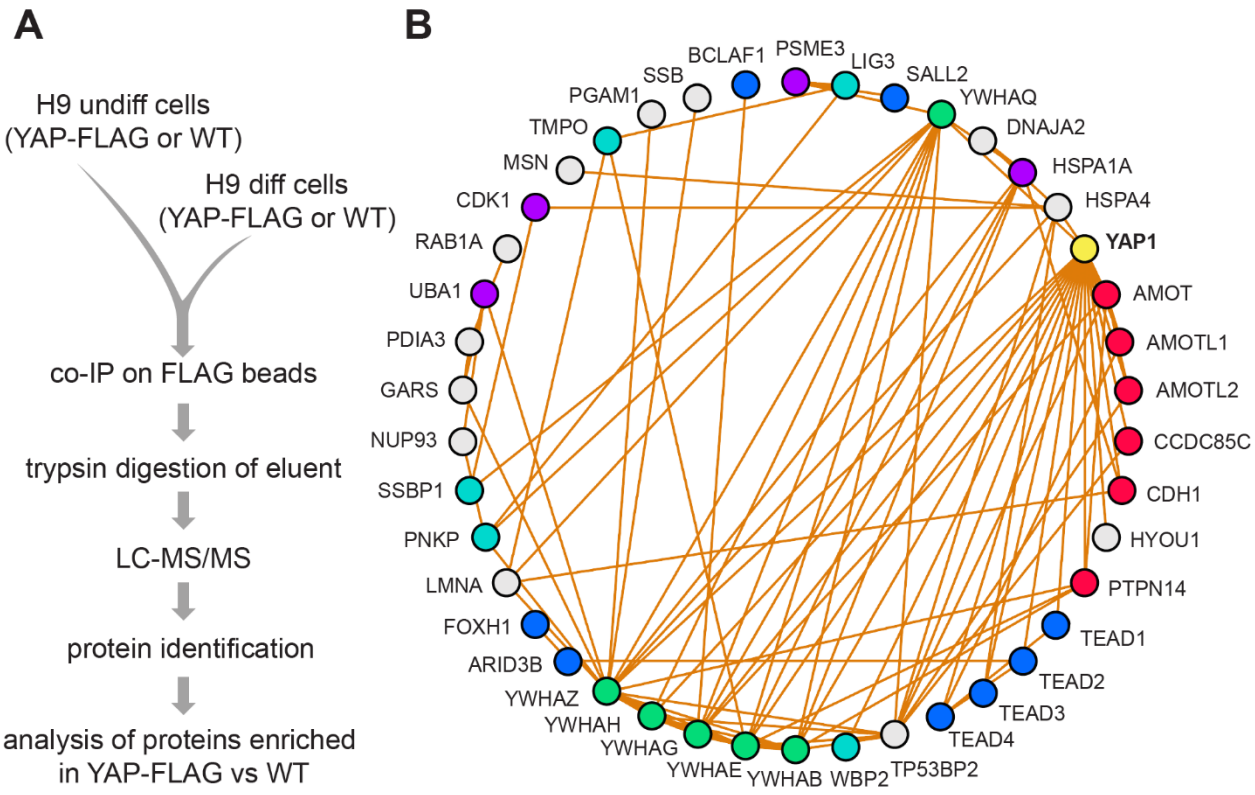

D

Gene name	Description	p-value	H9 YAP-flag undiff	H9 YAP-flag diff	H9 WT diff
AMOT	Angiomotin	< 0.00010	1	28	0
HSPA1A	Heat shock 70 kDa protein 1A/1B	< 0.00010	16	57	11
TMPO	Lamina-associated polypeptide 2	< 0.00010	15	2	4
TP53BP2	Apoptosis-stimulating of p53 protein 2	0.00023	1	10	0
UGDH	UDP-glucose 6-dehydrogenase	0.00024	0	7	1

Figure 3-2: AMOT interaction with YAP increases during neural differentiation

(A) Diagram of affinity purification-mass spectrometry for YAP-FLAG.

(B) Graphic representations of the top proteins enriched in FLAG co-IP from H9 YAP-FLAG cells. Edges denote previously characterized interactions. Node colors represent protein groupings as follows: yellow—bait (YAP-FLAG); red—junction proteins; blue—transcription factors; teal—DNA binding proteins; green—14-3-3 proteins; purple—ubiquitin-proteasome pathway.

(C) H9 YAP-FLAG cells differentiated to PAX6 and/or $SOX1^{+}$ neural progenitor cells.

(D) Top 5 protein interactions with YAP-FLAG that significantly increased or decreased during neural differentiation (H9 YAP-FLAG diff vs H9 YAP-FLAG undiff, H9 WT diff is control).

Scale bar, 50 μm.

3.3.3 AMOT upregulation and YAP downregulation during neuronal differentiation

Since we detected an increase in YAP-AMOT complexes during differentiation, we examined if the level of AMOT increases. AMOT was produced at low levels in hPS cells, but protein levels progressively increased as cells differentiated to the NSC and neuronal states (Figure 3-3A). AMOT has two paralogs, angiomotin-like 1 and -like 2 (AMOTL1 and AMOTL2). AMOTL1 and AMOTL2 are also expressed in H9-derived NSCs, however, at lower levels than AMOT, and only AMOT protein levels significantly increased in differentiated cells (Figure 3-3B). In NSCs, AMOT localized to tight junctions with both F-actin and YAP (Figures 3-3C and S3-2A). To examine AMOT and YAP dynamics during neuronal differentiation, we generated a stable H9 cell line harboring an inducible system in which expression of *Neurog2* drives neuronal differentiation (Figure S3-2B) (Zhang et al., 2013). By 12 hours following doxycycline induction, AMOT was upregulated and YAP was excluded from the nuclei of differentiated neuronal cells and downregulated (Figures 3-3D and S3-2C-D). Accordingly, expression of *CTGF*—a well characterized YAP target gene, including in hPS cells (Musah et al., 2014)—significantly decreased (Figure S3-2D).

Our detection of AMOT upregulation during neuronal differentiation of hPS cells, led us to hypothesize that a similar upregulation may occur during differentiation of adult mammalian NSCs. One of the main sites of adult neurogenesis occurs in the subgranular zone (SGZ) of the dentate gyrus (Eriksson et al., 1998). NSCs residing in the SGZ differentiate to intermediate neural progenitors, which migrate and eventually give rise to hippocampal granule neurons (Yu et al., 2014). YAP was expressed in NSCs in the SGZ of the mouse dentate gyrus and YAP levels were lower in differentiated cells with increased AMOT expression (Figure S3-2E). Taken together, these data indicate that AMOT expression increases as cells differentiate to NSCs and neurons, while YAP is excluded from nuclei and downregulated.

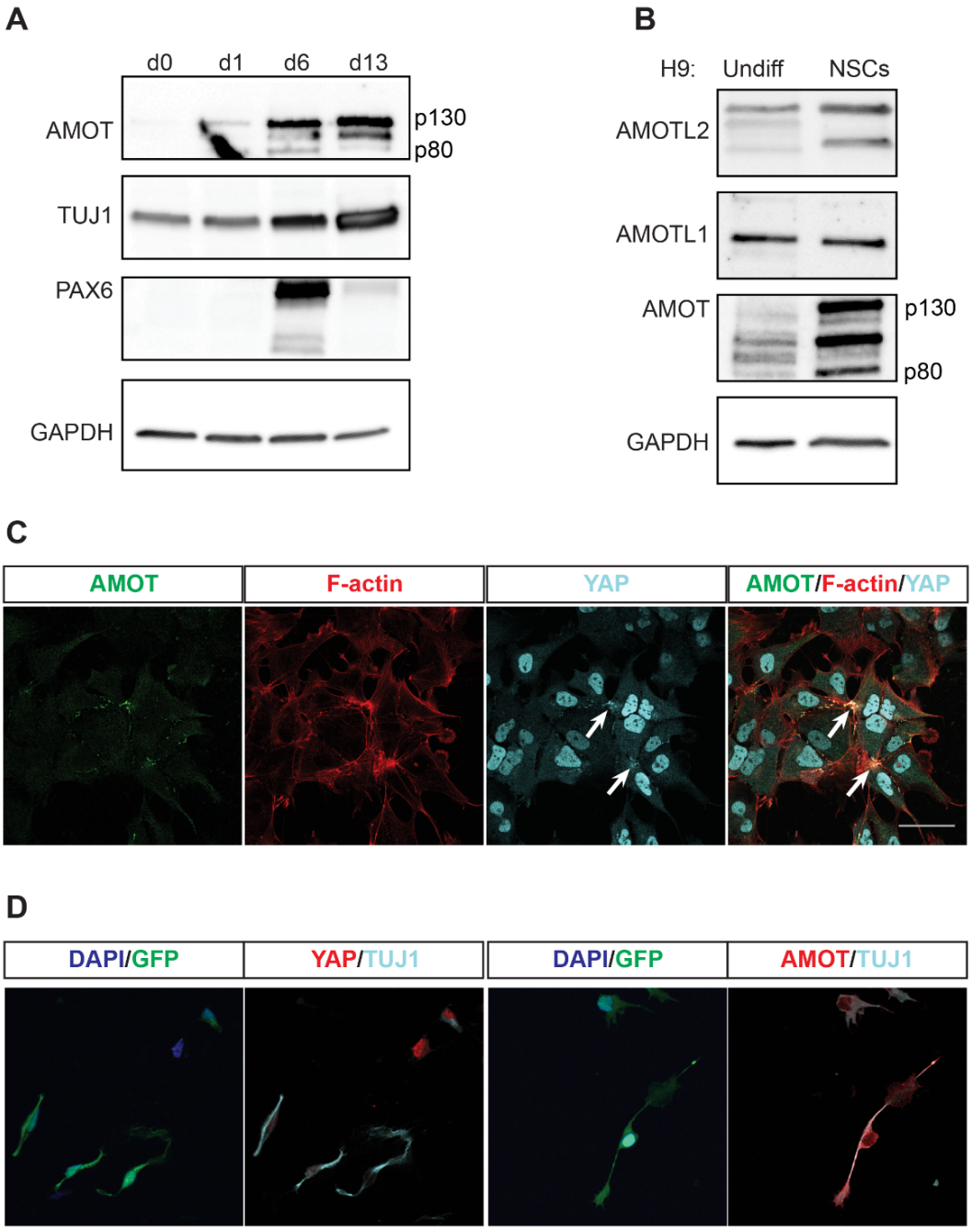

Figure 3-3: AMOT expression increases, while YAP is downregulated during neuronal differentiation

(A) Protein levels of AMOT, neuronal marker β-tubulin III (TUJ1), and NSC marker PAX6 during neuronal differentiation from H9 cells.

(B) Protein levels of AMOT, AMOTL1, and AMOTL2 in undifferentiated H9 cells vs H9-derived NSCs.

(C) Subcellular localization of AMOT, F-actin, and YAP in H9-derived NSCs. Filled arrows point out sites of co-localization.

(D) Expression of YAP and TUJ1 (left) or AMOT and TUJ1 (right) in Neurog2-T2A-GFP H9 cells, 12 hours after induction.

Scale bar, 50 μm.

3.3.4 AMOT regulates YAP localization in hPS cells

Because an increase in AMOT expression was associated with YAP nuclear exclusion during differentiation, we examined if AMOT mediates this process directly. AMOT has two main isoforms: p130 which contains binding sites for F-actin and YAP, and p80 which lacks these sites (Zhao et al., 2011). Forced expression of p130, but not p80, resulted in YAP nuclear exclusion (Figure 3-4A). Since F-actin depolymerization triggers YAP nuclear exclusion (Figure S3-1B) and promotes neuronal differentiation (Musah et al., 2014), we hypothesized that a reduction in F-actin would lead to increased AMOT-p130 interaction with YAP. Indeed, treatment with actin polymerization inhibitor latrunculin A had no effect on YAP interactions with the p80 AMOT isoform. In contrast, we detected a time-dependent increase in the interaction of AMOT-p130 with YAP (Figure 3-4B).

We also examined the effects of downregulating AMOT on YAP localization. Because AMOTL1 is also expressed in hPS cells and like AMOT contains F-actin and YAP binding sites, we employed inducible short hairpin RNAs to downregulate both proteins. *CTGF* expression was used as a readout of YAP nuclear localization. Knockdown of either AMOT-p130 or AMOTL1 increased YAP nuclear localization, while knockdown of AMOT-p80 had no affect (Figure S3-3A-C). If actin polymerization regulates YAP localization through AMOT, then knockdown of AMOT should rescue YAP nuclear localization in latrunculin A-treated cells. Cells treated with latrunculin A afforded a significant decrease in YAP nuclear localization, but concomitant knockdown of AMOT-p130 and AMOTL1 rescued YAP localization. In contrast, knockdown of

AMOT-p80, which cannot bind YAP, had no affect (Figure 3-4C). These results indicate that AMOT regulates YAP localization in hPS cells in response to the status of the cell's cytoskeleton.

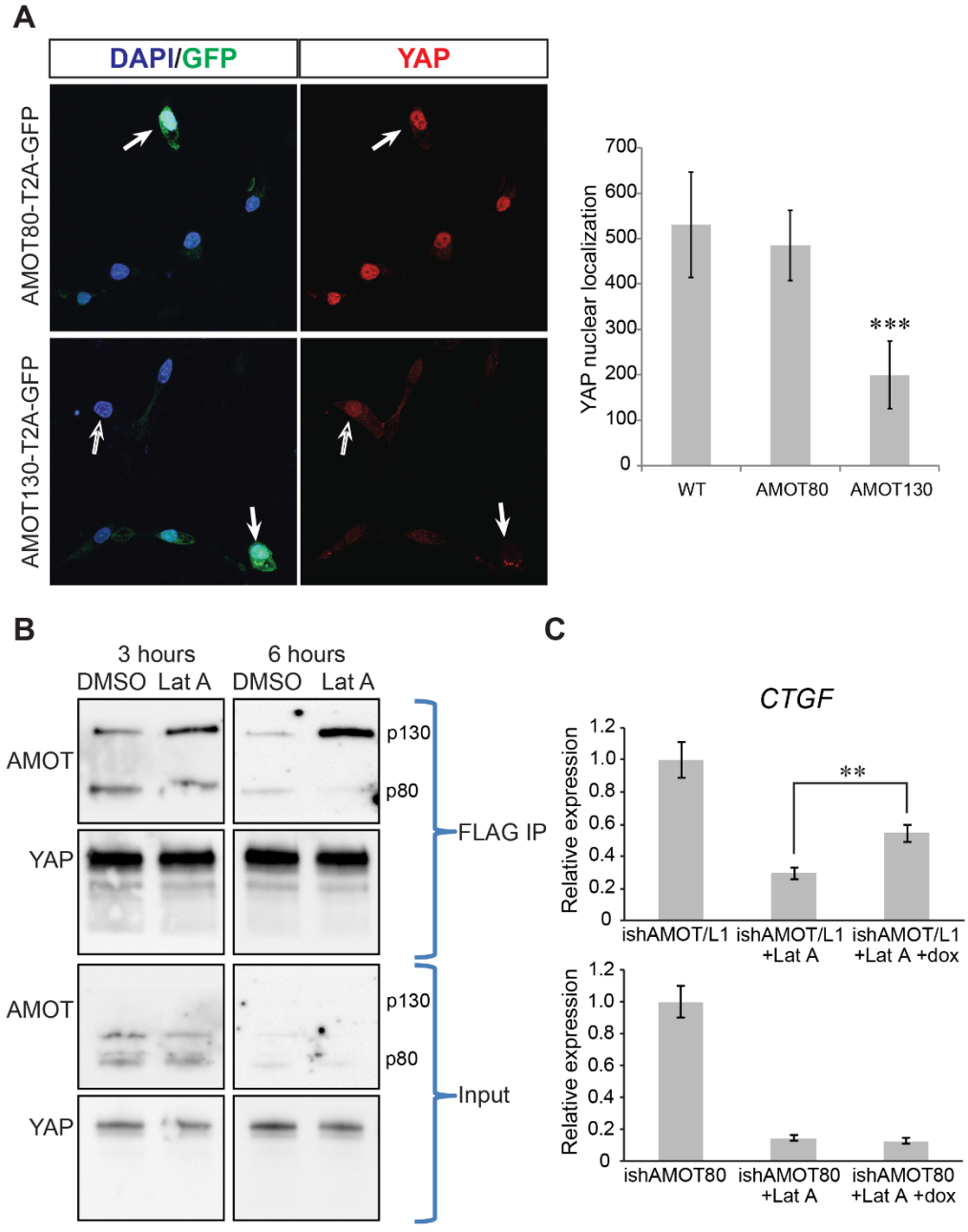

Figure 3-4: AMOT-p130 control of YAP localization in hPS cells in response to the actin cytoskeleton

(A) Left: Subcellular localization of YAP in AMOT130-T2A-GFP H9 cells (top) or AMOT80-T2A GFP H9 cells (bottom), 24 hours after induction. Filled arrows indicate cells producing

AMOT/GFP, hollow arrows indicate cells that fail to produce AMOT/GFP. Right: quantification of YAP nuclear localization (n=30 cells).

(B) Top: Immunoblots of FLAG co-immunoprecipitation after 3 and 6 hours of DMSO or 1 μM latrunculin A treatment. Bottom: IP input.

(C) Transcript levels of *CTGF* following hPS cell (H9) treatment with 1 μM latrunculin A, +/- dox-inducible knockdown of both AMOT130 and AMOTL1 (top), or AMOT80 (bottom).

Data are presented as the mean ± SEM, n=3, **p < 0.005, ***p < 0.0001. Scale bar, 50 μm.

3.4 Discussion

We previously reported that pliable microenvironments induce neuronal differentiation of hPS cells via nuclear exclusion of YAP. While we had linked F-actin polymerization status to YAP subcellular localization, the mechanism underlying the influence of the actin cytoskeleton on YAP localization remained unclear. In the present study, we found that during neuronal differentiation AMOT protein levels increase as does binding to YAP, which inhibits its nuclear translocation. Inhibition of F-actin polymerization, which promotes neuronal differentiation, increases the extent of AMOT-YAP interactions (Figure 3-5). These results suggest that AMOT acts as a link between the actin cytoskeleton state and YAP subcellular localization during neuronal differentiation.

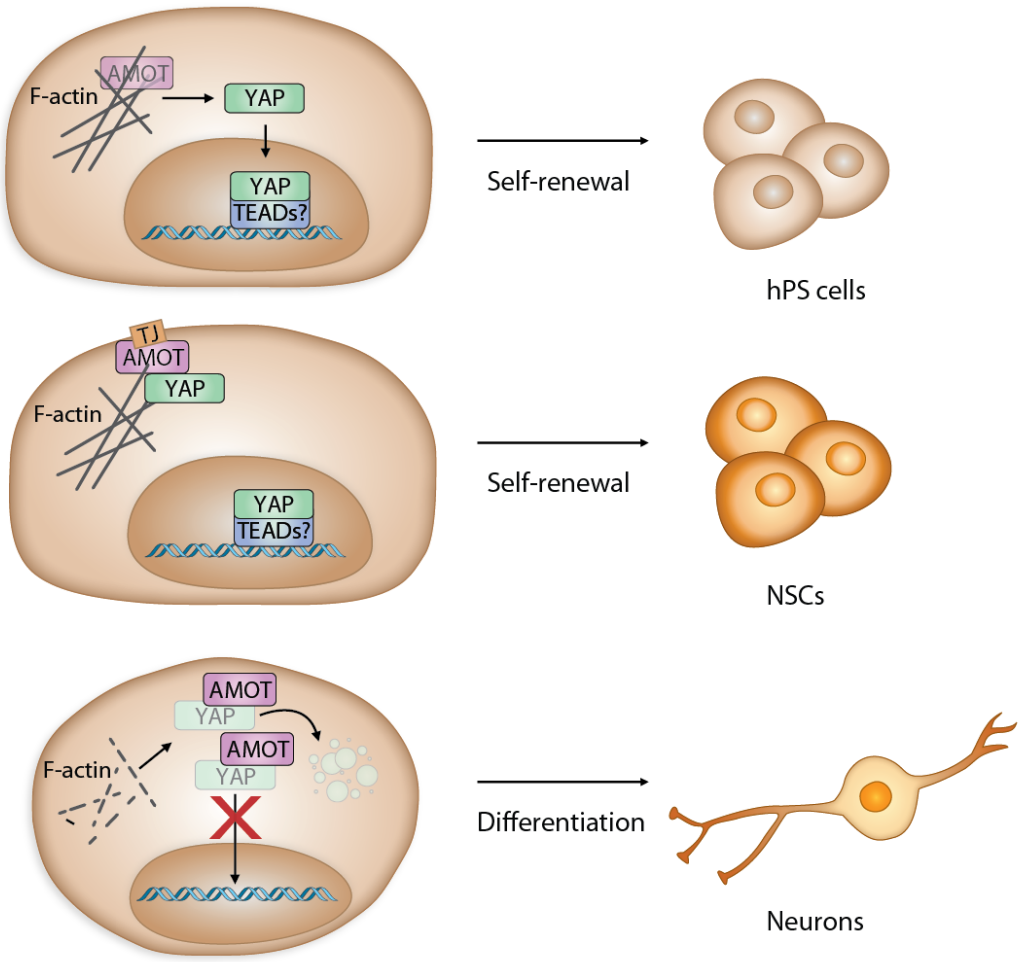

Figure 3-5: Proposed mechanism for AMOT-mediated regulation of YAP during neuronal differentiation. In hPS cells grown in stiff microenvironments, there are robust F-actin structures which bind to and sequester AMOT, which is expressed at low levels in undifferentiated cells. YAP therefore localizes to the nucleus where it helps regulate self-renewal. During neuronal differentiation, AMOT expression increases and binds YAP. In NSCs, AMOT sequesters YAP at tight junctions and a pool of nuclear YAP remains where it regulates self-renewal of NSCs. During initiation of neuronal commitment, tight junctions fall apart and AMOT expression further increases. In soft microenvironments, F-actin polymerization is reduced, thus liberating AMOT. These events enable AMOT to sequester YAP in the cytoplasm where YAP is proteasomally degraded. Absence of YAP from the nucleus helps to lift repression of neuronal differentiation. TJ: tight junction

Our identification of AMOT-dependent regulation of YAP during neuronal differentiation was facilitated by performing AP-MS on endogenously tagged YAP. This strategy for affinity purification of YAP complexes afforded several advantages over previous attempts. Methods which employ an antibody against YAP can suffer from lack of specificity, as most antibodies used for immunoprecipitation also recognize the paralogous TAZ protein. Exogenous expression of a tagged YAP construct also has disadvantages, as expression levels will likely differ from those of the endogenous protein and thus may not be representative of physiologically relevant interactions. Furthermore, YAP has 8 alternatively-spliced isoforms (Gaffney et al., 2012), and picking just one isoform for expression can miss isoform-specific interactions, which have been documented for YAP (Finch-Edmondson et al., 2016). Our system overcomes these challenges by tagging the endogenous protein, including all of its isoforms, and capturing it using magnetic beads conjugated to a highly specific antibody against the FLAG tag (Brizzard et al., 1994). Notably, our use of an hPS cell line also allowed to uncover YAP interactors in a cell line that is non-transformed, diploid, and clonal, whereas previous methods employed transformed cell lines (Couzens et al., 2013; Kohli et al., 2014; Wang et al., 2014b).

We observed that during differentiation AMOT sequesters YAP at tight junction sites in NSCs. Tight junctions not only form permeability barriers in cells, but also act as signaling platforms: They have been implicated in regulating the actin cytoskeleton, cell proliferation, and differentiation. For example, cingulin, a junctional adaptor, recruits the guanine nucleotide exchange factor GEFH1 (also known as ARHGEF2) to tight junctions, thus inhibiting RhoA signaling (Aijaz et al., 2005). Together, RhoA and GEFH1 regulate the actin cytoskeleton and focal adhesion formation; as such, they are also integral to cellular responses to changes in mechanical forces (Guilluy et al., 2011). Another example is illustrated by the tight junction protein, ZO-1, which regulates the subcellular localization of the ZO-1-associated nucleic acid binding protein (ZONAB) (Balda and Matter, 2000). ZONAB (also known as YBX3) is a Y box

transcription factor that determines when epithelial cells switch from a proliferative to a differentiated state (Lima et al., 2010). These observations along with our findings point to tight junctions as playing a key role in mechanosensing, and suggest that tight junction-mediated regulation of cell differentiation may be a more general phenomenon.

AMOT has previously been identified to regulate YAP in several biological contexts. In epithelial and endothelial cells, AMOT, along with its paralogs AMOTL1 and AMOTL2, localize to tight junctions and regulate apical-basal polarity (Moleirinho et al., 2014). All three AMOT proteins, with the exception of AMOT-p80, contain PPXY motifs that bind to the WW-domains of YAP (Zhao et al., 2011). These AMOT proteins also contain a separate F-actin binding domain that has been found in HEK293 and MCF10A cells to serve as a link between the actin cytoskeleton and YAP subcellular localization (Mana-Capelli et al., 2014). AMOT has also recently been found to regulate YAP localization in endothelial cells in response to sheer stress (Nakajima et al., 2017), but a role for AMOT in sensing substrate elasticity had not been described. This study demonstrates a novel role for AMOT in regulating YAP subcellular localization during hPS cell mechanosensing, as well as differentiation.

Considering the important roles that tissue mechanics and YAP play in cancer (Huang and Ingber, 2005; Moroishi et al., 2015), and the similarities between embryonic development and tumorigenesis (Aiello and Stanger, 2016), an attractive idea is that AMOT-dependent regulation of YAP is relevant to both processes. Our preliminary observations in mouse brain tissue suggest that AMOT regulates YAP during adult neurogenesis. It would be intriguing to assess whether these observations extend to brain tumorigenesis. Though AMOT had not been previously implicated in neural differentiation, AMOT has been linked to neural cancers. AMOT—the p130 isoform in particular—is upregulated in dormant versus fast-growing glioblastomas (Almog et al., 2009). YAP also is upregulated in human brain cancers and promotes glioblastoma growth (Orr et al., 2011). Our observations of AMOT-YAP interactions are consistent with a model in

which concurrent upregulation of AMOT in dormant glioblastomas results in AMOT sequestering YAP away from the nucleus, thereby inhibiting proliferation.

Several novel YAP interactors that we identified in undifferentiated cells point to a role for nuclear YAP in not only promoting self-renewal, but also in actively inhibiting differentiation. Specifically, during neuronal differentiation we detected a decrease in YAP complexes containing either the ARID3B or SALL4 transcription factors. ARID3B belongs to an AT-rich interaction domain (ARID) family of DNA binding proteins. ARID3B controls several genes responsible for pluripotency in hPS cells (Liao et al., 2016). In cancer cells, *ARID3B* expression results in the downregulation of genes associated with neuron development (Bobbs et al., 2015). SALL4 is a member of the *spalt*-like (SALL) C2H2-type zinc-finger transcription factors also involved in pluripotency. Specifically, SALL4 was recently shown in embryonic stem cells to contribute to maintaining pluripotency by preventing activation of neural development genes (Miller et al., 2016). Importantly, in addition to its role as a coactivator, YAP is also known to function as a transcriptional corepressor (Kim et al., 2015). Therefore, YAP's interaction with these transcription factors suggests a potential mechanism for how nuclear YAP represses neuronal differentiation in hPS cells.

We observed that increased AMOT levels during neuronal differentiation helped to drive YAP out of the nucleus, and subsequently YAP protein levels decreased. YAP is known to be targeted for degradation in the cytoplasm by the ubiquitin-proteasome pathway (Zhao et al., 2010). Accordingly, we observed that in undifferentiated cells YAP interacts with several components of the ubiquitin-proteasome system and that these interactions increased during differentiation. This proteasome-mediated degradation of YAP may serve as an additional mode of regulation to prevent YAP from translocating to the nucleus and repressing the neuronal differentiation program.

3.5 Methods

3.5.1 hES cell culture and differentiation

H9 human embryonic stem cells (WiCell) were maintained on Matrigel GFR (Corning)-coated tissue culture plastic plates in mTeSR1 medium (Stem Cell Technologies). Cells were passaged every 4-5 days using EDTA with the addition of 5 μM Y-27632 dihydrochloride (Tocris) during the first day. H9-derived NSCs (Han et al., 2009) (WiCell) were maintained on Matrigel GFR-coated plates in Neurobasal medium supplemented with 1x B27, 1x GlutaMAX, 1x MEM NEAA (all Gibco), and 10 ng/mL β-FGF (Waisman Biomanufacturing). NSCs were passaged every 3 days using StemPro Accutase (Gibco). Neuronal differentiation was performed as previously described (Wrighton et al., 2014). Briefly, on d-1 H9 cells (YAP FLAG or WT) were seeded on Matrigel-coated tissue culture plates at 200,000 cells/cm^2 in mTeSR1 medium supplemented with 5 μM Y-27632 dihydrochloride. On d0 through d5 the medium was changed to N2B27 (DMEM/F12:Neurobasal (1:1) supplemented with 1x GlutaMAX, 1x B27 and 1x N2 (all Gibco)) supplemented with 10 μM SB 431542, 100 nM LDN 193189 dihydrochloride, 1 μM SAG, and 1 μM retinoic acid (all Tocris). On d6-d13, the medium was changed to N2B27 supplemented with 1 μM SAG, 1 μM retinoic acid, 4 μM SU 5402, and 1 μM DAPT (all Tocris). Cells were analyzed on either d6 or d13. For evaluating responses to mechanical cues, compliant polyacrylamide hydrogels with 0.7 kPa Young's modulus substituted with vitronectin-derived heparin binding peptide (Klim et al., 2010) were synthesized as previously described (Musah et al., 2012). Rigid glass presenting vitronectin-derived heparin binding peptide was generated using the streptavidin-biotinylated peptide approach previously described (Klim et al., 2010). For inhibition of F-actin polymerization, cells were treated for the indicated length with indicated concentrations of latrunculin A (Tocris).

3.5.2 CRISPR/Cas9 genome engineering

For introduction of the FLAG-tag to the 3'end of the *YAP* coding gene, CRISPR/Cas9 genome editing was used. The Neo resistance cassette in pFETCh_Donor plasmid (Savic et al., 2015) (gift from Eric Mendenhall and Richard M. Myers, Addgene plasmid # 63934) was modified to Puro, and 1 kb homology arms targeting the 3'end of *YAP* were inserted to create a pFETCh_YAP plasmid. 2 µM Alt-R S.p. Cas9 Nuclease 3NLS (IDT) was complexed with 2.4 µM duplex consisting of Alt-R CRISPR-Cas9 crRNA (target sequence: TTAGAATTCAGTCTGCCTGA) and tracRNA (IDT) in nucleofection buffer. H9 cells were nucleofected with 5 µg pFETCH_YAP plasmid and the ribonucleoprotein complex using the Human Stem Cell Nucleofector Kit 2 (Lonza) and the B-16 program on the Amaxa Nucleofector II (Lonza) as per manufacturer instructions. Cells were allowed to recover for two days in mTeSR1 medium supplemented with 1x RevitaCell (Gibco) prior to selection with puromycin. Following puromycin selection, clones were derived using serial dilution and analyzed by PCR amplification and Sanger sequencing for correct modification at both alleles.

3.5.3 Lentiviral constructs

For inducible overexpression studies, the transfer plasmid was based on pCW-Cas9 (Wang et al., 2014a) (gift from Eric Lander & David Sabatini, Addgene plasmid # 50661), modified to include T2A-EGFP following Cas9 coding sequence. To construct pCW-Ngn2, Cas9 was replaced with Ngn2 amplified from pTet-O-Ngn2-puro (Zhang et al., 2013) (gift from Marius Wernig, Addgene plasmid # 52047). To construct pCW-AMOT80 or pCW-AMOT130, AMOT p80 or AMOT p130 were amplified from Lenti GFP-AMOT p80 or Lenti GFP-AMOT p130 (Zhao et al., 2011) (both gifts from Kunliang Guan, Addgene plasmids # 32830, 32828).
For inducible knockdown studies, the transfer plasmid was based on pLV-H1TetO-RFP-Puro (Biosettia). The target sequences were as follows: GCCTCCTCTTCTCTTAGTTCT (for

ishAMOT80), GCCACTTCCTAACCAGCATAG (for ishAMOT130), GGAGTTACGAGAGAAGCAAGC (for ishAMOTL1). For the ishAMOTL1 construct, RFP-Puro was replaced with the Neo resistance cassette.

To generate lentivirus, Lenti-X 293T cells (Clontech) were transfected using Lipofectamine 2000 (Invitrogen) with 2.63 μg psPAX2 (gift from Didier Trono, Addgene plasmid #12260), 1.32 μg pMD2.G (gift from Didier Trono, Addgene plasmid #12259), and 4 μg of the transfer plasmid. The medium was collected for 4 days and concentrated using Lenti-X Concentrator (Clontech). Concentrated lentiviral particles were added to H9 cells and selected by appropriate antibiotic selection (G418 and/or puromycin). mTeSR1 medium was supplemented with either 0.5 or 2.5 μg/mL doxycycline hyclate (Sigma-Aldrich) to induce knockdown or overexpression, respectively.

3.5.4 Immunoprecipitation

10 million H9 WT or H9 YAP-FLAG cells (undifferentiated or differentiated) were used for immunoprecipitation. Cell pellets were resuspended in Pierce IP Lysis Buffer (Thermo Fisher) supplemented with 1x Protease Inhibitor Cocktail (Promega) and 1x Halt Phosphatase Inhibitor Cocktail (Thermo Fisher), centrifuged to clarify the supernatant, and passed through 0.45 micron filters. Samples were diluted 2x in 1x Tris-buffered saline (TBS) and incubated with FLAG M2 Magnetic Beads (Sigma-Aldrich) for 2 hours at 4 °C. Beads were subsequently washed three times with wash buffer composed of 35 mM Tris-HCl (pH 7.5), 150 mM NaCl, 0.5 mM Na_2EDTA, 0.5 mM EGTA, 0.5 % Triton, 1.25 mM sodium pyrophosphate, 0.5 mM β-glycerophosphate, 0.5 mM Na_3VO_4, and 0.5 μg/mL leupeptin. Proteins were eluted with 300 ng/μL 3X FLAG peptide (Sigma-Aldrich) in TBS for 45 minutes at room temperature.

3.5.5 Mass spectrometry

Immunoprecipitated protein samples were TCA/acetone precipitated, and then re-solubilized and denatured in 8 M urea / 50 mM NH_4HCO_3 (pH8.5) / 1 mM Tris-HCl. Samples were then reduced, alkylated, and digested with trypsin/Lys-C. Peptides were analyzed by nanoLC-MS/MS using the Agilent 1100 nanoflow system (Agilent) connected to LTQ-Orbitrap Elite (Thermo Fisher Scientific) equipped with an EASY-Spray electrospray source. Chromatography of peptides prior to mass spectral analysis was accomplished using PepMap column (Thermo Fisher Scientific) on a NanoHPLC system. As peptides eluted from the HPLC-column/electrospray source survey MS scans were acquired in the Orbitrap with a resolution of 120,000 followed by MS2 fragmentation of the 20 most intense peptides detected in the MS1 scan from 350 to 1800 m/z; redundancy was limited by dynamic exclusion. Raw MS/MS data were converted to mgf file format using MSConvert (ProteoWizard) for downstream analysis. Resulting mgf files were used to search against the Uniprot Homo sapiens amino acid sequence database with decoy reverse entries and a list of common contaminants using in-house Mascot search engine 2.2.07 [Matrix Science]. Peptide mass tolerance was set at 15 ppm and fragment mass at 0.6 Da. Protein annotations, significance of identification and spectral based quantification was performed on Scaffold (Proteome Software). Protein threshold was set at 2% FDR and the peptide threshold at 1% FDR with a minimum number of 2 identified peptides. Quantitative analysis was carried out using Fisher's Exact Test using the Benjamini-Hochberg correction. Network graph was generated using esyN (Bean et al., 2014).

3.5.6 Immunoblotting

Cells were lysed in RIPA Buffer (Pierce) supplemented with 1x Halt Protease Inhibitor Cocktail and 1x Halt Phosphatase Inhibitor Cocktail (Thermo Fisher). Lysates were resolved by SDS-PAGE and transferred onto a PVDF membrane. The primary antibodies and dilutions used

are described in Table S3. The secondary antibodies used were HRP-conjugated anti-rabbit IgG or anti-mouse IgG (1:10000, Jackson ImmunoResearch). ECL Prime (Amersham) was used for chemiluminescent detection, which was recorded using ImageQuant LAS4000 (GE Healthcare).

3.5.7 Immunostaining

For immunocytochemistry analysis, cells were fixed with 4% formaldehyde and permeabilized with 0.125% Triton X-100. For immunohistochemistry analysis, FFPE 5 micron thick sections from C57BL/6J adult mouse brains were obtained from the RARC pathology lab. Tissues were deparaffinized and subjected to citrate buffer-based antigen retrieval. The primary antibodies and dilutions used are described in Table S3. The secondary antibodies used were Alexa Fluor 488, 594, or 647 anti-mouse, rabbit, chicken, or goat IgG (1:1000, Molecular Probes). Cell nuclei were counterstained with DAPI dilactate (1:10000, Molecular Probes). Confocal microscopy was performed on a Nikon A1R-Si+. Images were analyzed and quantified using Fiji (Schindelin et al., 2012) with the Coloc 2 plugin for nuclear localization quantification.

3.5.8 Quantitative PCR

RNA extraction was performed using RNeasy Plus Mini (QIAGEN) as per manufacturer instructions. RNA was reverse transcribed using iScript cDNA Synthesis Kit (Bio-Rad). qPCR was performed on either the 7500 Fast Real-Time PCR System (Applied Biosciences) or CFX Connect (Bio-Rad) using iTaq Universal SYBR Green Supermix (Bio-Rad). The primer sequences used are described in Table S4. *GAPDH* was used as the reference gene for normalization.

3.5 Supplementary Information

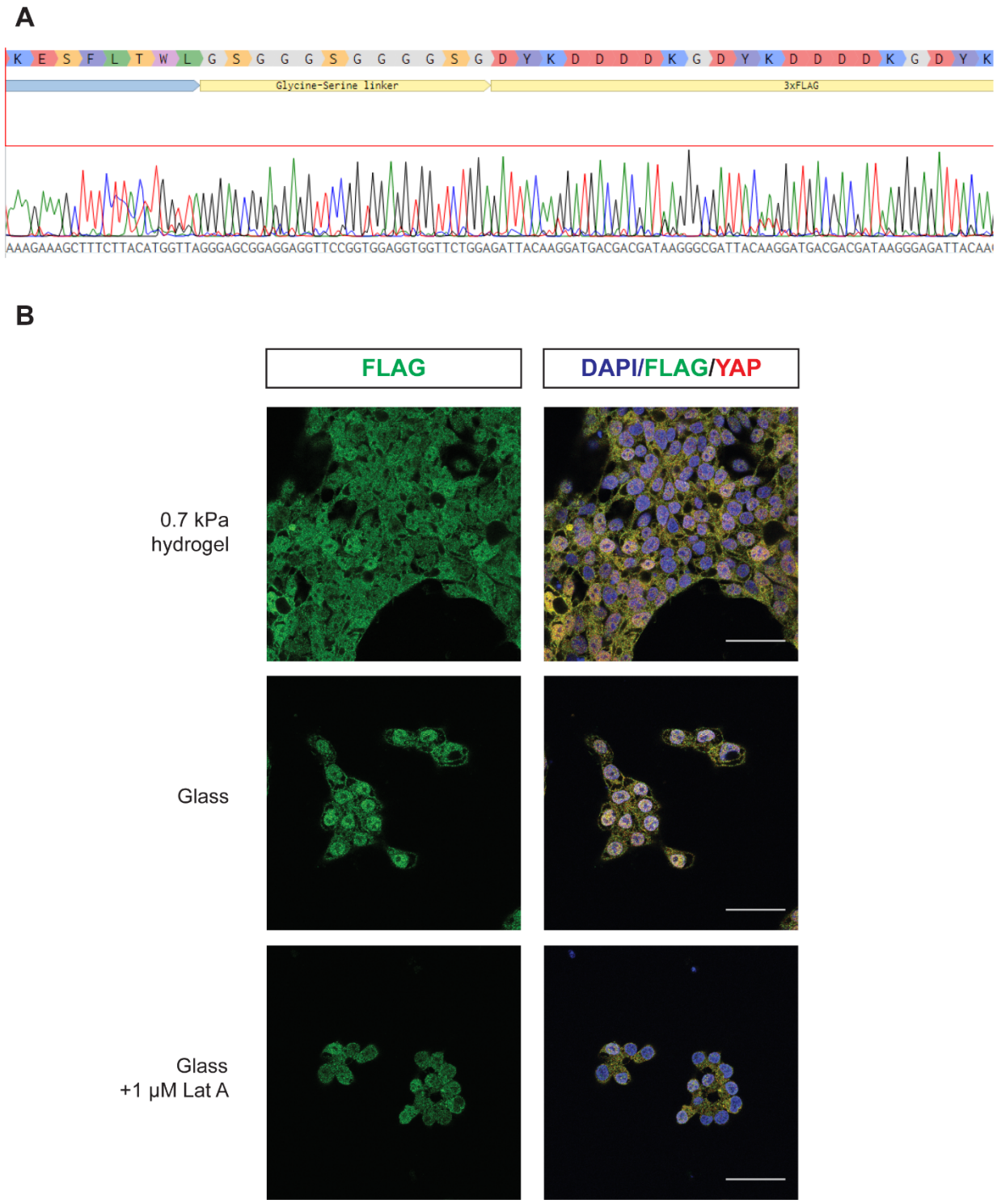

Figure S3-1: Characterization of H9 YAP-FLAG cell line

(A) DNA chromatogram of CRISPR/Cas9-edited region in the H9 YAP-FLAG cell line.

(B) Subcellular localization of YAP-FLAG in H9 YAP-FLAG cells cultured on soft 0.7 kPa hydrogels (top) or on rigid glass without (middle) or with (bottom) 1 μM latrunculin A treatment for 2 hours.

Scale bar, 50 μm.

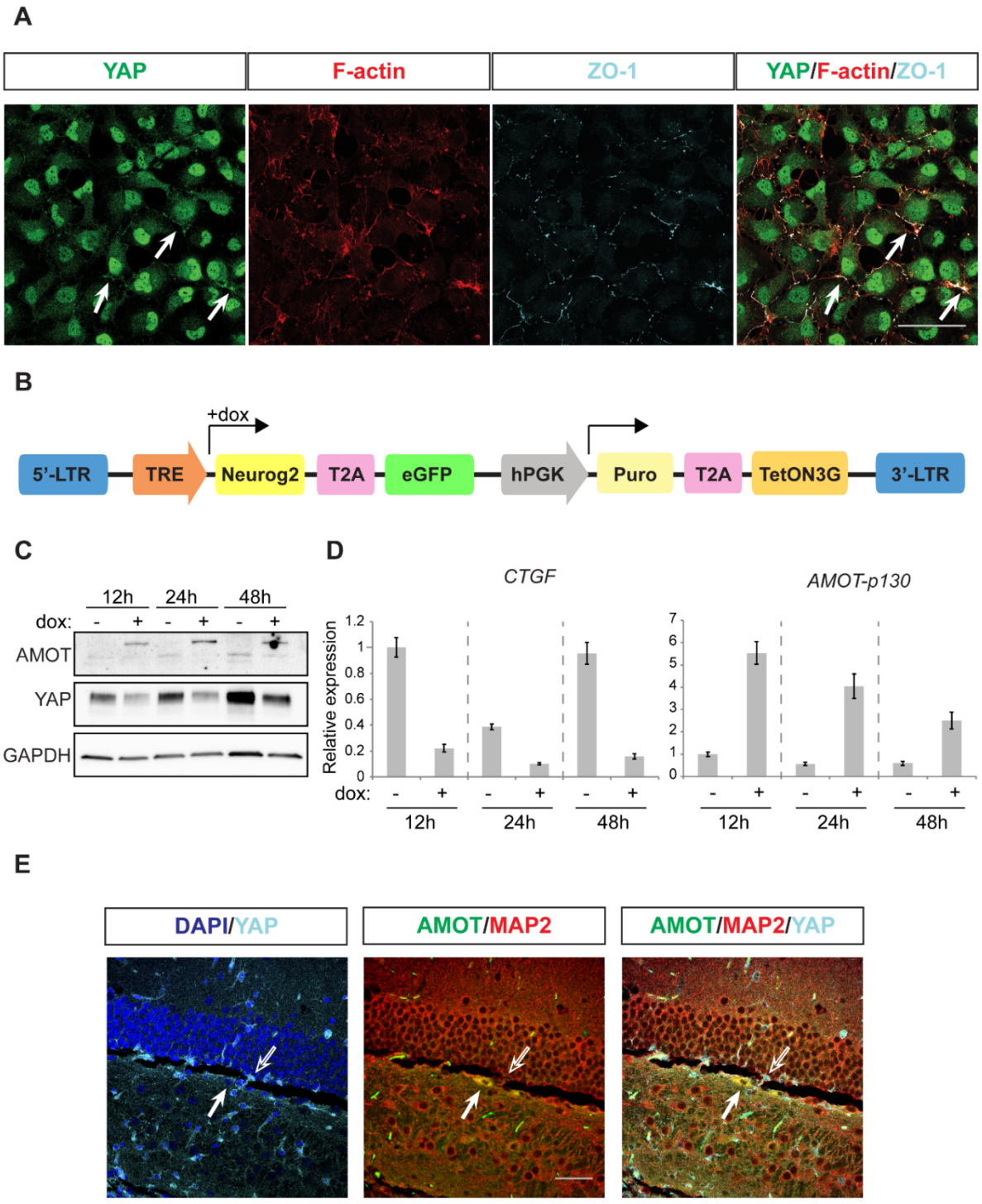

Figure S3-2: AMOT expression increases, while YAP is downregulated during neuronal differentiation.

(A) Subcellular localization of YAP, F-actin, and tight junction marker ZO-1 in NSCs. Filled arrows point out sites of co-localization.

(B) A schematic diagram of Neurog2-T2A-GFP H9 cell line.

(C) Protein levels of AMOT and YAP with or without dox induction of *Neurog2* for 12-48 hour

(D) Transcript levels of *AMOT-p130* and *CTGF* with or without dox induction of *Neurog2* for 12-48 hours

(E) Expression of YAP, AMOT, and MAP2 in differentiating NSCs in the SGZ of the mouse dentate gyrus. Filled arrow point out differentiated neurons, which have migrated away from precursor cells (hollow arrows).

Data are presented as the mean ± SEM, n=3. Scale bar, 50 μm.

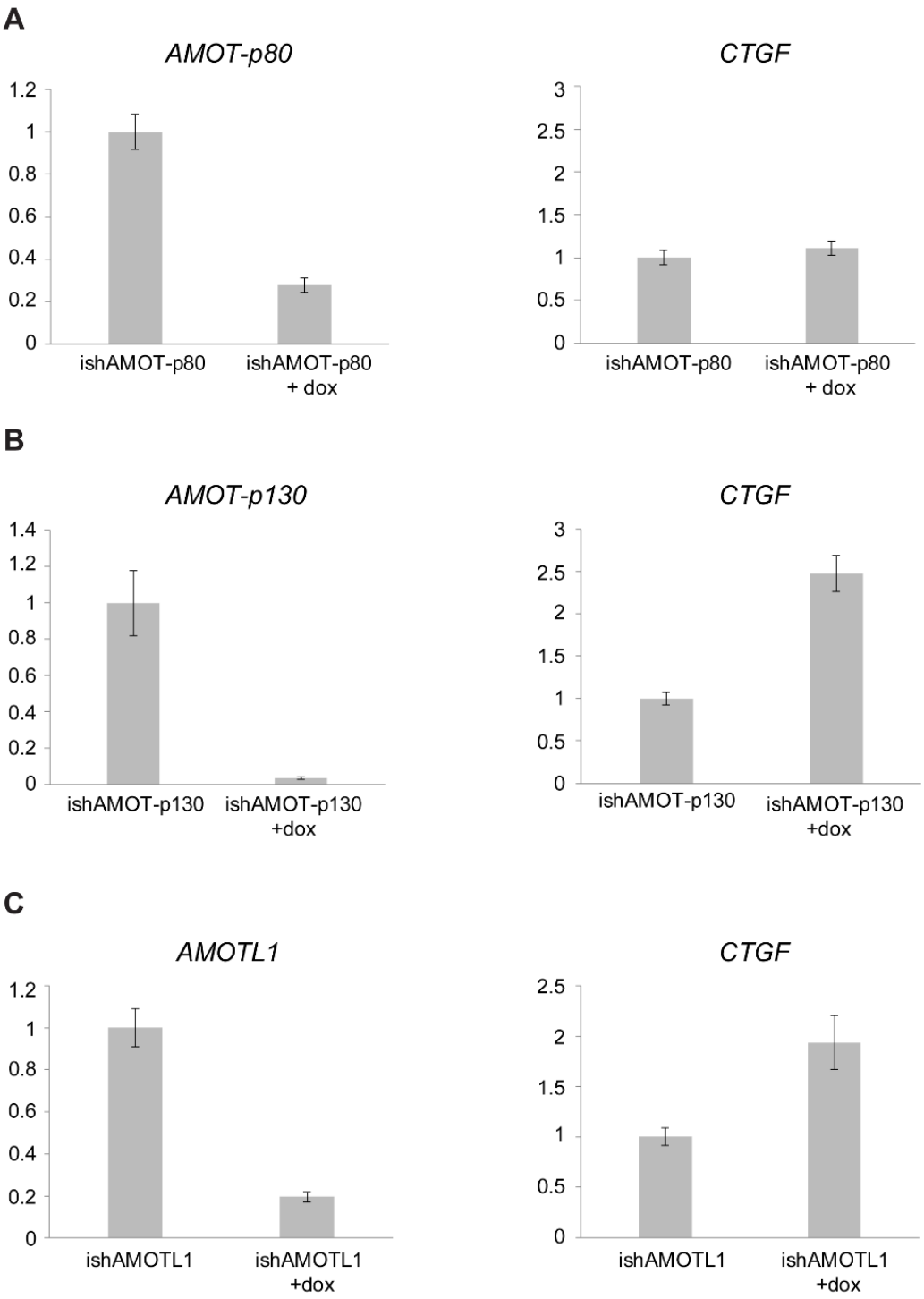

Figure S3-3: Characterization of AMOT and AMOTL1 knockdowns.

(A) Transcript levels of *AMOT-p80* and *CTGF* with or without dox induction of AMOT-p80 shRNA for 24 hours.

(B) Transcript levels of *AMOT-p130* and *CTGF* with or without dox induction of AMOT-p130

shRNA for 24 hours.

(C) Transcript levels of *AMOTL1* and *CTGF* with or without dox induction of AMOTL1 shRNA for 24 hours.

Data are presented as the mean ± SEM, n=3.

Table S3-1: List of proteins enriched in FLAG co-IP from H9 YAP-FLAG cells

Gene name	Description	Accession Number	p-value	YAP-FLAG avg	WT avg
YAP1	Transcriptional coactivator YAP1	P46937	< 0.00010	355	2
PTPN14	Tyrosine-protein phosphatase non-receptor type 14	Q15678	< 0.00010	17	0
YWHAE	14-3-3 protein epsilon	P62258	< 0.00010	32	6
TEAD3	Transcriptional enhancer factor TEF-5	Q99594	< 0.00010	11	0
TEAD2	Transcriptional enhancer factor TEF-4	Q15562	< 0.00010	9	0
HSPA1A	Heat shock 70 kDa protein 1A/1B	P08107	< 0.00010	16	3
YWHAG	14-3-3 protein gamma	P61981	< 0.00010	12	2
YWHAH	14-3-3 protein eta	Q04917	< 0.00010	8	0
TMPO	Lamina-associated polypeptide 2, isoform alpha	P42166	< 0.00010	15	3
ARID3B	AT-rich interactive domain-containing protein 3B	Q8IVW6	< 0.00010	8	1
LIG3	DNA ligase 3	P49916	< 0.00010	5	0
WBP2	WW domain-binding protein 2	A6NG10	0.00019	5	0
SSBP1	Single-stranded DNA-binding protein, mitochondrial	Q04837	0.00019	5	0
YWHAQ	14-3-3 protein theta	P27348	0.0002	12	3
YWHAB	14-3-3 protein beta/alpha	P31946	0.00047	5	0
YWHAZ	14-3-3 protein zeta/delta	P63104	0.00084	8	2
HSPA4	Heat shock 70 kDa protein 4	P34932	0.0032	18	8
AMOTL1	Angiomotin-like protein 1	Q8IY63	0.0042	4	0
TEAD1	Transcriptional enhancer factor TEF-1	H0YE88	0.0075	3	0
UBA1	Ubiquitin-like modifier-activating enzyme 1	P22314	0.023	6	2
PDIA3	Protein disulfide-isomerase A3	P30101	0.025	4	1
TEAD4	Transcriptional enhancer factor TEF-3	Q15561	0.026	2	0
FOXH1	Forkhead box protein H1	F5H8D7	0.026	2	0
SALL4	Sal-like protein 4	Q9UJQ4	0.035	3	0
ENAH	Protein enabled homolog	Q8N8S7	0.047	2	0
HYOU1	Hypoxia up-regulated protein 1	Q9Y4L1	0.058	2	0
RAB1A	Ras-related protein Rab-1A	E7END7	0.087	1	0
GARS	Glycine--tRNA ligase	P41250	0.087	1	0
PGAM1	Phosphoglycerate mutase 1	P18669	0.087	1	0
TMPO	Lamina-associated polypeptide 2, isoforms beta/gamma	P42167	0.087	1	0
TPM4	Tropomyosin alpha-4 chain	P67936	0.087	1	0
DNAJA2	DnaJ homolog subfamily A member 2	O60884	0.092	3	1

SALL2	Sal-like protein 2	Q9Y467	0.15	2	0
BCLAF1	Bcl-2-associated transcription factor 1	E9PK91	0.15	2	0
CCDC85C	Coiled-coil domain-containing protein 85C	A6NKD9	0.16	1	0
MSN	Moesin	P26038	0.16	1	0
NUP93	Nuclear pore complex protein Nup93	H3BVG0	0.16	1	0
PTPN11	Tyrosine-protein phosphatase non-receptor type 11	Q06124	0.16	1	0
LMNA	Prelamin-A/C	P02545	0.16	1	0
EML4	Echinoderm microtubule-associated protein-like 4	B5MBZ0	0.16	1	0
PNKP	Bifunctional polynucleotide phosphatase/kinase	M0QYH2	0.16	1	0
SSB	Lupus La protein	P05455	0.16	1	0
CDK1	Cyclin-dependent kinase 1	P06493	0.16	1	0
ARHGEF10	Rho guanine nucleotide exchange factor 10	O15013	0.25	1	0
CDH1	Cadherin-1	P12830	0.25	1	0
TP53BP2	Apoptosis-stimulating of p53 protein 2	Q13625	0.29	1	0
PDZD2	PDZ domain-containing protein 2	O15018	0.29	1	0
AMOTL2	Angiomotin-like protein 2	Q9Y2J4	0.29	1	0
COPE	Coatomer protein complex, subunit epsilon, isoform d	M0QXB4	0.29	1	0
POLR1B	DNA-directed RNA polymerase I subunit RPA2	Q9H9Y6	0.29	1	0
NME1	Nucleoside diphosphate kinase A	P15531	0.3	2	1
AMOT	Angiomotin	Q4VCS5	0.38	1	0
DPP7	Dipeptidyl peptidase 2	Q9UHL4	0.38	1	0
PSME3	Proteasome activator complex subunit 3	K9J957	0.38	1	0

Table S3-2: List of YAP-FLAG interactors that increase or decrease during neural differentiation

Gene name	Description	Accession Number	p-value	YAP-FLAG undiff	YAP-FLAG diff	WT diff
AMOT	Angiomotin	Q4VCS5	< 0.00010	1	28	0
HSPA1A	Heat shock 70 kDa protein 1A/1B	P08107	< 0.00010	16	57	11
TMPO	Lamina-associated polypeptide 2, isoform alpha	P42166	< 0.00010	15	2	4
TP53BP2	Apoptosis-stimulating of p53 protein 2	Q13625	0.00023	1	10	0
UGDH	UDP-glucose 6-dehydrogenase	O60701	0.00024	0	7	1
YWHAE	14-3-3 protein epsilon	P62258	0.00038	32	72	16
DPP7	Dipeptidyl peptidase 2	Q9UHL4	0.00072	1	10	2
SNAP29	Synaptosomal-associated protein 29	O95721	0.00078	0	6	1
ARID3B	AT-rich interactive domain-containing protein 3B	Q8IVW6	0.0014	8	1	0
LIG3	DNA ligase 3	P49916	0.0031	5	0	0
HUWE1	E3 ubiquitin-protein ligase HUWE1	Q7Z6Z7	0.004	0	6	2
IPO8	Importin-8	O15397	0.0085	0	4	1
CCDC85C	Coiled-coil domain-containing protein 85C	A6NKD9	0.011	1	7	0
DDX1	ATP-dependent RNA helicase DDX1	Q92499	0.012	0	5	0
HSPA2	Heat shock-related 70 kDa protein 2	P54652	0.012	0	5	0

RTCB	tRNA-splicing ligase RtcB homolog	Q9Y3I0	0.012	1	6	1
UBA1	Ubiquitin-like modifier-activating enzyme 1	P22314	0.022	6	16	5
HYOU1	Hypoxia up-regulated protein 1	Q9Y4L1	0.028	2	9	2
CHD1L	Chromodomain-helicase-DNA-binding protein 1-like	Q86WJ1	0.028	0	3	0
UGGT1	UDP-glucose:glycoprotein glucosyltransferase 1	Q9NYU2	0.028	0	3	0
LRRC59	Leucine-rich repeat-containing protein 59	Q96AG4	0.028	0	3	0
KLC2	Kinesin light chain 2	Q9H0B6	0.028	0	3	0
ARHGAP17	Rho GTPase-activating protein 17	Q68EM7	0.028	0	3	0
HM13	Minor histocompatibility antigen H13	Q8TCT9	0.028	0	3	0
CDH2	Cadherin-2	P19022	0.028	0	3	1
BAG4	BAG family molecular chaperone regulator 4	O95429	0.028	0	3	0
AMOTL2	Angiomotin-like protein 2	Q9Y2J4	0.03	1	5	0
CAPZB	Capping protein (Actin filament) muscle Z-line, beta, isoform 4	B1AK88	0.03	1	5	1
ATP6V1B2	V-type proton ATPase subunit B, brain isoform	P21281	0.032	0	4	1
YWHAZ	14-3-3 protein zeta/delta	P63104	0.048	8	19	2
TJP2	Tight junction protein ZO-2	Q9UDY2	0.055	3	0	0
SALL4	Sal-like protein 4	Q9UJQ4	0.055	3	0	0
PSMC1	26S protease regulatory subunit 4	P62191	0.061	1	5	2
PFN2	Profilin-2	C9J0J7	0.073	1	4	1
EPS15L1	Epidermal growth factor receptor substrate 15-like 1	Q9UBC2	0.086	0	3	0
HADHB	Trifunctional enzyme subunit beta, mitochondrial	P55084	0.086	0	3	1
GSN	Gelsolin	P06396	0.086	0	3	0
TEAD3	Transcriptional enhancer factor TEF-5	Q99594	0.087	11	8	0
DYNC1H1	Cytoplasmic dynein 1 heavy chain 1	Q14204	0.092	0	2	0
EPB41L2	Band 4.1-like protein 2	O43491	0.092	0	2	0
TJP1	Tight junction protein ZO-1	Q07157	0.092	0	2	0
ADD3	Gamma-adducin	Q9UEY8	0.092	0	2	0
FOXP4	Forkhead box protein P4	B7ZBM3	0.092	0	2	0
PFKL	ATP-dependent 6-phosphofructokinase, liver type	P17858	0.092	0	2	0
DNAJA1	DnaJ homolog subfamily A member 1	P31689	0.092	0	2	0
PLIN3	Perilipin-3	O60664	0.092	0	2	0
HSPA4	Heat shock 70 kDa protein 4	P34932	0.1	18	32	7
FOXH1	Forkhead box protein H1	F5H8D7	0.11	2	0	0
PTPN14	Tyrosine-protein phosphatase non-receptor type 14	Q15678	0.13	17	29	0
NME1	Nucleoside diphosphate kinase A	P15531	0.16	2	0	0
BCLAF1	Bcl-2-associated transcription factor 1	E9PK91	0.16	2	0	0
YWHAB	14-3-3 protein beta/alpha	P31946	0.17	5	11	1
DIAPH1	Protein diaphanous homolog 1	E9PEZ3	0.17	1	3	0
PDZD2	PDZ domain-containing protein 2	O15018	0.17	1	3	1
RPA1	Replication protein A 70 kDa DNA-binding subunit	P27694	0.17	1	3	0
YWHAG	14-3-3 protein gamma	P61981	0.18	12	21	1

IPO5	Importin-5	O00410	0.18	3	7	3
SND1	Staphylococcal nuclease domain-containing protein 1	Q7KZF4	0.19	4	8	1
LAMB1	Laminin subunit beta-1	G3XAI2	0.22	0	2	0
TCEA1	Transcription elongation factor A protein 1	P23193	0.22	0	2	0
HAT1	Histone acetyltransferase type B catalytic subunit	O14929	0.22	0	2	0
USP11	Ubiquitin carboxyl-terminal hydrolase	G5E9A6	0.22	0	2	0
SRSF3	Serine/arginine-rich-splicing factor 3	P84103	0.22	0	2	0
EZR	Ezrin	P15311	0.23	3	6	2
ARHGEF10	Rho guanine nucleotide exchange factor 10	O15013	0.24	1	0	0
PGAM1	Phosphoglycerate mutase 1	P18669	0.24	1	0	0
CDH1	Cadherin-1	P12830	0.24	1	0	0
SPRR2E	Small proline-rich protein 2E	P22531	0.26	1	3	1
PTPN11	Tyrosine-protein phosphatase non-receptor type 11	Q06124	0.26	1	3	0
YWHAH	14-3-3 protein eta	Q04917	0.28	8	13	1
CYFIP1	Cytoplasmic FMR1-interacting protein 1	Q7L576	0.3	0	1	0
WBP2	WW domain-binding protein 2	A6NG10	0.32	5	4	0
TEAD4	Transcriptional enhancer factor TEF-3	Q15561	0.32	2	1	0
LMNA	Prelamin-A/C	P02545	0.34	1	0	0
PNKP	Bifunctional polynucleotide phosphatase/kinase	M0QYH2	0.34	1	0	0
TMPO	Lamina-associated polypeptide 2, isoforms beta/gamma	P42167	0.36	1	3	0
SALL2	Sal-like protein 2	Q9Y467	0.46	2	3	1
TEAD2	Transcriptional enhancer factor TEF-4	Q15562	0.46	9	11	0
YWHAQ	14-3-3 protein theta	P27348	0.48	12	17	4
AMOTL1	Angiomotin-like protein 1	Q8IY63	0.48	4	6	0
EML4	Echinoderm microtubule-associated protein-like 4	B5MBZ0	0.48	1	2	0

Table S3-3: Primary antibodies used in this study

Antigen	Species	Source	Dilutions
14-3-3 (pan)	Rabbit	Cell Signaling 8312	IB: 1:1000
AMOT	Rabbit	Cell Signaling 43130	IB: 1:500, ICC: 1:500
AMOT	Mouse	Santa Cruz sc-515262	ICC: 1:100, IHC: 1:100
AMOTL1	Rabbit	Abcam ab84049	IB: 1:1000
AMOTL2	Rabbit	Sigma-Aldrich SAB1304596	IB: 1:1000
β-Tubulin III (TUJ1)	Mouse	BioLegend 801201	IB: 1:1000, ICC: 1:1000
FLAG (M2)	Mouse	Sigma-Aldrich F1804	ICC: 1:500
GAPDH	Rabbit	Cell Signaling 5174	IB: 1:20000
MAP2	Chicken	Abcam ab5392	IHC: 1:2000
PAX6	Rabbit	BioLegend 901301	IB: 1:1000, ICC: 1:300
SOX1	Goat	R&D AF3369	ICC: 1:200
TEAD (pan)	Rabbit	Cell Signaling 13295	IB: 1:1000
YAP	Rabbit	Cell Signaling 14074	IB: 1:2000, ICC: 1:300, IHC: 1:300
ZO-1	Mouse	Invitrogen 33-9100	ICC: 1:300

Table S3-4: RT-qPCR primer sequences used in this study

Gene name	Forward primer	Reverse primer
AMOT (p80)	GAGTCGTCACCTTGTCTTCTTT	CCTTTAGTTTCTCAGCCTTCCT
AMOT (p130)	GCCACTTCCTAACCAGCATAG	GGGCTTGCACACTACAGATT
AMOTL1	GAGGATCTCAGAGGTGGAAATG	TGCCATACCGCAGTTGTT
CTGF	GTGCATCCGTACTCCCAAA	CTCCACAGAATTTAGCTCGGTAT
GAPDH	GTGGTCTCCTCTGACTTCAAC	CCTGTTGCTGTAGCCAAATTC

3.6 Acknowledgments

I thank Grzegorz Sabat at the UW–Madison Biotechnology Center Mass Spectrometry Facility for mass spectrometry analysis. I thank the UW–Madison Biochemistry Optical Core for microscopy support. I thank Dr. A. Gendron-Fitzpatrick and Beth Gray (UW–Madison Research Animal Resource Center) for mouse tissue sections. I acknowledge Christine Isabella, Dr. Sayaka Masuko, Dr. Joseph Klim, and Deena-al Mahbuba for helpful feedback.

3.7 References

Aiello, N.M., and Stanger, B.Z. (2016). Echoes of the embryo: using the developmental biology toolkit to study cancer. Dis Model Mech *9*, 105-114.

Aijaz, S., D'Atri, F., Citi, S., Balda, M.S., and Matter, K. (2005). Binding of GEF-H1 to the tight junction-associated adaptor cingulin results in inhibition of Rho signaling and G1/S phase transition. Dev Cell *8*, 777-786.

Almog, N., Ma, L., Raychowdhury, R., Schwager, C., Erber, R., Short, S., Hlatky, L., Vajkoczy, P., Huber, P.E., Folkman, J., *et al.* (2009). Transcriptional switch of dormant tumors to fast-growing angiogenic phenotype. Cancer Res *69*, 836-844.

Balda, M.S., and Matter, K. (2000). The tight junction protein ZO-1 and an interacting transcription factor regulate ErbB-2 expression. EMBO J *19*, 2024-2033.

Bean, D.M., Heimbach, J., Ficorella, L., Micklem, G., Oliver, S.G., and Favrin, G. (2014). esyN: network building, sharing and publishing. PLoS One *9*, e106035.

Beyer, T.A., Weiss, A., Khomchuk, Y., Huang, K., Ogunjimi, A.A., Varelas, X., and Wrana, J.L. (2013). Switch enhancers interpret TGF-beta and Hippo signaling to control cell fate in human embryonic stem cells. Cell Rep *5*, 1611-1624.

Bobbs, A., Gellerman, K., Hallas, W.M., Joseph, S., Yang, C., Kurkewich, J., and Cowden Dahl, K.D. (2015). ARID3B Directly Regulates Ovarian Cancer Promoting Genes. PLoS One *10*, e0131961.

Brizzard, B.L., Chubet, R.G., and Vizard, D.L. (1994). Immunoaffinity purification of FLAG epitope-tagged bacterial alkaline phosphatase using a novel monoclonal antibody and peptide elution. Biotechniques *16*, 730-735.

Cao, X., Pfaff, S.L., and Gage, F.H. (2008). YAP regulates neural progenitor cell number via the TEA domain transcription factor. Genes Dev *22*, 3320-3334.

Chen, K.G., Mallon, B.S., McKay, R.D., and Robey, P.G. (2014). Human pluripotent stem cell culture: considerations for maintenance, expansion, and therapeutics. Cell Stem Cell *14*, 13-26.

Couzens, A.L., Knight, J.D., Kean, M.J., Teo, G., Weiss, A., Dunham, W.H., Lin, Z.Y., Bagshaw, R.D., Sicheri, F., Pawson, T., *et al.* (2013). Protein interaction network of the mammalian Hippo pathway reveals mechanisms of kinase-phosphatase interactions. Sci Signal *6*, rs15.

Davis-Dusenbery, B.N., Williams, L.A., Klim, J.R., and Eggan, K. (2014). How to make spinal motor neurons. Development *141*, 491-501.

Dupont, S., Morsut, L., Aragona, M., Enzo, E., Giulitti, S., Cordenonsi, M., Zanconato, F., Le Digabel, J., Forcato, M., Bicciato, S., *et al.* (2011). Role of YAP/TAZ in mechanotransduction. Nature *474*, 179-183.

Engler, A.J., Sen, S., Sweeney, H.L., and Discher, D.E. (2006). Matrix elasticity directs stem cell lineage specification. Cell *126*, 677-689.

Eriksson, P.S., Perfilieva, E., Bjork-Eriksson, T., Alborn, A.M., Nordborg, C., Peterson, D.A., and Gage, F.H. (1998). Neurogenesis in the adult human hippocampus. Nat Med *4*, 1313-1317.

Finch-Edmondson, M.L., Strauss, R.P., Clayton, J.S., Yeoh, G.C., and Callus, B.A. (2016). Splice variant insertions in the C-terminus impairs YAP's transactivation domain. Biochem Biophys Rep *6*, 24-31.

Gaffney, C.J., Oka, T., Mazack, V., Hilman, D., Gat, U., Muramatsu, T., Inazawa, J., Golden, A., Carey, D.J., Farooq, A.*, et al.* (2012). Identification, basic characterization and evolutionary analysis of differentially spliced mRNA isoforms of human YAP1 gene. Gene *509*, 215-222.

Guilluy, C., Swaminathan, V., Garcia-Mata, R., O'Brien, E.T., Superfine, R., and Burridge, K. (2011). The Rho GEFs LARG and GEF-H1 regulate the mechanical response to force on integrins. Nat Cell Biol *13*, 722-727.

Han, D., Byun, S.H., Park, S., Kim, J., Kim, I., Ha, S., Kwon, M., and Yoon, K. (2015). YAP/TAZ enhance mammalian embryonic neural stem cell characteristics in a Tead-dependent manner. Biochem Biophys Res Commun *458*, 110-116.

Han, Y., Miller, A., Mangada, J., Liu, Y., Swistowski, A., Zhan, M., Rao, M.S., and Zeng, X. (2009). Identification by automated screening of a small molecule that selectively eliminates neural stem cells derived from hESCs but not dopamine neurons. PLoS One *4*, e7155.

Huang, S., and Ingber, D.E. (2005). Cell tension, matrix mechanics, and cancer development. Cancer Cell *8*, 175-176.

Kim, M., Kim, T., Johnson, R.L., and Lim, D.S. (2015). Transcriptional co-repressor function of the hippo pathway transducers YAP and TAZ. Cell Rep *11*, 270-282.

Klim, J.R., Li, L., Wrighton, P.J., Piekarczyk, M.S., and Kiessling, L.L. (2010). A defined glycosaminoglycan-binding substratum for human pluripotent stem cells. Nat Methods *7*, 989-994.

Kohli, P., Bartram, M.P., Habbig, S., Pahmeyer, C., Lamkemeyer, T., Benzing, T., Schermer, B., and Rinschen, M.M. (2014). Label-free quantitative proteomic analysis of the YAP/TAZ interactome. Am J Physiol Cell Physiol *306*, C805-818.

Li, L., Bennett, S.A., and Wang, L. (2012). Role of E-cadherin and other cell adhesion molecules in survival and differentiation of human pluripotent stem cells. Cell Adh Migr *6*, 59-70.

Lian, I., Kim, J., Okazawa, H., Zhao, J., Zhao, B., Yu, J., Chinnaiyan, A., Israel, M.A., Goldstein, L.S., Abujarour, R.*, et al.* (2010). The role of YAP transcription coactivator in regulating stem cell self-renewal and differentiation. Genes Dev *24*, 1106-1118.

Liao, T.T., Hsu, W.H., Ho, C.H., Hwang, W.L., Lan, H.Y., Lo, T., Chang, C.C., Tai, S.K., and Yang, M.H. (2016). let-7 Modulates Chromatin Configuration and Target Gene Repression through Regulation of the ARID3B Complex. Cell Rep *14*, 520-533.

Lima, W.R., Parreira, K.S., Devuyst, O., Caplanusi, A., N'Kuli, F., Marien, B., Van Der Smissen, P., Alves, P.M., Verroust, P., Christensen, E.I.*, et al.* (2010). ZONAB promotes proliferation and represses differentiation of proximal tubule epithelial cells. J Am Soc Nephrol *21*, 478-488.

Mana-Capelli, S., Paramasivam, M., Dutta, S., and McCollum, D. (2014). Angiomotins link F-actin architecture to Hippo pathway signaling. Mol Biol Cell *25*, 1676-1685.

Miller, A., Ralser, M., Kloet, S.L., Loos, R., Nishinakamura, R., Bertone, P., Vermeulen, M., and Hendrich, B. (2016). Sall4 controls differentiation of pluripotent cells independently of the Nucleosome Remodelling and Deacetylation (NuRD) complex. Development *143*, 3074-3084.

Moleirinho, S., Guerrant, W., and Kissil, J.L. (2014). The Angiomotins - From discovery to function. FEBS Letters *588*, 2693-2703.

Moroishi, T., Hansen, C.G., and Guan, K.L. (2015). The emerging roles of YAP and TAZ in cancer. Nat Rev Cancer *15*, 73-79.

Murphy, W.L., McDevitt, T.C., and Engler, A.J. (2014). Materials as stem cell regulators. Nat Mater *13*, 547-557.

Musah, S., Morin, S.A., Wrighton, P.J., Zwick, D.B., Jin, S., and Kiessling, L.L. (2012). Glycosaminoglycan-binding hydrogels enable mechanical control of human pluripotent stem cell self-renewal. ACS Nano *6*, 10168-10177.

Musah, S., Wrighton, P.J., Zaltsman, Y., Zhong, X., Zorn, S., Parlato, M.B., Hsiao, C., Palecek, S.P., Chang, Q., Murphy, W.L.*, et al.* (2014). Substratum-induced differentiation of human pluripotent stem cells reveals the coactivator YAP is a potent regulator of neuronal specification. Proc Natl Acad Sci U S A *111*, 13805-13810.

Nakajima, H., Yamamoto, K., Agarwala, S., Terai, K., Fukui, H., Fukuhara, S., Ando, K., Miyazaki, T., Yokota, Y., Schmelzer, E.*, et al.* (2017). Flow-Dependent Endothelial YAP Regulation Contributes to Vessel Maintenance. Dev Cell *40*, 523-536 e526.

Orr, B.A., Bai, H., Odia, Y., Jain, D., Anders, R.A., and Eberhart, C.G. (2011). Yes-associated protein 1 is widely expressed in human brain tumors and promotes glioblastoma growth. J Neuropathol Exp Neurol *70*, 568-577.

Panciera, T., Azzolin, L., Fujimura, A., Di Biagio, D., Frasson, C., Bresolin, S., Soligo, S., Basso, G., Bicciato, S., Rosato, A.*, et al.* (2016). Induction of Expandable Tissue-Specific Stem/Progenitor Cells through Transient Expression of YAP/TAZ. Cell Stem Cell *19*, 725-737.

Piccolo, S., Dupont, S., and Cordenonsi, M. (2014). The biology of YAP/TAZ: hippo signaling and beyond. Physiol Rev *94*, 1287-1312.

Saha, K., Keung, A.J., Irwin, E.F., Li, Y., Little, L., Schaffer, D.V., and Healy, K.E. (2008). Substrate modulus directs neural stem cell behavior. Biophys J *95*, 4426-4438.

Savic, D., Partridge, E.C., Newberry, K.M., Smith, S.B., Meadows, S.K., Roberts, B.S., Mackiewicz, M., Mendenhall, E.M., and Myers, R.M. (2015). CETCh-seq: CRISPR epitope tagging ChIP-seq of DNA-binding proteins. Genome Res *25*, 1581-1589.

Schindelin, J., Arganda-Carreras, I., Frise, E., Kaynig, V., Longair, M., Pietzsch, T., Preibisch, S., Rueden, C., Saalfeld, S., Schmid, B.*, et al.* (2012). Fiji: an open-source platform for biological-image analysis. Nat Methods *9*, 676-682.

Sun, Y., Yong, K.M., Villa-Diaz, L.G., Zhang, X., Chen, W., Philson, R., Weng, S., Xu, H., Krebsbach, P.H., and Fu, J. (2014). Hippo/YAP-mediated rigidity-dependent motor neuron differentiation of human pluripotent stem cells. Nat Mater *13*, 599-604.

Wang, T., Wei, J.J., Sabatini, D.M., and Lander, E.S. (2014a). Genetic screens in human cells using the CRISPR-Cas9 system. Science *343*, 80-84.

Wang, W., Li, X., Huang, J., Feng, L., Dolinta, K.G., and Chen, J. (2014b). Defining the protein-protein interaction network of the human hippo pathway. Mol Cell Proteomics *13*, 119-131.

Wrighton, P.J., Klim, J.R., Hernandez, B.A., Koonce, C.H., Kamp, T.J., and Kiessling, L.L. (2014). Signals from the surface modulate differentiation of human pluripotent stem cells through glycosaminoglycans and integrins. Proc Natl Acad Sci U S A *111*, 18126-18131.

Yang, C., Tibbitt, M.W., Basta, L., and Anseth, K.S. (2014). Mechanical memory and dosing influence stem cell fate. Nat Mater *13*, 645-652.

Yu, D.X., Marchetto, M.C., and Gage, F.H. (2014). How to make a hippocampal dentate gyrus granule neuron. Development *141*, 2366-2375.

Yu, F.X., and Guan, K.L. (2013). The Hippo pathway: regulators and regulations. Genes Dev *27*, 355-371.

Zhang, Y., Pak, C., Han, Y., Ahlenius, H., Zhang, Z., Chanda, S., Marro, S., Patzke, C., Acuna, C., Covy, J.*, et al.* (2013). Rapid single-step induction of functional neurons from human pluripotent stem cells. Neuron *78*, 785-798.

Zhao, B., Li, L., Lu, Q., Wang, L.H., Liu, C.Y., Lei, Q., and Guan, K.L. (2011). Angiomotin is a novel Hippo pathway component that inhibits YAP oncoprotein. Genes Dev *25*, 51-63.

Zhao, B., Li, L., Tumaneng, K., Wang, C.Y., and Guan, K.L. (2010). A coordinated phosphorylation by Lats and CK1 regulates YAP stability through SCF(beta-TRCP). Genes Dev *24*, 72-85.

Chapter 4

Future directions: tools for monitoring YAP interactions during hPS cell self-renewal and differentiation

4.1 Overview

In the preceding chapters, I documented my investigations of the molecular mechanisms underlying substrate-induced differentiation of hPS cells. We identified YAP as a key mechanotransducer of substrate elasticity in hPS cells. On stiff surfaces YAP localizes to the nucleus, whereas on soft surfaces YAP is excluded from the nucleus and in the cytoplasm its concentration is decreased by degradation by the proteosome. The neuronal differentiation observed when hPS cells are cultured the soft surface can be recapitulated by depleting YAP in cells cultured on a stiff surface. I showed that during neuronal differentiation YAP localization is regulated by AMOT. AMOT-YAP complexes increase during differentiation and forced expression of AMOT drives YAP out of the nucleus. These studies demonstrate that modulation of YAP subcellular localization can potently influence the cell fate decisions of hPS cells.

In this chapter, I will discuss ongoing work and future directions aimed at further characterizing the protein-protein interactions that mediate YAP stability and localization during hPS cell self-renewal and differentiation. I generated hPS cell lines that facilitate the monitoring of YAP interactions in live cells. I propose a strategy by which these cell lines can be used to discover novel small molecules that influence YAP stability and subcellular localization. I expect that these directions will enable a greater understanding of YAP's role in human development and disease and can deliver new compounds for controlling YAP-mediated biological processes such as differentiation and tumorigenesis.

4.2 Results and Discussion

4.2.1 YAP-FLAG cell line reveals novel YAP interactors

In chapter 3, I used CRISPR/Cas9-mediated engineering to generate a YAP-FLAG hPS cell line, which I employed to identify YAP interactors in undifferentiated hPS cells. Given that YAP interactors in hPS cells had not been previously characterized and my strategy provided the means to examine endogenously tagged YAP, I wanted to determine if new interactions could be identified. In addition to capturing many of the previously identified YAP interactors (Chapter 3), the list indeed presented several novel interactors including ARID3B and thymopoietin (TMPO).

ARID3B was one of the top significant hits in the AP-MS of YAP-FLAG in undifferentiated cells, but had not been previously identified to be a YAP interactor. I confirmed the ARID3B interaction by immunoblot following FLAG immunoprecipitation in YAP-FLAG cells (Figure 4-1). ARID3B is a transcription factor that belongs to an AT-rich interaction domain (ARID) family of DNA binding proteins. Since the ARID3B interaction was enriched in undifferentiated cells and ARID3B-YAP complexes decreased during neuronal differentiation, I hypothesize that by binding ARID3B and thereby modulating the transcription of ARID3B target genes, YAP either promotes pluripotency or represses differentiation. Consistent with this hypothesis, a recent study found that *ARID3B* expression levels were enriched in undifferentiated hPS cells relative to differentiated cells and ARID3B depletion attenuated the expression of most pluripotency genes (Liao et al., 2016).

Additionally, several studies indicate a role for ARID3B in neural cancers. ARID3B is overexpressed in neuroblastoma and cooperates with MYCN to afford increased oncogenicity and proliferation (Kobayashi et al., 2006; Kobayashi et al., 2013). In cancer cells, genes associated with neuron development were enriched for ARID3B binding sites, and forced

expression of *ARID3B* led to their downregulation (Bobbs et al., 2015). These studies indicate that by inducing proliferation in neural tissue, ARID3B drives malignancy. Given that YAP has also been observed to be overexpressed in malignant neural cancers (Orr et al., 2011), the YAP-ARID3B interaction may mediate the observed neural tumorigenesis in these pathologies. This hypothesis suggests that targeting ARID3B-YAP interactions might hold promise for the discovery of novel therapeutic interventions for neural cancers.

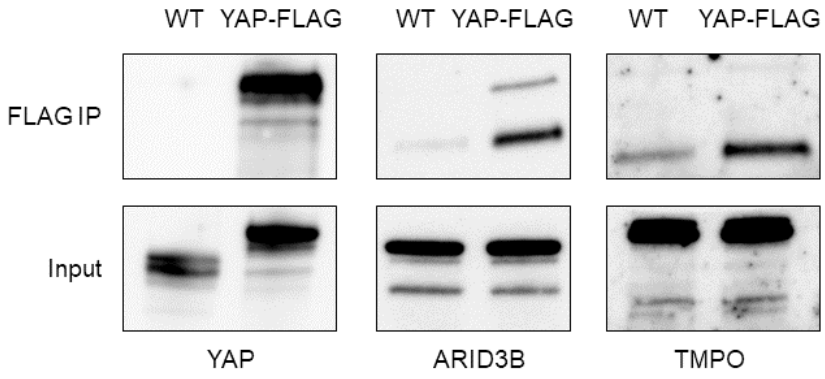

Figure 4-1: YAP-FLAG cell line reveals novel YAP interactors.
Top: Immunoblots following FLAG co-immunoprecipitation from H9 WT and H9 YAP-FLAG cell lines. Bottom: IP input.

One of the additional YAP interactors that is uncharacterized, but was a significant hit in undifferentiated cells is TMPO, also known as lamina-associated polypeptide 2 (LAP2). Another study identified TMPO in a list of potential YAP interactors, but whether this interaction is relevant was unclear (Kohli et al., 2014). I confirmed by immunoblot the enrichment of TMPO in YAP-FLAG cells after FLAG-immunoprecipitation (Figure 4-1). TMPO has six splice variants, including LAP2α. Although this was not the isoform detected in the aforementioned immunoblot, the potential of YAP to interact with LAP2α was nonetheless intriguing. LAP2α is necessary for maintaining nucleoplasmic lamins A/C (Naetar et al., 2017). Lamins have been identified as key molecules for mediating mechanosensing (Osmanagic-Myers et al., 2015). Lamin A expression is correlated to matrix elasticity: Cells in stiff microenvironments have

increased lamin A expression, while low levels of lamin A are produced in soft microenvironments (Swift et al., 2013). Since YAP subcellular localization is altered by substrate stiffness, perhaps TMPO provides an additional point of regulation by linking lamin A expression to YAP localization.

To examine if TMPO controls YAP subcellular localization, I used CRISPR-mediated editing to target a region common to all TMPO slice variants. In this way, I generated hPS cells heterogeneous ($TMPO^{+/-}$) and homogenous ($TMPO^{-/-}$) for TMPO deletion. Since cells on soft substrates display low levels of lamin A and decreased nuclear YAP, and TMPO is necessary for maintaining lamin A, I hypothesized that $TMPO^{-/-}$ hPS cells would downregulate nuclear YAP. Indeed, $TMPO^{+/-}$ cells displayed lower levels of TMPO and nuclear YAP, and TMPO expression was absent in $TMPO^{-/-}$ cells, which displayed further downregulated nuclear YAP (Figure 4-2). Generation of isoform-specific deletions or rescue with specific TMPO isoforms will be necessary to identify which TMPO isoforms influence YAP subcellular localization in hPS cells.

In summary, using endogenously tagged YAP for AP-MS in hPS cells led to the identification of several novel YAP interactors. Further characterization of these interactions and their influence on hPS cell fate is needed. Additional novel YAP interactors were also identified by AP-MS, but their relevance will require further characterization. In analogy with our observations with AMOT, some of these novel interactors increased their interaction with YAP during neuronal differentiation. These interactors include heat shock 70 kDa protein 1A/1B (HSPA1A), a heat shock protein involved in cell growth and differentiation (Mayer and Bukau, 2005), and UDP-glucose 6-dehydrogenase (UGDH), an enzyme involved in the biosynthesis of glycosylated extracellular matrix molecules (Wang et al., 2010). Finally, it will be worthwhile to examine how YAP-protein interactions change during differentiation to non-neuroectodermal lineages, such as during mesodermal and endodermal differentiation. These experiments would shed further light into the role of YAP in human development.

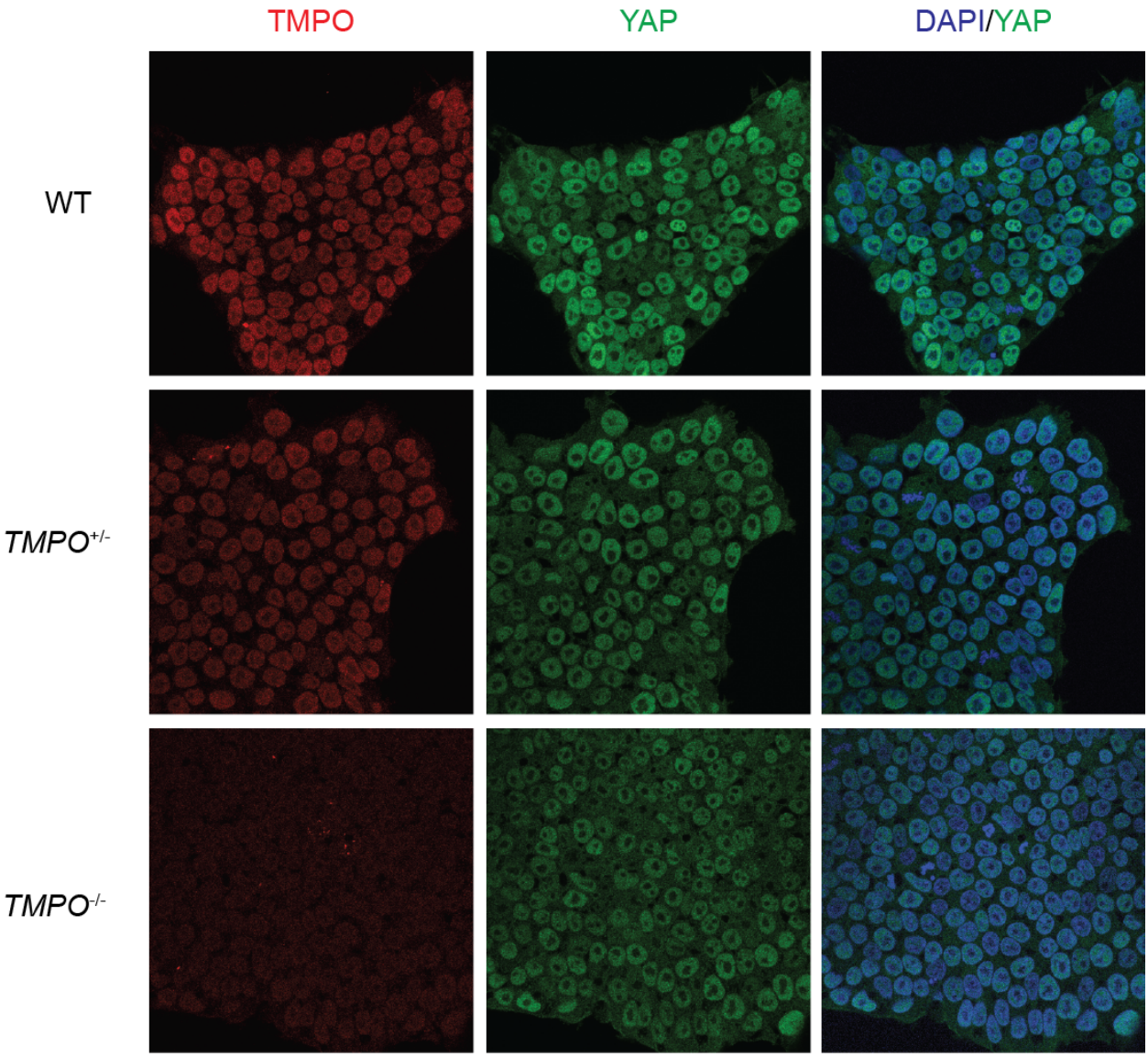

Figure 4-2: Nuclear YAP is reduced in *TMPO*-deficient hPS cells.

Protein levels of TMPO (left) and YAP subcellular localization (middle and right) in WT (top), $TMPO^{+/-}$ (middle), and $TMPO^{-/-}$ (bottom) H9 cells.

4.2.2 Monitoring YAP post-translational modifications

While I've identified changes in the composition of YAP-protein complexes during neuronal differentiation, the influence of post-translational modifications (PTMs) on these interactions remains to be understood. YAP can undergo a wide variety of PTMs including phosphorylation,

ubiquitylation, acetylation, methylation, and O-GlcNAcylation (Piccolo et al., 2014; Zhang et al., 2017). The contributions of these YAP PTMs to the protein's roles in differentiation and mechanotransduction are largely unclear. Recent advances in mass spectrometry are enabling the detection of these PTMs (Doll and Burlingame, 2015), therefore it will be worthwhile to identify their functional roles in YAP biology.

My preliminary work points to PTMs influencing YAP interactions in response to matrix mechanics. As discussed in chapter 2, I showed that in hPS cells cultured on soft microenvironments YAP is targeted by the ubiquitin-proteasome pathway. Additionally, as discussed in chapter 3, several ubiquitin-proteasome pathway proteins were enriched in YAP-FLAG AP-MS. Since we observed that in soft microenvironments hPS cells display reduced F-actin, I examined whether reduction of F-actin polymerization influences YAP interactions. I hypothesized that a short-term (6 h) treatment with an F-actin inhibitor should not significantly alter protein expression. Thus, if differences for YAP interactions were detected they are likely due to differences in PTMs, which generally occur on much shorter time scales. Indeed AP-MS showed several significant differences in YAP-protein interactions during inhibition of F-actin polymerization compared to a DMSO control (Table 4-1). Consistent with YAP nuclear exclusion following latrunculin A treatment, an increase in interactions with cytoplasmic proteins (14-3-3s, AMOTs) was observed concomitant with a decrease in interactions with nuclear proteins (TEADs). During this short-term treatment, the amount of immunoprecipitated YAP-FLAG in latrunculin A-treated cells was slightly lower than in DMSO control, but the difference had low statistical significance. In summary, these preliminary results suggest that PTMs influence YAP subcellular localization and stability in response to changes in matrix elasticity or hPS cell cytoskeletal state.

Table 4-1: YAP interactors in the absence and presence of latrunculin A

Gene name	Description	Accession number	p-value	YAP-FLAG DMSO	YAP-FLAG Lat A	WT
YWHAE	14-3-3 protein epsilon	P62258	0.0012	42	62	6
AMOTL2	Angiomotin-like protein 2	Q9Y2J4	0.046	2	7	0
YWHAQ	14-3-3 protein theta	P27348	0.065	14	20	3
TEAD2	Transcriptional enhancer factor TEF-4	Q15562	0.065	13	4	0
TJP2	Tight junction protein ZO-2	Q9UDY2	0.083	2	6	3
MSN	Moesin	P26038	0.088	0	3	0
YWHAG	14-3-3 protein gamma	P61981	0.089	15	20	2
AMOT	Angiomotin	Q4VCS5	0.095	3	7	0
AMOTL1	Angiomotin-like protein 1	Q8IY63	0.11	6	10	0
HSPA1A	Heat shock 70 kDa protein 1A/1B	P08107	0.13	19	9	3
HSPA4	Heat shock 70 kDa protein 4	P34932	0.15	36	21	8
TEAD3	Transcriptional enhancer factor TEF-5	Q99594	0.21	11	5	0
YWHAZ	14-3-3 protein zeta/delta	P63104	0.22	11	13	2
ARID3B	AT-rich interactive domain-containing protein 3B	Q8IVW6	0.25	2	4	1
ARHGEF10	Rho guanine nucleotide exchange factor 10	O15013	0.25	2	4	0
TEAD4	Transcriptional enhancer factor TEF-3	Q15561	0.27	4	1	0
RAB1A	Ras-related protein Rab-1A	E7END7	0.27	4	1	0
HUWE1	E3 ubiquitin-protein ligase HUWE1	Q7Z6Z7	0.31	2	0	0
UBA1	Ubiquitin-like modifier-activating enzyme 1	P22314	0.32	8	9	2
DNAJA2	DnaJ homolog subfamily A member 2	O60884	0.33	5	2	1
YAP1	Transcriptional coactivator YAP1	P46937	0.33	393	303	2

4.2.3 YAP-Nanoluc cell line for monitoring protein-protein interactions in live hPS cells

To aid in further characterization of YAP-protein interactions, as well as to help identify small molecules that influence these interactions, I set out to engineer an hPS cell line in which YAP is endogenously tagged with Nanoluc. Nanoluc is an engineered luciferase that in comparison to traditional variants is smaller in size and exhibits greatly enhanced sensitivity

(Hall et al., 2012). These properties make Nanoluc an attractive tag for bioluminescence applications in live cells. The improved luminescence activity makes Nanoluc useful for bioluminescence resonance transfer (BRET) experiments, which can be used for quantifying protein-protein interactions in live cells. A robust assay termed NanoBRET has been developed for this purpose (Machleidt et al., 2015).

Using CRISPR/Cas9-mediated genome engineering I produced a YAP-Nanoluc hPS cell line. The C-terminal Nanoluc tag was present in both alleles (Figure 4-3A). Importantly, the tag did not alter YAP subcellular localization, as YAP remained nuclear in hPS cells (Figure 4-3B). High luminescence activity was detected in YAP-Nanoluc cells, but not in WT cells, following incubation with a cell permeable luciferase substrate (data not shown).

A

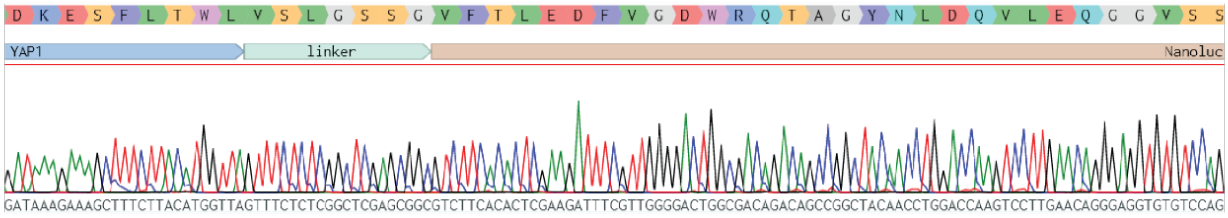

B

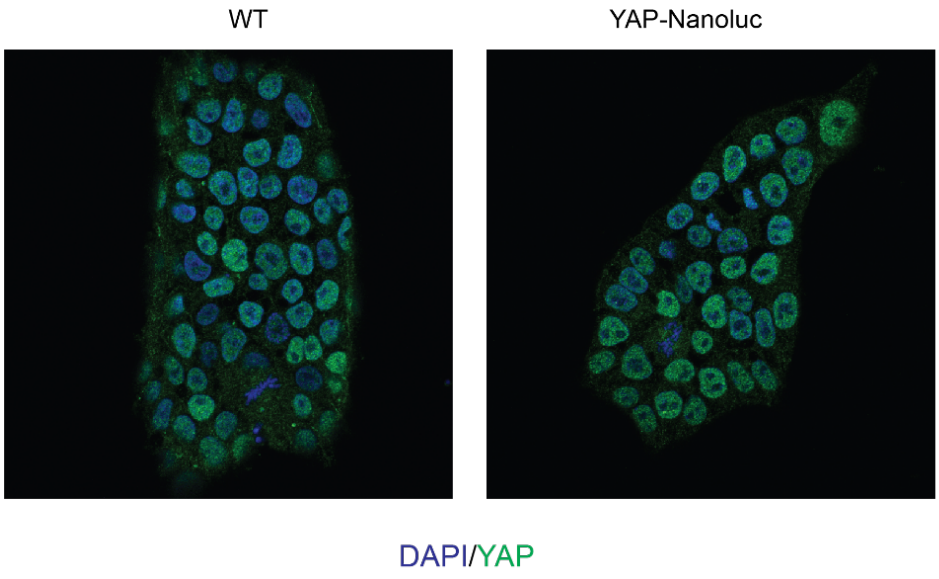

Figure 4-3: Generation of H9 YAP-Nanoluc cell line

(A) DNA chromatogram of CRISPR/Cas9-edited region in the H9 YAP-Nanoluc cell line.

(B) YAP subcellular localization in H9 WT and H9 YAP-Nanoluc cell lines

I envision that the YAP-Nanoluc hPS cell line can be used to quantify YAP-protein interactions in live cells using NanoBRET. This strategy provides a convenient platform for identifying changes in interactions between YAP and a given protein of interest in hPS cells or their differentiated progeny in response to soluble or insoluble signaling cues. Additionally, NanoBRET is highly amendable to high-throughput small molecule-based screens. Therefore, the YAP-Nanoluc cell line can be used for discovering novel compounds that alter YAP-protein interactions or YAP stability. Such compounds could be useful for driving cell differentiation or for targeting YAP's role in tumorigenesis.

4.2.4 YAP-SNAP cell line for monitoring YAP subcellular localization in live hPS cells

To enable monitoring of YAP subcellular localization in hPS cells, I generated a YAP-SNAP hPS cell line. The SNAP-tag provides a strategy for covalent labeling of proteins inside living cells (Xue et al., 2015). It was derived from an alkyltransferase DNA repair protein and allows for highly specific labeling using benzylguanine derivatives, including ones that are fluorescently conjugated (Keppler et al., 2003).

Using CRISPR-Cas9 genome engineering I produced an hPS cell line in which YAP is endogenously tagged with the SNAP tag. The C-terminal SNAP tag was present in both alleles of the YAP-SNAP cell line (Figure 4-4A). Next, I incubated WT and YAP-SNAP cells with cell-permeable fluorescent SNAP ligands and monitored YAP subcellular localization in live cells by confocal microscopy. Labeling with either SNAP-Cell 505-Star or SNAP-Cell 647-SiR could be used to detect YAP-SNAP subcellular localization in YAP-SNAP cells but not in WT cells (Figure

4-4B). Importantly, the SNAP tag did not lead to YAP mislocalization, as YAP-SNAP was detected in the nucleus of hPS cells.

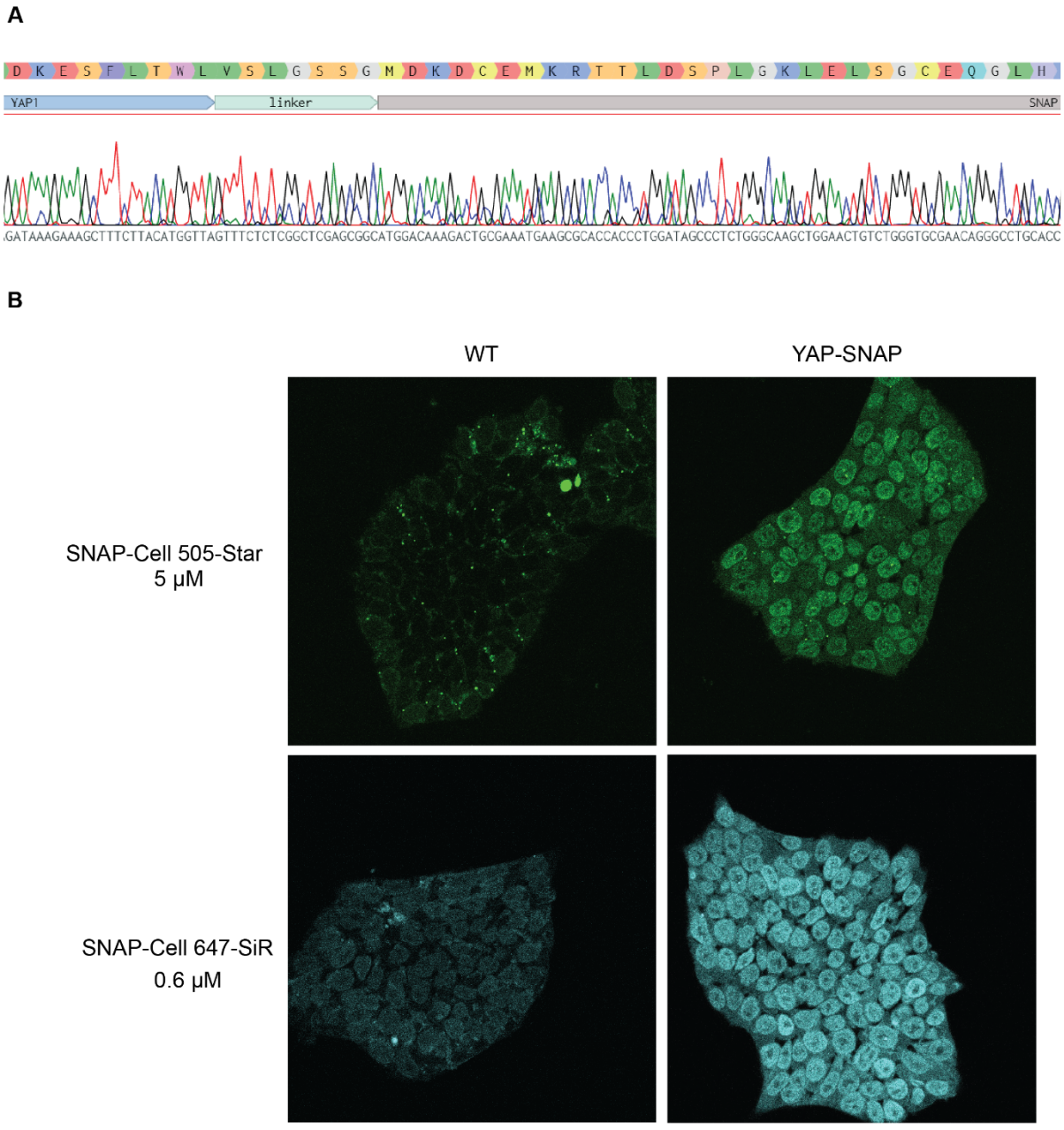

Figure 4-4: Generation of H9 YAP-SNAP cell line

(A) DNA chromatogram of CRISPR/Cas9-edited region in the H9 YAP-SNAP cell line.

(B) SNAP labeling in live H9 WT (left) and H9 YAP-SNAP (right) cells with 5 µM SNAP-Cell 505-Star (top) or 0.6 µM SNAP-Cell 647-SiR (bottom).

Next, I investigated whether the YAP-SNAP cell line recapitulates the changes in YAP subcellular localization that I previously characterized in Chapter 3. Indeed, I detected a decrease in YAP nuclear localization in live hPS cells with forced expression of AMOT-p130 or Neurog2 (Figure 4-5A, B). Therefore, the SNAP tag does not hinder YAP interaction with AMOT and can be used to detect changes in YAP subcellular localization in live cells.

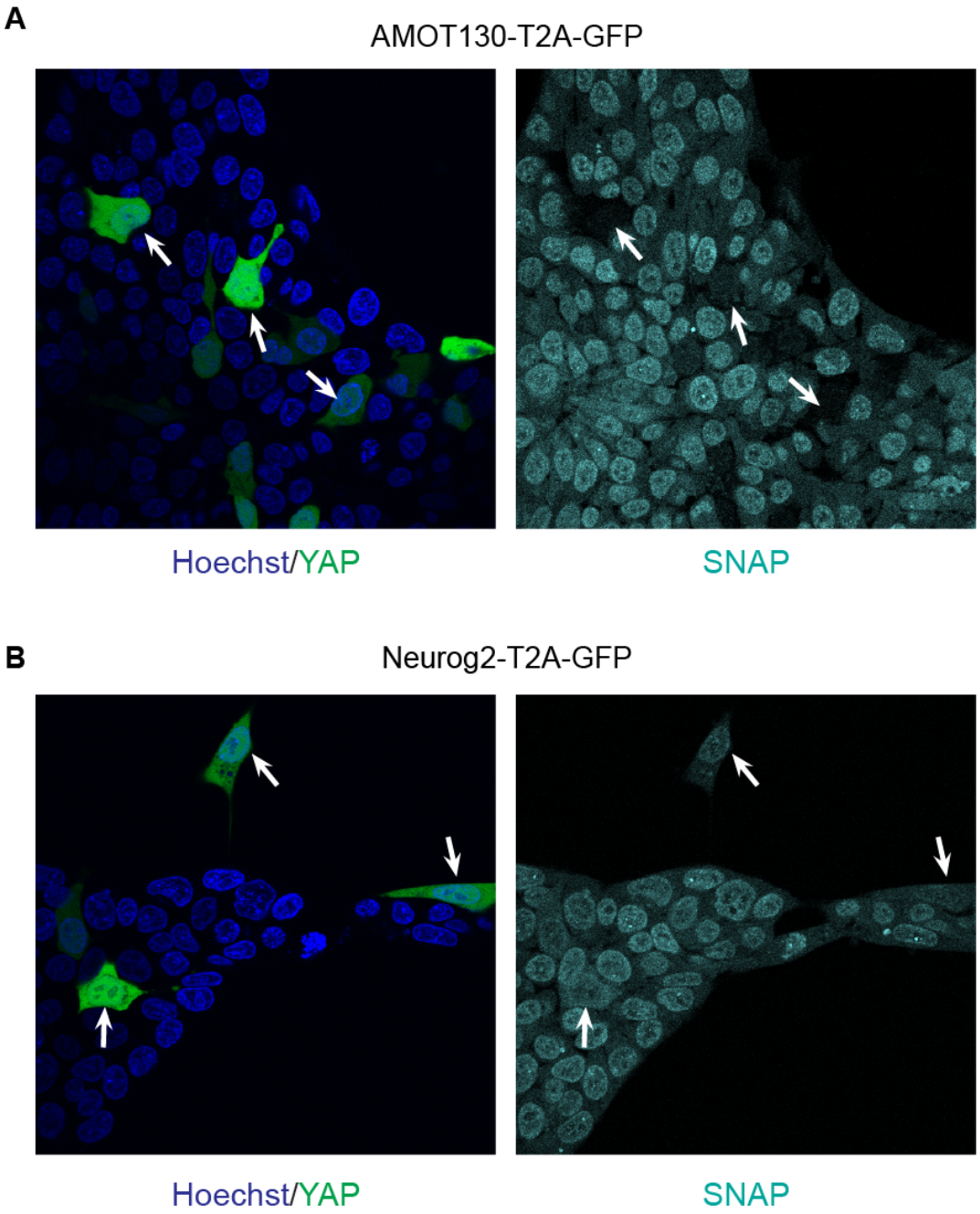

Figure 4-5: YAP-SNAP cell line allows for monitoring changes in YAP subcellular localization in response to forced AMOT expression or Neurog2 induction
(A) H9 YAP-SNAP AMOT130-T2A-GFP cells labeled with 0.6 μM SNAP-Cell 647-SiR, 24 hours after induction. Arrows indicate cells producing AMOT/GFP.
(B) H9 YAP-SNAP Neurog2-T2A-GFP cells labeled with 0.6 μM SNAP-Cell 647-SiR, 24 hours after induction. Arrows indicate cells producing Neurog2/GFP.

Next, I examined if the YAP-SNAP cell line can be used to monitor the dynamics of YAP subcellular localization in live cells. I labeled the YAP-SNAP cells, and recorded the change in YAP-SNAP localization for two hours after addition of the F-actin polymerization inhibitor latrunculin A. YAP-SNAP nuclear localization progressively decreased over time during inhibitor treatment, consistent with previous observations (Figure 4-6A,B).

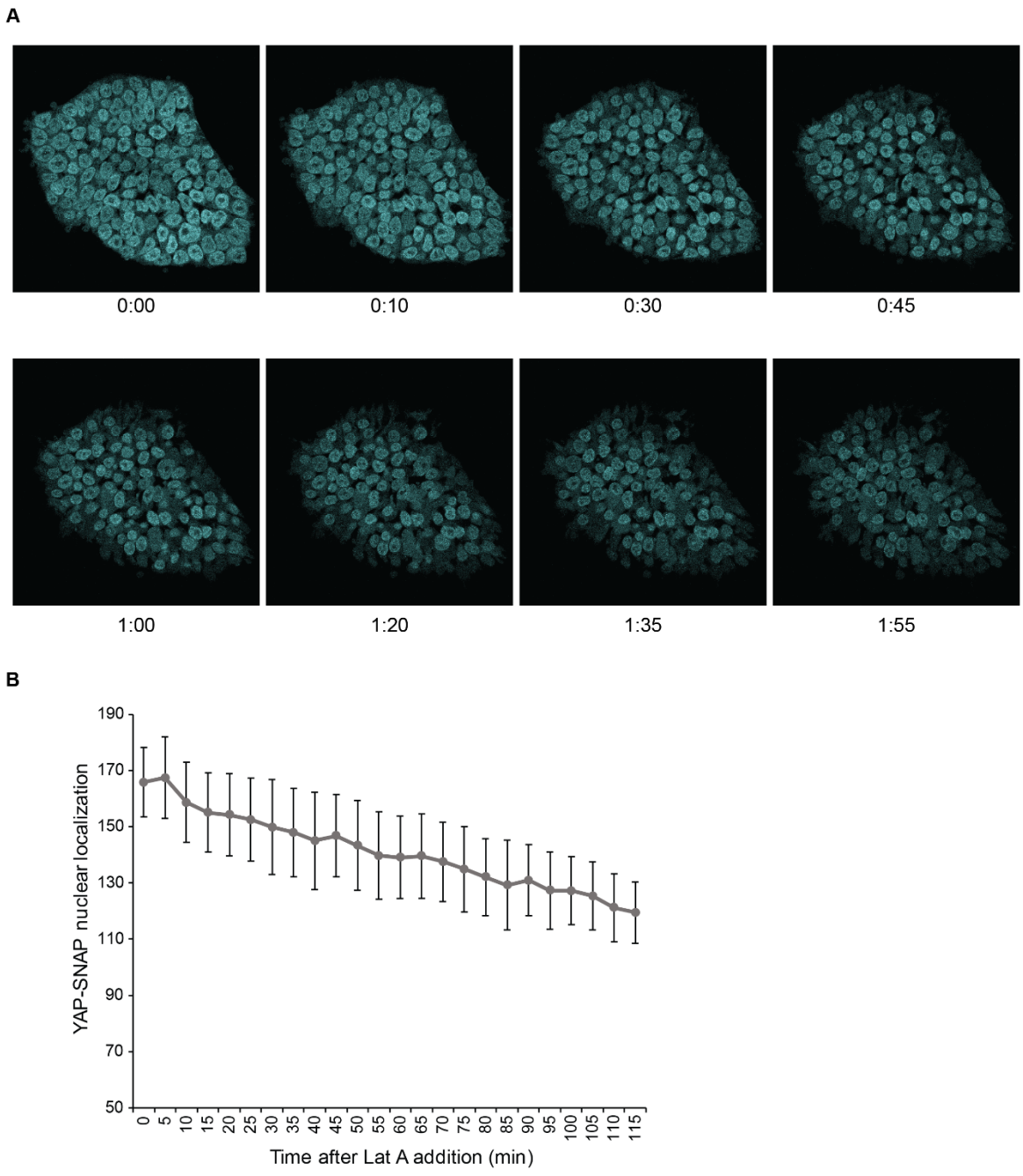

Figure 4-6: YAP-SNAP cell line allows for monitoring changes in YAP subcellular localization in response to F-actin inhibition.

(A) Time lapse imaging of H9 YAP-SNAP cells labeled with 0.6 μM SNAP-Cell 647-SiR for two hours following addition of 1 μM latrunculin A.

(B) Quantification of YAP-SNAP nuclear localization (n=30 cells).

I envision that the YAP-SNAP cell line can be used to monitor YAP subcellular localization during differentiation, as well as in more complex systems like organoids. This latter application could shed further light into YAP's regulation of organ size. Additionally, the YAP-SNAP cell line can be applied to high throughput small molecule-based screens for discovery of compounds that influence YAP subcellular localization.

In conclusion, the YAP-FLAG, YAP-Nanoluc, and YAP-SNAP hPS cell lines will be useful tools for characterizing YAP protein-interactions and discovering novel compounds that influence YAP-protein interactions, stability, or subcellular localization.

4.3 Methods

4.3.1 hPS cell culture

H9 hES cells were cultured as described in previous chapters.

4.3.2 Immunoprecipitation and mass spectrometry

H9 YAP-FLAG cells were cultured in mTeSR1 supplemented with DMSO or 1 μM latrunculin A for 6 hours. FLAG immunoprecipitation and mass spectrometry analysis was performed as described in chapter 3.

4.3.3 CRISPR-mediated genome engineering of hPS cells

For targeting *TMPO* in H9 hES cells, CRISPR/Cas9 genome editing was used. TMPO target sequence (GCGGCCGGTTGCGAGCCGTG) was cloned into PX459 (gift from Feng Zhang, Addgene plasmid # 62988) (Ran et al., 2013). H9 cells were nucleofected with 5 μg PX459 and the ribonucleoprotein complex using the Human Stem Cell Nucleofector Kit 2 (Lonza) and the B-16 program on the Amaxa Nucleofector II (Lonza) as per manufacturer instructions. Cells were allowed to recover for two days in mTeSR1 medium supplemented with 1x RevitaCell

(Gibco) prior to selection with puromycin. Following puromycin selection, clones were derived using serial dilution and analyzed by PCR amplification and Sanger sequencing for to identify modifications at both alleles.

The introduction of the Nanoluc and SNAP tags was carried out as described in Chapter 3 for the FLAG-tag with the following modications. The FLAG sequence in the pFETCh_Donor plasmid (gift from Eric Mendenhall and Richard M. Myers, Addgene plasmid # 63934) was modified to Nanoluc amplified from pNLF1 (Promega) or SNAP amplified from pSNAPf (New England BioLabs).

4.3.4 SNAP labeling

Live cell labeling of WT and H9 YAP-SNAP cells was performed using fresh solutions prepared from SNAP-Cell 505-Star or SNAP-Cell 647-SiR stocks (New England BioLabs). Ligands were diluted in mTeSR1 to indicated concentrations by mixing thoroughly by pipetting up and down 10 times. Cells on Matrigel-coated Lab-Tek Chambered Coverglass (Nunc) were incubated with the solutions at 37 °C, 5% CO_2 for 30 minutes. Cells were washed 4 times with mTeSR1 and incubated in fresh medium at 37 °C, 5% CO_2 for 30 minutes. For nuclei labeling, the fresh medium was first supplemented with 1:10000 Hoechst 33342 trihydrochloride trihydrate (Molecular Probes). Cells were washed 3 times with mTeSR1 with the medium left on the cells after the last wash. Cells were imaged in an environmental chamber at 37 °C on a Nikon A1R-Si+.

4.3.5 Lentiviral generation of stable cell lines

Lentiviruses for hPS cell transduction of AMOT-T2A-GFP and Neurog2-T2A were generated as described in chapter 3.

4.3.6 Immunoblotting and immunostaining

Western blots and immunofluorescence was performed as described in previous chapters. The primary antibodies used are listed in Table 4-2.

Table 4-2: List of primary antibodies used in this study

Antigen	Species	Source	Dilutions
ARID3B	Mouse	Santa Cruz sc-514741	IB: 1:500
TMPO	Mouse	Cell Signaling 5369	IB: 1:1000, ICC: 1:500
YAP	Rabbit	Cell Signaling 14074	IB: 1:2000, ICC: 1:300

4.4 Acknowledgments

I thank Grzegorz Sabat at the UW–Madison Biotechnology Center Mass Spectrometry Facility for mass spectrometry analysis. I thank Deena-Al Mahbuba for future contributions to this work.

4.5 References

Bobbs, A., Gellerman, K., Hallas, W.M., Joseph, S., Yang, C., Kurkewich, J., and Cowden Dahl, K.D. (2015). ARID3B Directly Regulates Ovarian Cancer Promoting Genes. PLoS One *10*, e0131961.

Doll, S., and Burlingame, A.L. (2015). Mass spectrometry-based detection and assignment of protein posttranslational modifications. ACS Chem Biol *10*, 63-71.

Hall, M.P., Unch, J., Binkowski, B.F., Valley, M.P., Butler, B.L., Wood, M.G., Otto, P., Zimmerman, K., Vidugiris, G., Machleidt, T.*, et al.* (2012). Engineered luciferase reporter from a deep sea shrimp utilizing a novel imidazopyrazinone substrate. ACS Chem Biol *7*, 1848-1857.

Keppler, A., Gendreizig, S., Gronemeyer, T., Pick, H., Vogel, H., and Johnsson, K. (2003). A general method for the covalent labeling of fusion proteins with small molecules in vivo. Nat Biotechnol *21*, 86-89.

Kobayashi, K., Era, T., Takebe, A., Jakt, L.M., and Nishikawa, S. (2006). ARID3B induces malignant transformation of mouse embryonic fibroblasts and is strongly associated with malignant neuroblastoma. Cancer Res *66*, 8331-8336.

Kobayashi, K., Jakt, L.M., and Nishikawa, S.I. (2013). Epigenetic regulation of the neuroblastoma genes, Arid3b and Mycn. Oncogene *32*, 2640-2648.

Kohli, P., Bartram, M.P., Habbig, S., Pahmeyer, C., Lamkemeyer, T., Benzing, T., Schermer, B., and Rinschen, M.M. (2014). Label-free quantitative proteomic analysis of the YAP/TAZ interactome. Am J Physiol Cell Physiol *306*, C805-818.

Liao, T.T., Hsu, W.H., Ho, C.H., Hwang, W.L., Lan, H.Y., Lo, T., Chang, C.C., Tai, S.K., and Yang, M.H. (2016). let-7 Modulates Chromatin Configuration and Target Gene Repression through Regulation of the ARID3B Complex. Cell Rep *14*, 520-533.

Machleidt, T., Woodroofe, C.C., Schwinn, M.K., Mendez, J., Robers, M.B., Zimmerman, K., Otto, P., Daniels, D.L., Kirkland, T.A., and Wood, K.V. (2015). NanoBRET--A Novel BRET Platform for the Analysis of Protein-Protein Interactions. ACS Chem Biol *10*, 1797-1804.

Mayer, M.P., and Bukau, B. (2005). Hsp70 chaperones: cellular functions and molecular mechanism. Cell Mol Life Sci *62*, 670-684.

Naetar, N., Ferraioli, S., and Foisner, R. (2017). Lamins in the nuclear interior - life outside the lamina. J Cell Sci *130*, 2087-2096.

Orr, B.A., Bai, H., Odia, Y., Jain, D., Anders, R.A., and Eberhart, C.G. (2011). Yes-associated protein 1 is widely expressed in human brain tumors and promotes glioblastoma growth. J Neuropathol Exp Neurol *70*, 568-577.

Osmanagic-Myers, S., Dechat, T., and Foisner, R. (2015). Lamins at the crossroads of mechanosignaling. Genes Dev *29*, 225-237.

Piccolo, S., Dupont, S., and Cordenonsi, M. (2014). The biology of YAP/TAZ: hippo signaling and beyond. Physiol Rev *94*, 1287-1312.

Ran, F.A., Hsu, P.D., Wright, J., Agarwala, V., Scott, D.A., and Zhang, F. (2013). Genome engineering using the CRISPR-Cas9 system. Nat Protoc *8*, 2281-2308.

Swift, J., Ivanovska, I.L., Buxboim, A., Harada, T., Dingal, P.C., Pinter, J., Pajerowski, J.D., Spinler, K.R., Shin, J.W., Tewari, M.*, et al.* (2013). Nuclear lamin-A scales with tissue stiffness and enhances matrix-directed differentiation. Science *341*, 1240104.

Wang, T.P., Pan, Y.R., Fu, C.Y., and Chang, H.Y. (2010). Down-regulation of UDP-glucose dehydrogenase affects glycosaminoglycans synthesis and motility in HCT-8 colorectal carcinoma cells. Exp Cell Res *316*, 2893-2902.

Xue, L., Karpenko, I.A., Hiblot, J., and Johnsson, K. (2015). Imaging and manipulating proteins in live cells through covalent labeling. Nat Chem Biol *11*, 917-923.

Zhang, X., Qiao, Y., Wu, Q., Chen, Y., Zou, S., Liu, X., Zhu, G., Zhao, Y., Chen, Y., Yu, Y.*, et al.* (2017). The essential role of YAP O-GlcNAcylation in high-glucose-stimulated liver tumorigenesis. Nat Commun *8*, 15280.

Appendix 1

Generating heparan sulfate-deficient human pluripotent stem cells

A1.1 Overview

As discussed in Chapter 1, hPS cell matrix adhesion is mediated by cell-surface integrins and GAGs. Engagement of cell-surface GAGs is necessary for maintaining pluripotency, and surfaces that selectively engage GAGs can maintain hPS cell self-renewal (Klim et al., 2010). Additionally, GAG engagement in the absence of integrin activation promotes mesendoderm differentiation (Wrighton et al., 2014). These studies suggest that GAGs play important roles in regulating hPS cell self-renewal and differentiation.

Indeed, studies in mice have shown that the GAG heparan sulfate is crucial for proper animal development. Notably, complete interruption of heparan sulfate biosynthesis leads to early termination of mouse embryonic development (Lin et al., 2000). The contribution of heparan sulfate to mammalian development is likely mediated by heparan sulfate's role in regulating the binding of a wide variety of growth factors to their proper receptors (Forsten-Williams et al., 2008). The molecular mechanisms linking these processes, however, are not well elucidated—particularly in humans. As discussed in Chapter 1, there exist important differences between mouse and human development, therefore more studies are needed to understand the role of heparan sulfate during human development.

In this appendix, I generated and characterized heparan sulfate-deficient hPS cells. Our ongoing efforts, not covered here, are examining the impact of heparan sulfate-deficiency in hPS cell self-renewal and differentiation toward specific lineages, as well as the underlying molecular mechanisms.

A1.2 Results and Discussion

A1.2.1 CRISPR/Cas9-mediated generation of heparan sulfate-deficient hPS cells

To aid in determining the functional roles of heparan sulfate (HS) in hPS cells, I set out to generate an HS-deficient hPS cell line by CRISPR-mediated targeting of the HS biosynthetic gene *EXT1* (Figure A1-1A). *EXT1* encodes exostosin glycosyltransferase 1, a polymerase that heterodimerizes with exostosin glycosyltransferase 2 (EXT2) to form a complex that's responsible for the chain extension of the HS backbone. HS production is completely abolished in *Ext1*$^{-/-}$ mouse embryos (Lin et al., 2000) and *Ext1*$^{-/-}$ mouse ES cells (Johnson et al., 2007). Therefore, I expected that knockout of *EXT1* should result in a completely HS-deficient hPS cell line. Following CRISPR-mediated editing, we isolated a clone in which both alleles incorporated frameshift mutations at the targeted site (Figure A1-1B). To determine whether HS biosynthesis was blocked, we assessed cell-surface HS levels by flow cytometry using the anti-HS antibody 10E4. Whereas HS was detected in wildtype cells, it was absent in the *EXT1*$^{-/-}$ cells (Figure A1-1C). These results indicate that we successfully produced an hPS cell line that is HS-deficient.

Lack of cell-surface HS on hPS cells should inhibit cell binding to surfaces which selectively engage GAGs. WT and *EXT1*$^{-/-}$ cells adhered equally well to a surface coated with vitronectin, an ECM protein that contains binding sites for both GAGs and integrins (Figure A1-1D). In contrast, *EXT1*$^{-/-}$ hPS cells did not adhere to a synthetic surface that displays the GAG-binding VHBD peptide (Figure A1-E). These results indicate that adhesion of hPS cells to the VHBD peptide is mediated by HS.

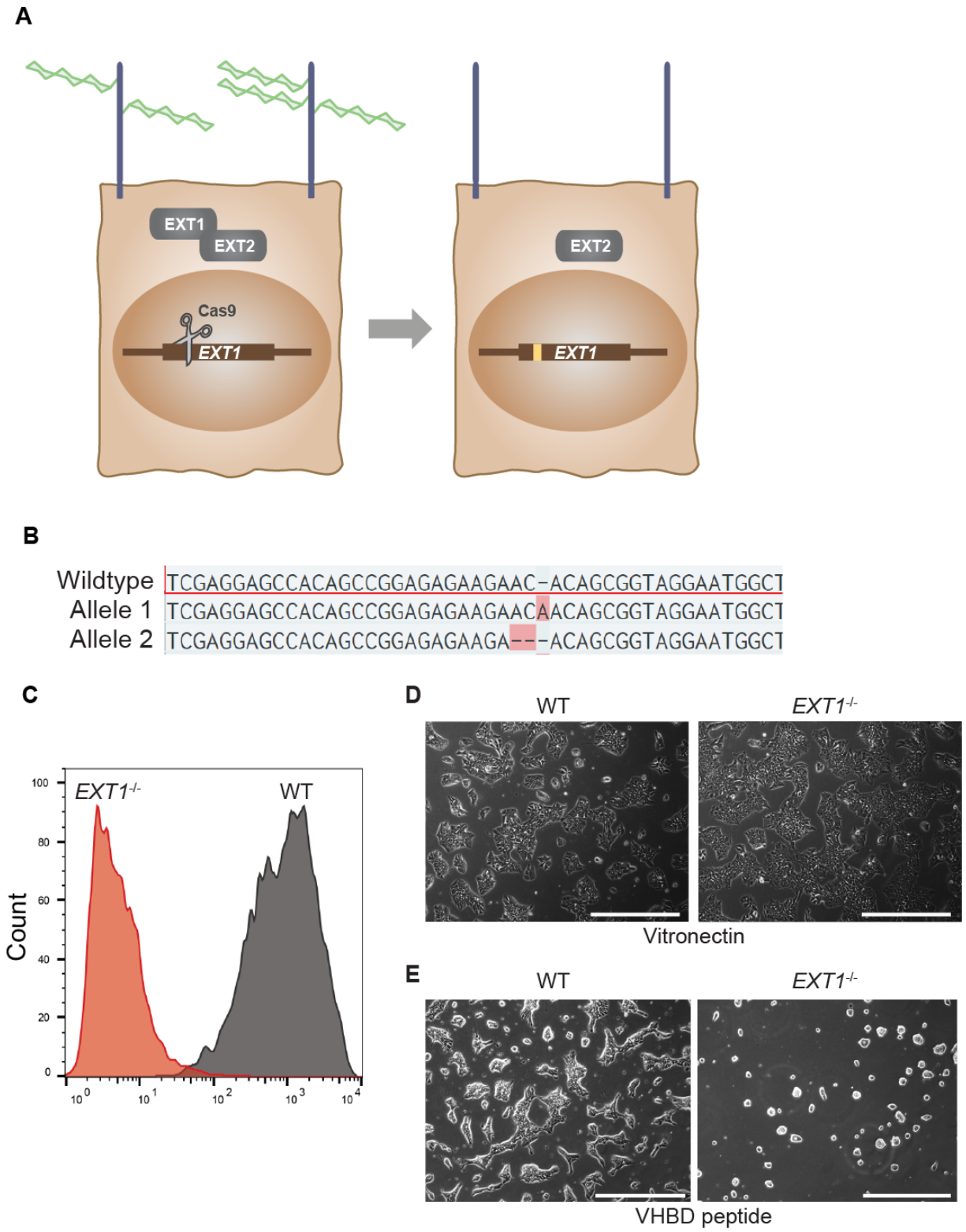

Figure A1-1: Generation of an HS-deficient hPS cell line.

(A) Scheme for generating HS-deficient hPS cells via CRISPR-mediated targeting of *EXT1*.

(B) Biallelic sequence in the sgRNA-targeted region of *EXT1* of an isolated H9 hES cell clone following CRISPR editing.

(C) Histogram plot of HS fluorescence intensity measured by flow cytometry in WT and *EXT1*$^{-/-}$ H9 cells.

(D) Binding of WT (left) and *EXT1*$^{-/-}$ (right) H9 cells to vitronectin-coated tissue culture polystyrene.

(E) Binding of WT (left) and *EXT1*$^{-/-}$ (right) H9 cells to streptavidin-coated tissue culture polystyrene incubated with a biotinylated VHBD peptide.

Next, I examined whether HS-deficiency in *EXT1*$^{-/-}$ hPS cells is exclusively due to lack of EXT1 activity. Using confocal imaging, I confirmed that WT cells display HS on their cell surface whereas *EXT1*$^{-/-}$ hPS cells do not (Figure A1-2A). If HS-deficiency is EXT1-dependent than rescue of *EXT1* expression should rescue HS biosynthesis. Indeed, *EXT1*$^{-/-}$ cells with forced expression of exogenous EXT1 exhibited rescued display of HS on their cell surface (Figure A1-2B). These results indicate that the observed HS deficiency in *EXT1*$^{-/-}$ hPS cells is EXT1-dependent, thereby ruling out potential off-target effects.

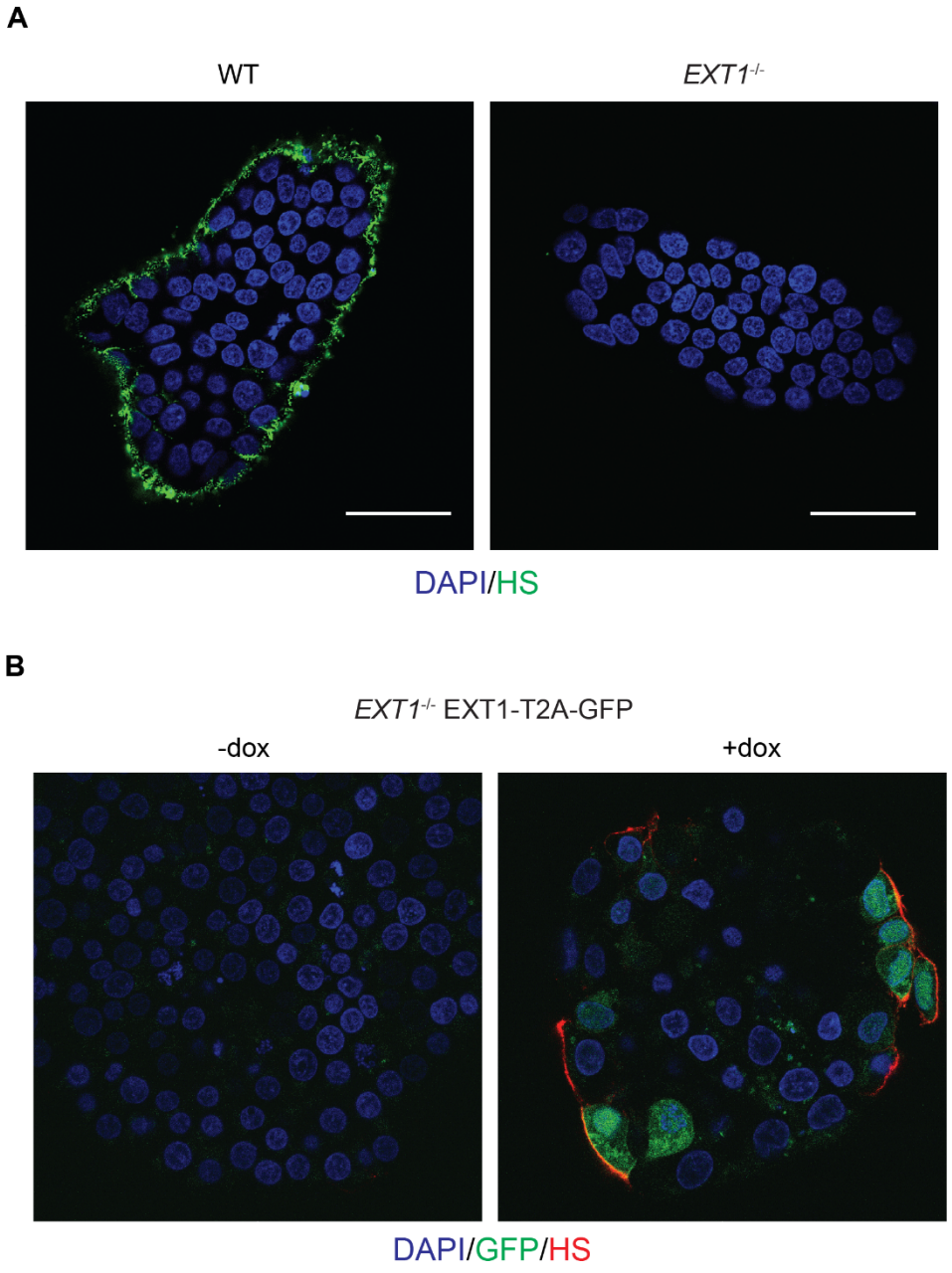

Figure A1-2: HS-deficiency is EXT1 dependent.

(A) HS levels in WT (left) and *EXT1*$^{-/-}$ (right) H9 cells

(B) HS levels in *EXT1*$^{-/-}$ EXT1-T2A-GFP H9 cells with (right) or without (left) doxycycline-induction for 24 hours. The GFP^{+} cells co-express exogenous *EXT1*.

A1.2.2 Heparan sulfate-deficient hPS cells form focal adhesions

Next, I examined whether focal adhesion formation was compromised in *EXT1*$^{-/-}$ cells. Focal adhesions are complexes that provide a link between the cell cytoskeleton and the ECM, and as such are important in cell mechanosensing (Humphrey et al., 2014). Proteoglycans, such as syndecan-4, participate in focal adhesion formation, and overexpression of HS-deficient mutants reduces focal adhesion formation (Gopal et al., 2010; Saoncella et al., 1999). To determine whether HS mediates hPS cell focal adhesion, I cultured WT and *EXT1*$^{-/-}$ cells under chemically-defined heparin-free culture conditions and stained the cells for vinculin, a marker of focal adhesions. Focal adhesion formation, however, appeared to be uncompromised in *EXT1*$^{-/-}$ hPS cells (Figure A1-3). Consistent with proper mechanosensing of a stiff microenvironment, YAP remained nuclearly localized in *EXT1*$^{-/-}$ hPS cells. These results suggest that HS-deficiency in hPS cells does not hinder focal adhesion formation and mechanotransduction.

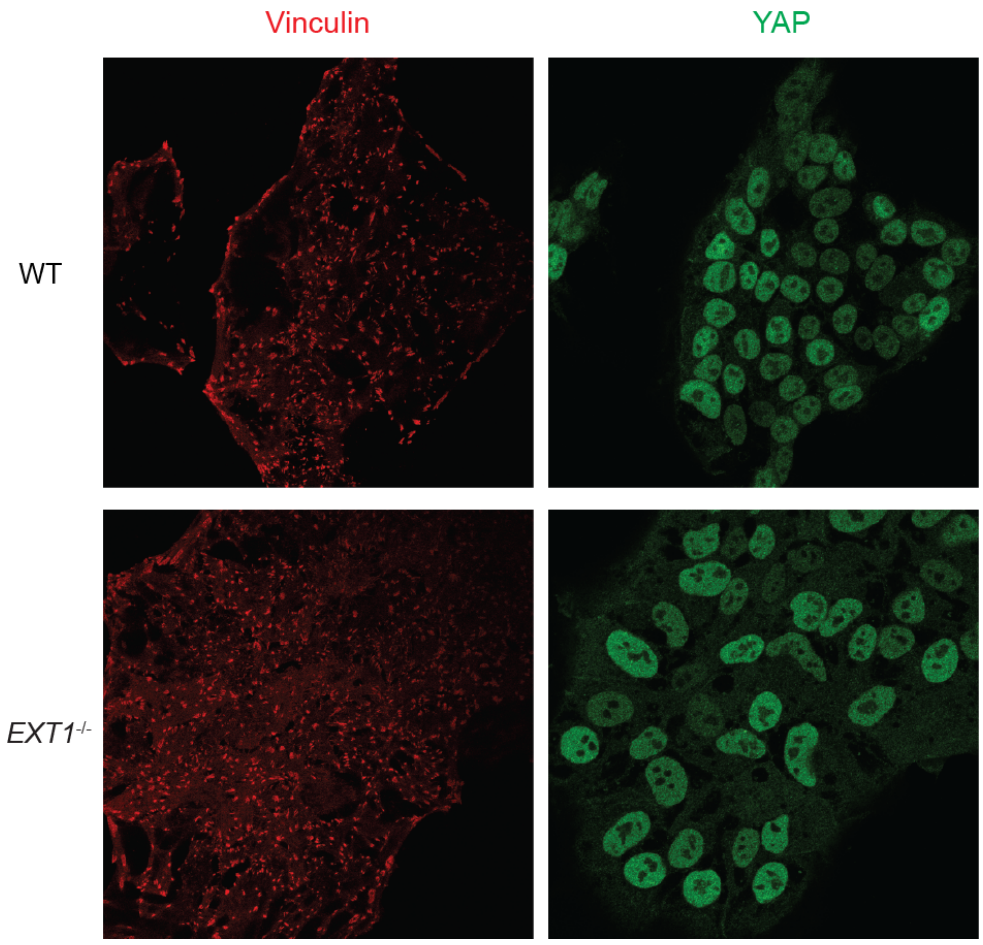

Figure A1-3: HS-deficient hPS cells form focal adhesions and retain nuclear YAP. Vinculin (left) and YAP (right) protein levels and localization in WT (top) and *EXT1*$^{-/-}$ (bottom) H9 cells cultured on vitronectin-coated glass in E8 medium.

A1.3 Methods

A1.3.1 hPS cell culture

H9 hES cells were cultured as described in previous chapters. Tissue culture polystyrene presenting the VHBD peptide was generated as described in chapter 2. For vitronectin coating, tissue culture polystyrene was incubated with 2.5 μg/mL vitronectin (R&D Systems) in PBS for 24 hours at 4 °C.

A1.3.2 CRISPR editing of hPS cells

For targeting *EXT1* in H9 hES cells, CRISPR/Cas9 genome editing was used. 2 μM Alt-R S.p. Cas9 Nuclease 3NLS (IDT) was complexed with 2.4 μM duplex consisting of Alt-R CRISPR-Cas9 crRNA (target sequence: AGCCGGAGAGAAGAACACAG) and tracRNA (IDT) in nucleofection buffer. H9 cells were nucleofected with the ribonucleoprotein complex using the Human Stem Cell Nucleofector Kit 2 (Lonza) and the B-16 program on the Amaxa Nucleofector II (Lonza) as per manufacturer instructions. Cells were allowed to recover for two days in mTeSR1 medium supplemented with 1x RevitaCell (Gibco) Clones were derived using serial dilution and analyzed by PCR amplification and Sanger sequencing to identify the modifications at both alleles.

A1.3.3 Flow cytometry

For analysis of HS cell surface levels, WT and $EXT^{-/-}$ H9 cells were detached with 1 mM EDTA, centrifuged, and resuspended in 1 mL cold PBS containing 1 μL LIVE/DEAD fixable far-red dead cell stain. Cells were then centrifuged and resuspended in PBS containing 2% BSA (w/v) supplemented with 1:200 anti-mouse HS IgM 10E4 (United States Biological) for 1 hour on ice. Antibody exposure was followed by two washes. Cells were then resuspended in PBS containing 2% BSA (w/v) supplemented with goat anti-mouse IgM-PE for 1 hour on ice,

followed by two washes. Data were obtained using a FACSCalibur instrument (BD) and analyzed using FlowJo software (Tree Star, Inc.).

A1.3.4 Immunofluorescence

Immunofluorescence was performed as described in previous chapter. The primary antibodies used in this study are described in Table A1-1.

Table A1-1: List of primary antibodies used in this study

Antigen	Species	Source	Dilutions
HS (10E4)	Mouse	US Biological H1890	ICC: 1:100, FC: 1:200
Vinculin	Mouse	Sigma Aldrich V9131	ICC: 1:300
YAP	Rabbit	Cell Signaling 14074	ICC: 1:300

A1.3.5 Lentiviral generation of stable cell lines

Lentiviruses for hPS cell transduction of EXT1-T2A-GFP were generated as described in chapter 3. EXT1, amplified from hPS cell-derived cDNA, was cloned in the modified pCW vector.

A1.4 Acknowledgments

I thank Dr. Paul Wrighton for starting this project, and Dr. Sayaka Masuko and Qiao Li for continuing it. I thank Sayaka for analysis of HS by flow cytometry and for conducting cell binding experiments.

A1.5 References

Forsten-Williams, K., Chu, C.L., Fannon, M., Buczek-Thomas, J.A., and Nugent, M.A. (2008). Control of growth factor networks by heparan sulfate proteoglycans. Ann Biomed Eng *36*, 2134-2148.

Gopal, S., Bober, A., Whiteford, J.R., Multhaupt, H.A., Yoneda, A., and Couchman, J.R. (2010). Heparan sulfate chain valency controls syndecan-4 function in cell adhesion. J Biol Chem *285*, 14247-14258.

Humphrey, J.D., Dufresne, E.R., and Schwartz, M.A. (2014). Mechanotransduction and extracellular matrix homeostasis. Nat Rev Mol Cell Biol *15*, 802-812.

Johnson, C.E., Crawford, B.E., Stavridis, M., Ten Dam, G., Wat, A.L., Rushton, G., Ward, C.M., Wilson, V., van Kuppevelt, T.H., Esko, J.D.*, et al.* (2007). Essential alterations of heparan sulfate during the differentiation of embryonic stem cells to Sox1-enhanced green fluorescent protein-expressing neural progenitor cells. Stem Cells *25*, 1913-1923.

Klim, J.R., Li, L., Wrighton, P.J., Piekarczyk, M.S., and Kiessling, L.L. (2010). A defined glycosaminoglycan-binding substratum for human pluripotent stem cells. Nat Methods *7*, 989-994.

Lin, X., Wei, G., Shi, Z., Dryer, L., Esko, J.D., Wells, D.E., and Matzuk, M.M. (2000). Disruption of gastrulation and heparan sulfate biosynthesis in EXT1-deficient mice. Dev Biol *224*, 299-311.

Saoncella, S., Echtermeyer, F., Denhez, F., Nowlen, J.K., Mosher, D.F., Robinson, S.D., Hynes, R.O., and Goetinck, P.F. (1999). Syndecan-4 signals cooperatively with integrins in a Rho-dependent manner in the assembly of focal adhesions and actin stress fibers. Proc Natl Acad Sci U S A *96*, 2805-2810.

Wrighton, P.J., Klim, J.R., Hernandez, B.A., Koonce, C.H., Kamp, T.J., and Kiessling, L.L. (2014). Signals from the surface modulate differentiation of human pluripotent stem cells through glycosaminoglycans and integrins. Proc Natl Acad Sci U S A *111*, 18126-18131.